

Reinforcement interfaces in low-carbon concretes

Meimei Song

Submitted in accordance with the requirements for the degree of
Doctor of Philosophy

The University of Leeds

School of Civil Engineering

June 2015

The candidate confirms that the work submitted is her own and that appropriate credit has been given where reference has been made to the work of others.

This copy has been supplied on the understanding that it is copyright material and that no quotation from the thesis may be published without proper acknowledgement.

The right of Meimei Song to be identified as Author of this work has been asserted by her in accordance with the Copyright, Designs and Patents Act 1988.

© 2015 The University of Leeds and Meimei Song

Acknowledgements

Three years life in Leeds is a truly a great memory for me, it is a process not only obtaining academic knowledge but also discovering myself in many ways. Sincere acknowledgements are given to my primary supervisor Professor Philip Purnell for his academic supervision during my PhD study and all the professional comments given on my thesis. Thanks are also given to my supervisor Professor Ian Richardson for his academic guidance in microanalysis and image analysis. Financial supports from China Scholarship Council in association with University of Leeds for this project are greatly appreciated. It is my honour to meet lots friends here; time we spent together will always be remembered. In particular, thanks should be given to Chuanlin who helped me a lot in thesis printing. Special dedication should be given to my parents, my brother and my fiancé, thanks for your love.

Abstract

Calcium sulfoaluminate cement (CSA) is a potential low-carbon binder that has a markedly less alkaline matrix environment compared to traditional Portland cement. Investigations on its long-term chemical compatibility with different reinforcements (i.e. glass fibre and steel rebar) are necessary before widespread adoption could occur. In this project, studies mainly focus on the microstructural evolution at interfacial zones over time, which has a significant impact on the durability properties of reinforced concretes.

Glass fibre reinforced composites made with two matrix formulations (OPC, and OPC plus calcium sulfoaluminate based matrices) aged for 10 years at 25°C and steel reinforced CSA concretes aged for 28 days and 1.5 years are studied. Optical transmitted microscopy and SEM/EDX on the thin section petrographic specimens of composites are employed to give a straightforward interfacial zone characterization. Quantitative imaging analysis techniques are newly updated by using quantified elemental mappings for the first time.

The results suggest that CSA cement is highly compatible with the embedded glass fibre and steel reinforcement in the long term. Aged GRC composite modified by CSA cement shows greatly retained toughness, accompanied by considerably flexible interfacial and interfilamentary areas around the glass fibres. This is in contrary to the aged OPC/GRC, which demonstrates significantly brittle behaviour with substantial densification of C-S-H/CH intermixture occurring around glass fibres. In the steel reinforced CSA concrete, elemental mappings clearly show that there is a non-

continuous aluminium-rich layer at the steel/concrete interface; and the aluminium gel is slightly consumed over time by chemical reactions. Imaging analysis results indicate less active ion transport at the steel/concrete interface than that in the traditional OPC concrete system.

Table of content

ACKNOWLEDGEMENTS	I
ABSTRACT	II
TABLE OF CONTENT	IV
LIST OF FIGURES	IX
LIST OF TABLES	XIII
LIST OF ABBREVIATIONS	XIV
LIST OF CEMENT CHEMISTRY	XV
CHAPTER 1- INTRODUCTION	1
1.1 General introduction	1
1.2 Aims and objectives	5
1.3 Thesis structure	7
CHAPTER 2- LITERATURE REVIEW ON CALCIUM SULFOALUMINATE CEMENT	8
2.1 Introduction	8
2.2 Chemical compositions	10
2.2.1 Calcium sulfoaluminate	11
2.2.2 Belite.....	11
2.3 Durability	12
2.3.1 Carbonation	12
2.3.2 Corrosion resistance.....	13
CHAPTER 3- LITERATURE REVIEW ON GRC COMPOSITES	15
3.1 Introduction	15
3.2 Historical	17
3.3 Theoretical mechanism of GRC composite	20
3.4 Durability	22
3.4.1 Mechanisms	23
3.4.1.1 Fibre corrosion	24
3.4.1.2 Matrix densification and interfilamentary precipitation	24
3.4.2 Accelerated ageing.....	26

3.5 Improvement of GRC from matrix modification.....	30
3.5.1 GRC from Pozzolanas additives.....	31
3.5.1.1 Metakaolin.....	31
3.5.1.2 GGBS.....	32
3.5.1.3 Silica fume.....	32
3.5.2 GRC from non-Portland cement.....	33
3.6 Role of interface.....	34
3.7 Discussion	36
CHAPTER 4- LITERATURE REVIEW ON INTERFACES IN STEEL	
REINFORCED CONCRETE	38
4.1 Introduction	38
4.2 Reinforcement corrosion.....	39
4.2.1 Chloride-induced corrosion.....	40
4.2.2 Corrosion by carbonation	41
4.3 The role of steel/concrete interface	41
4.4 Microstructure at steel/concrete interface.....	43
4.5 Quantification analysis.....	47
4.5.1 Overview.....	47
4.5.2 Phase segmentation.....	48
4.5.3 Quantification at the steel/concrete interface	50
4.6 Discussion	53
CHAPTER 5- EXPERIMENTAL	55
5.1 Materials and mix design	55
5.1.1 GRC composites	55
5.1.2 Steel reinforced concrete.....	56
5.2 Experimental design	60
5.3 Thin section petrography (TSP) production	62
5.3.1 Overview.....	62
5.3.2 Initial cutting.....	64
5.3.3 Initial grinding	64
5.3.4 Hydration stop	65
5.3.5 Resin impregnation.....	66

5.3.6 First face grinding	66
5.3.7 Bonding	67
5.3.8 Removal of excess material	68
5.3.9 Final grinding	68
5.3.10 Storage	72
5.4 Bulk analysis	72
5.4.1 DTA/TG	72
5.4.2 X-ray Diffraction (XRD).....	73
5.5 Bending test.....	75
5.6 Thin section (optical) microscope	75
5.7 SEM/EDX.....	77
5.7.1 General introduction to SEM	77
5.7.2 Coating	79
5.7.3 SEM set up.....	79
5.7.3.1 Working distance.....	80
5.7.3.2 Accelerated voltage.....	80
5.7.3.3 Magnification	81
5.7.3.4 Image resolution.....	81
5.7.4 EDX	81
5.7.4.1 Elemental mappings.....	81
5.7.4.2 Spot analysis.....	83
5.8 Image analysis	84
CHAPTER 6- RESULTS AND DISCUSSION: GRC	89
6.1 DTA.....	89
6.2 XRD	91
6.3 Microstructural study of Nashrin/GRC	93
6.3.1 Thin section image	93
6.3.2 SEM on polished sample.....	98
6.3.3 Microanalysis.....	105
6.3.4 SEM on fractured surface.....	107
6.3.5 SEM on fibre surface	108
6.4 Microstructural study of OPC/GRC	109

6.4.1 Thin section image	109
6.4.2 SEM on polished sample.....	112
6.4.3 Microanalysis.....	116
6.4.4 SEM on fractured surface.....	118
6.4.5 SEM on fibre surface	119
6.5 Bending tests	120
6.6 Summary of main findings	124
CHAPTER 7- RESULTS AND DISCUSSION: STEEL REINFORCED CONCRETE	125
7.1 DTA.....	125
7.1.1 CSA paste	125
7.1.2 OPC paste	128
7.2 XRD	130
7.2.1 CSA paste	130
7.2.2 OPC paste	132
7.3 Microstructure in steel reinforced CSA concrete	134
7.3.1 Early-age microstructure	134
7.3.1.1 SEM.....	134
7.3.1.2 Microanalysis.....	138
7.3.2 Long-term microstructure	139
7.3.2.1 SEM.....	139
7.3.2.2 Microanalysis.....	143
7.4 Microstructure in steel reinforced OPC concrete	145
7.4.1 Early-age microstructure	145
7.4.1.1 SEM.....	145
7.4.1.2 Microanalysis.....	148
7.4.2 Long-term microstructure	149
7.4.2.1 SEM.....	149
7.4.2.2 Microanalysis.....	153
7.5 Image analysis	154
7.5.1 Steel reinforced CSA concrete	154
7.5.2 Steel reinforced OPC concrete.....	158

7.6 Summary of main findings	161
CHAPTER 8- GENERAL DISCUSSION.....	163
8.1 Chemical composition at the interface	163
8.1.1 Glass fibre/cement interface.....	163
8.1.2 Steel/concrete interface.....	164
8.2 Ion transport at steel/concrete interface	165
8.3 Accuracy of hot water accelerated ageing tests	167
8.4 General discussion on the importance of interface.....	173
8.5 Application of CSA cement.....	175
CHAPTER 9- CONCLUSIONS AND FUTURE WORK	177
9.1 General conclusions	177
9.2 Future work.....	178
REFERENCES.....	179
APPENDIX A	193
APPENDIX B	195

List of figures

Figure 3.3.1 Typical stress-strain curve for GRC composite reinforced by short fibres with high fibre content ($V_f > V_{f_{crit}}$, $l \leq l_c$), from reference (Purnell, 2007).....	22
Figure 3.4.1 Illustration of strand-in-cement tensile specimen test.....	27
Figure 3.4.2 SIC strength retention in water at various temperatures, from reference (Litherland, 1981).....	28
Figure 3.4.3 Arrhenius graphs from SIC tests, from reference (Litherland, 1981).....	29
Figure 3.5.1 Stress-strain performance of (a) OPC/GRC and (b) CSA-based GRC composites aged at 50°C, from reference (Purnell and Beddows, 2005).....	34
Figure 4.4.1 Microstructure images shown that CH is often absent at the steel/concrete interface, from reference (Glass <i>et al.</i> , 2001).....	46
Figure 4.5.1 Phase segmentation in cement paste and a combined image used for area analysis, from reference (Stutzman, 2004).....	50
Figure 4.5.2 An example for regional growing at the interface from reference (Horne, 2004).....	51
Figure 4.5.3 Microstructural gradients in the interfacial region between cement paste and vertically cast steel in a concrete with a w/c ratio of 0.49; from reference (Horne <i>et al.</i> , 2007).....	52
Figure 5.1.1 Particle size distribution of aggregates used in the project.....	57
Figure 5.1.2 An example of the arrangement of four reinforced bars in CSA concrete.....	59
Figure 5.3.1 Flowchart of the sequences to produce a thin section petrography specimen.....	63
Figure 5.3.2 The grinding machine (Rotopol 35 by Struers) used in the final grinding process.....	69
Figure 5.3.3 Sequence of the procedure of final grinding process.....	71
Figure 5.4.1 Illustration of X-ray generation.....	74
Figure 5.5.1 Experimental setup of four-point bending test on GRC slabs..	75
Figure 5.7.1 Overview of signal generation in SEM.....	77

Figure 5.8.1 Different SEM settings for iron mappings in one of the examples of reinforced concrete sample	85
Figure 5.8.2 Smartmap in Inca used to collect elemental mappings for image analysis	86
Figure 5.8.3 An example of reading elemental information pixel by pixel using Inca software	87
Figure 5.8.4 An example of obtaining the quantitative Microsoft Excel data on atomic information for each pixel	87
Figure 6.1.1 STA results of 10y aged OPC/GRC and GRC modified by Nashrin	90
Figure 6.2.1 XRD results of 10y aged GRC modified by Nashrin and OPC	92
Figure 6.3.1 Observation of unaged Nashrin/GRC composite under plain polarised and uncrossed polarised light (polar at 80 degree), based on a thin section petrography sample made in a previous project; width of field 0.32mm	95
Figure 6.3.2 Observation of 10-years aged Nashrin/GRC composite under (a) plain polarised (b) uncrossed polarised light, polar at 78 degree and (c) backscattered image at the same location, width of field 0.32mm.....	96
Figure 6.3.3 Observation of 10-years aged Nashrin/GRC composite under (a) plain polarised (b) uncrossed polarised light, polar at 75 degree and (c) backscattered image at the same location, width of field 0.32mm.....	97
Figure 6.3.4 First example of microstructure of Nashrin/GRC aged for 10 years	101
Figure 6.3.5 Second example of microstructure of Nashrin/GRC aged for 10 years	104
Figure 6.3.6 Scatter graphs of Nashrin-based GRC composites aged for 10 year at 25°C	106
Figure 6.3.7 SEM images of fractured 10 years-aged Nashrin/GRC at various magnifications.....	108
Figure 6.3.8 Microstructure of fibre surfaces in aged Nashrin/GRC composite	109
Figure 6.4.1 Thin section images of OPC-based GRC aged for 28 days at 25°C, under partial plain polarised and crossed polarised light, based on a thin section petrography sample made in a previous project; width of field 0.32mm	111

Figure 6.4.2 Thin section images of OPC-based GRC aged for 10 years at 25°C, under partial plain polarised and crossed polarised light, width of field 0.32mm	112
Figure 6.4.3 Microstructure of OPC/GRC aged for 10 years at 25°C	115
Figure 6.4.4 Scatter graphs of OPC/GRC composites aged for 10 years at 25°C	117
Figure 6.4.5 SEM images of fractured 10 years-aged OPC/GRC at various magnifications	119
Figure 6.4.6 Microstructure of fibre surface in aged OPC/GRC composite	120
Figure 6.5.1 Stress-strain curves for unaged GRC composites, data from reference (Purnell and Beddows, 2005).....	123
Figure 6.5.2 Stress-strain curves of GRC composites aged for 10 years ..	123
Figure 7.1.1 STA results of CSA paste cured at 21°C for 7, 28, 90 days and 1.5 years	127
Figure 7.1.2 STA results of OPC paste cured at 21°C for 7, 28, 90 days and 1.5 years	129
Figure 7.2.1 XRD analysis of CSA cements powder and hydrated CSA paste	131
Figure 7.2.2 XRD analysis of hydrated OPC paste at w/c 0.69	133
Figure 7.3.1 Backscattered electron image of steel reinforced CSA concrete aged for 28 days	137
Figure 7.3.2 Microanalysis at the steel/concrete interface in CSA concrete aged for 28 days	139
Figure 7.3.3 Microstructure study of steel reinforced CSA concrete aged for 1.5 years	142
Figure 7.3.4 Scatter graph of atomic ratios at the steel/concrete interface of reinforced CSA concrete, aged for 1.5 years	144
Figure 7.4.1 Microstructural study of steel reinforced OPC concrete cured for 28 days.....	147
Figure 7.4.2 Scatter graph of atomic ratios at the steel/concrete interface of reinforced OPC concrete, aged for 28 days.....	149
Figure 7.4.3 Microstructure study of steel reinforced OPC concrete aged for 1.5 years	152

Figure 7.4.4 Scatter graph of atomic ratios at the steel/concrete interface of reinforced OPC concrete, aged for 1.5 years.....	154
Figure 7.5.1 Image analysis on atomic ratios at the steel/concrete interface in reinforced CSA concrete	158
Figure 7.5.2 Image analysis on atomic ratios at the steel/concrete interface in reinforced OPC concrete.....	161
Figure 8.2.1 Calcium hydroxide phase gradient in the interfacial region between cement paste and vertically cast steel at four ages in a concrete with a w/c ratio of 0.70, from reference (Horne <i>et al.</i> , 2007).....	166
Figure 8.3.1 Evolution of bending performance of OPC/GRC by hot water accelerated ageing at 50°C; from reference (Purnell and Beddows, 2005)	169
Figure 8.3.2 Stress-strain curves for the GRC specimens made of CEMI 32.5R, accelerated at 40°C/99% RH with reference sample cured at 20°C/66% RH for 28 days, from reference (Butler <i>et al.</i> , 2010).....	169
Figure 8.3.3 Evolution of bending performance of Nashrin/GRC by hot water accelerated ageing at 50°C; from reference (Purnell and Beddows, 2005)	172
Figure 10.1 Image analysis on S/Ca at the interface between CSA cement and steel.....	194

List of tables

Table 3.1.1 Properties of hardened cement paste, from reference (Majumdar and Laws, 1991).....	16
Table 3.1.2 Typical properties of unaged GRC composites.....	17
Table 3.2.1 Chemical compositions of various glass fibres (wt.%) from reference (Majumdar and Laws, 1991)	18
Table 3.2.2 Comparison of mechanical properties of GRC composites reinforced by both Cem-FIL and Cem-FIL 2 under natural weathering at BRS, from reference (Majumdar and Laws, 1991).....	20
Table 3.4.1 Examples of the measured strength properties of spray-dewatered OPC/GRC reinforced by 5 wt.% Cem-FIL AR glass fibre) with ageing, from reference (Majumdar and Laws, 1991)	23
Table 4.4.1 Chemical compositions at the interface between steel disc and ordinary cement paste (wt.%), from reference (Li and Hu, 2001)	44
Table 5.1.1 XRF results of OPC and Nashrin modified GRC aged for 10 years at 25°C	56
Table 5.1.2 Mix design of C35 CSA concrete	58
Table 5.1.3 Chemical composition of CSA cement and OPC cement by XRF analysis	60
Table 5.2.1 Design of the experimental work on GRC part.....	61
Table 5.2.2 Design of the experimental work on steel reinforced concrete part.....	61
Table 5.3.1 Illustration of grit sizes and their corresponding grade standard	68
Table 5.7.1 General SEM setup.....	80
Table 5.7.2 General Mapping setup.....	82

List of abbreviations

AR: Alkalis resistant
BSE: Backscattered electron
CSA: calcium sulfoaluminate cement
CTL: Chloride threshold level
DSC: Differential scanning calorimetry
DTA: Differential thermal analysis
E: elastic modulus
EDX: Energy dispersive X-ray spectroscopy
FS: Failure strain
GGBS: Ground granulated blast furnace slag
GRC: Glass fibre reinforced concrete
HAC: High alumina cement
IS: Impact strength
LOP: Limit of proportionality
MOR: Modulus of rupture
OPC: Ordinary Portland cement
Pfa: Pulverised fuel ash
SEM: Scanning electron microscopy
SIC: Strand in cement
SSC: Super-sulfated cement
TG: Thermogravimetry
TSP: Thin section petrography
UTS: Ultimate tensile strength
XRD: X-ray diffraction

List of cement chemistry

AFm: monosulfate

AFt: ettringite

C₃A: tri-calcium alumina

C₄AF: calcium alumina-ferrite

C₄A₃ \bar{S} : calcium sulfoaluminate

CH: calcium hydroxide

C₂S: de-calcium silicate

C-S-H: calcium silicate hydrate

C₂ASH₈: stratlingite

Chapter 1- Introduction

1.1 General introduction

In the global push for greener energy and less carbon emission, the cement industry is inevitably challenged because it contributes perhaps 6% to total global anthropogenic CO₂ emission every year (Damtoft *et al.*, 2008; Juenger *et al.*, 2011). Production of 1t Portland cement clinker generates about 800Kg of CO₂ emissions (Gartner, 2004; Damtoft *et al.*, 2008; Winnefeld and Lothenbach, 2010); more than 60% of the generated CO₂ derives from the decarbonation of limestone (Popescu *et al.*, 2003) and the remainder from energy consumptions (e.g. heating raw materials to a temperature of 1450°C and grinding clinkers). Hence much more attention has been given by researchers to developing a new generation of environmentally friendly cement systems with the aim of achieving less direct CO₂ emission and/or energy savings.

Calcium sulfoaluminate cement (CSA) is one such cement having been described as a low-carbon binder, the production of which is expected to reduce CO₂ emission by up to 35% relative to the traditional Portland cement production (Carmen Martin-Sedeno *et al.*, 2010; Zhou *et al.*, 2006). It was first produced in China in the 1970s by heating mixtures of limestone, bauxite and gypsum to about 1250°C, generating a clinker with the main compositions of calcium sulfoaluminate and belite. One of the prominent characteristics of hydrated CSA paste is that it is free of calcium hydroxide, which consequently leads to a less alkaline pore solution with a pH value between 10 and 11.5 (Zhou *et al.*, 2006). Rapid formation of ettringite in

Chapter 1- Introduction

hydrated CSA cement system within the first few hours puts CSA cement well suited on the production of high-early strength concretes (Beretka *et al.*, 1997); the intrinsically expansive property of ettringite is beneficial in some special situations, e.g. shrinkage-compensation materials, self-levelling screed and self-levelling topping mortar (Pera and Ambroise, 2004). However, its carbonation rate has been suspected to be much more rapid than that in Portland cement concrete due to the dominant formation of ettringite (Quillin, 2001); this may cause a moderate concrete strength loss (Juenger *et al.*, 2011). Moreover in steel reinforced CSA concrete system, reduced alkalinity in the pore solution caused by carbonation may also activate the reinforcement corrosion.

Glass fibre reinforced concrete (GRC for short) is a versatile construction material of considerable potential, normally made in the form of thin sheets. Nevertheless its long-term durability has aroused some concerns, which has limited its wider application in engineering. GRC composites made with normal Portland cement may suffer significant reductions in tensile strength and ductility with ageing and it tends to deteriorate more rapidly under humid environment. The exact mechanisms underlying this degradation process are still debated but it is normally accepted that it involves a combination of glass fibre corrosion caused by the hydroxyl in the pore solution, and significant CH precipitation between and around fibres that causes loss of flexibility. Therefore efforts have been directed towards the study of modified matrix formulation with markedly reduced alkalinity and/or propensity to precipitate calcium hydroxide. CSA cement is one such solution that meets these two criteria, in which calcium hydroxide is absent during hydration and

Chapter 1- Introduction

a considerably less alkaline pore solution is developed. The addition of CSA cement in GRC has been studied and encouraging results of improved retention of tensile strength and toughness has been reported (Purnell *et al.*, 1999; Purnell and Beddows, 2005) by using hot water accelerated ageing tests.

Due to a lack of long research periods available for the long-term curing of GRC at normal temperatures, hot water accelerated ageing has been developed to assess the likely behaviour of GRC durability within manageable time scales. However, the side effects by hot water accelerating ageing cannot be ignored. It may not simply accelerate the hydration as expected originally, but may also have an influence on the intrinsic nature of the hydrated matrix to some degree (e.g. totally different hydration products can be generated at elevated ageing temperature), which is a key factor controlling the degradation mechanism, thus limiting the usefulness of this testing procedure. This could lead to overestimations or underestimations of the durability of the tested GRC composites.

In traditional OPC-based steel reinforced concrete systems, the steel/concrete interface tends to become more porous than the bulk matrix. Previous studies (Li and Hu, 2001; Horne *et al.*, 2007) generally agree that there are considerable amounts of crystalline CH in a layer at the interface, which may or may not be continuous along the whole perimeter of steel, only adhering on the steel surface partially. This leads to the assumption that enhanced pH buffering capacity is maintained at the interface, which consequently helps protect the embedded steel from corrosion as a high pH is retained in the vicinity of steel under most conditions. However, when

Chapter 1- Introduction

embedded in a less alkaline solution developed by the CSA-based material, steel reinforcement is no longer protected by a solid lime-rich layer as no CH is formed during hydration; and the tendency of rapid carbonation of the abundant ettringite formed during hydration further reduces its buffering capacity against de-alkalization. Therefore concerns have been raised for the passivation of the steel bars that are embedded in CSA cement matrix in the long term.

The interfacial zone is the weakest part in concrete and it is usually from this region that cracks initiate and propagate, followed by a destructive stress failure. To some extent, physical condition and composition of the hydrated phases in this region are among the deciding factors controlling the durability properties of reinforced concrete systems. Much research has studied steel reinforced CSA concrete (Kalogridis *et al.*, 2000; Janotka *et al.*, 2002; Glasser and Zhang, 2001), but most of the work has concentrated on the strength development and various macro-properties (e.g. carbonation, sulfate resistance, frost and corrosion resistant capacities). Little is known about how its microstructure evolves with ageing, in particular at the steel/concrete interfacial region, despite this being a fundamental factor which has an influential effect on the macro-properties development of reinforced CSA concretes.

Image analysis techniques make it possible to achieve quantitative calculations of different phases (e.g. unhydrated cement, CH, porosity) at the interface in reinforced OPC concretes. This is based on phase segmentations according to their unique microstructural features as well as several computer-based arithmetic programs. Although elemental mappings

Chapter 1- Introduction

are able to provide straightforward and qualitative digital information on the spatial distributions of different elements in general, quantitative evolution of various atomic ratios (e.g. Ca/Si, Al/Ca, S/Ca) with curing at the interfacial region remains unclear. This suggests that careful examination in pursuit of a better understanding of the mobility of different ions during hydration in the vicinity of steel, and how it may be influenced by various factors, e.g. w/c ratios, curing conditions and the matrix type, is likely to be useful. Similar quantitative analysis on reinforced CSA concrete is also needed in order to clarify the intrinsic differences between OPC and CSA cement in how they distribute different ions in order to protect the embedded steel and give confidence in the long-term behaviour of CSA concrete.

1.2 Aims and objectives

In both composite systems, the interface is of paramount importance. Thus, studies in this project focus on the investigation of CSA-based concretes reinforced by different reinforcements, e.g. glass fibres and steel bar reinforcement, with particular focus on the interfacial region. Research will emphasize whether those embedded reinforcements are still physically and chemically compatible within the newly made CSA cement matrix, by means of microstructural observations at the interfacial zones. This information is of vital importance for assessment of the predicted durability properties of CSA-based materials, which is critical before the widespread application of CSA cement concrete can occur in the construction industry and the potential low-carbon benefits be realised.

Chapter 1- Introduction

This project provides the opportunity to study the 'real aged' GRC composites cured for 10 years at 25°C. Both durability and microstructure studies of these CSA modified GRC are investigated, with a reference from normal GRC composites under the same ageing condition. In addition, CSA concretes reinforced by steel bars (with a diameter of 10mm) are also made to study the microstructural evolution at the steel/cement interface at ages for up to 1.5 year, in both qualitative and quantitative ways.

The primary objectives of this project are:

- Study on the hydration process of CSA cement pastes hydrated at different curing regimes (7 days, 28 days, 90 days and 1.5 years).
- Appraisal of the long-term compatibility between glass fibre and CSA-modified cement matrix in GRC systems.

Bending performances and microstructural evolution at the interfilamentary and fibre/cement interfacial zone of the GRC composites are examined; the latter is a critical aspect in describing the long-term durability properties of GRC.

- Assessment of the time-dependent microstructure development at the steel/concrete interface in reinforced CSA concrete cured for up to 1.5 year, in comparison to a corresponding OPC concrete system.
- Image analysis to study the chemical composition at the steel/concrete interface in both steel reinforced CSA and OPC concrete systems.

Quantitative distributions of atomic ratios (e.g. Ca/Si, Al/Ca, S/Ca) as a function of distance away from steel (within 30 μ m) are attempted, aiming at figuring out the intrinsic difference between these CSA and

Chapter 1- Introduction

OPC-based concrete systems and the preferable precipitation and transport of varying ions in the vicinity of the embedded steel with curing.

1.3 Thesis structure

The thesis is started with three chapters of literature review (chapter two on CSA cement, chapter three on GRC composites and chapter four on interfaces in steel reinforced concrete). Then it follows chapter five for the experimental work, mainly introducing the materials and technical methodologies used in this research. Chapter six presents the experimental results on GRC composites, by combining different analytical techniques. Chapter seven refers to the results on interfaces in steel reinforced concrete. Discussion is included in chapter eight, comparing the results obtained in this research with the previous research. A general conclusion can be found in chapter nine, focusing on the different features of interfacial zone in reinforced composites with modified matrix and varying reinforcements.

Chapter 2- Literature review on calcium sulfoaluminate cement

This chapter summarises the history of CSA cement and the influences of different clinker compositions (e.g. contents of gypsum) on the macro-properties of CSA-based materials. Hydration mechanism of CSA cement is also introduced in this text below. Durability properties of CSA-based materials (e.g. carbonation and corrosion resistance) are summarised in this chapter.

2.1 Introduction

CSA cement was first produced in China in the 1970s (Glasser and Zhang, 2001; L.Zhang, 1999; Zhang and Glasser, 2005; Shi *et al.*, 2011). Raw materials including limestone, bauxite together with gypsum or anhydrite are fired at 1250-1350°C; the firing temperature is therefore ~200°C lower than that for Portland cement manufacture. Its main clinker composition is calcium sulfoaluminate $C_4A_3\bar{S}$ (or called Ye'elimitite); other phases such as belite, aluminate or ferrite may also present depending on the raw mixes.

Calcium sulfoaluminate is considerably lower in calcium content compared with other clinker phases in Portland cement; this leads to a favourable reduction in CO₂ emission during the calcination of limestone in cement kilns. In detail, CaO content by weight of several cement phases are listed as follows: C₃S 73.7%, C₂S 65.1%, C₃A 62.2%, C₄AF 46.2%, $C_4A_3\bar{S}$ 36.7%. Among these clinker phases, calcium sulfoaluminate can be summarised to

Chapter 2- Literature review on calcium sulfoaluminate cement

be the most attractive option for developing low-energy cements (Arjunan *et al.*, 1999).

Varying contents of gypsum or anhydrite are added to the raw mix in order to control the dimensional stability properties of CSA cement (Winnefeld and Barlag, 2009; Glasser and Zhang, 2001; García-Maté *et al.*, 2012; Telesca *et al.*, 2014). This is tailored to different engineering applications, e.g. a CaSO_4 content between 18-20% causes slight shrinkage during setting; a value between 22-24% provides a minimal dimensional change; and at value at or above 25%, CSA cement can be quite expansive due to the presence of large amounts of ettringite formation (Glasser and Zhang, 2001). Therefore one of the main applications of CSA cement is used as an expansive binder in shrinkage-compensated cement, e.g. leakage and seepage prevention projects (Juenger *et al.*, 2011; Glasser and Zhang, 2001; Janotka *et al.*, 2003; Janotka and Krajci, 1999; Pera and Ambroise, 2004; Georgin *et al.*, 2008). CSA cement usually gives very high early strength because of the rapid formation of ettringite within the first few hours, bonding and interlocking between ettringite is assumed to contribute to the strength development (Arjunan *et al.*, 1999; Glasser and Zhang, 2001; Hargis *et al.*, 2013). Due to its low alkaline pore solution compared to OPC, addition of CSA cement has been used to produce high-performance glass fibre reinforced composites (Pera and Ambroise, 2004; Purnell *et al.*, 1999). On the other hand, the formation of ettringite and AFm phases makes CSA cement paste able to bind heavy metals (as ettringite and AFm can accommodate substitutions in their SO_4^{2-} , Ca^{2+} or Al^{3+} sites), therefore CSA cement is also considered as a potential material in the field of hazardous

Chapter 2- Literature review on calcium sulfoaluminate cement

waste encapsulation (Peysson *et al.*, 2005; Zhou *et al.*, 2006; Luz *et al.*, 2006; Juenger *et al.*, 2011; Albino *et al.*, 1996; Winnefeld and Lothenbach, 2010; Berger *et al.*, 2013).

In summary, the advantages of CSA cement over Portland cement can be summarised as:

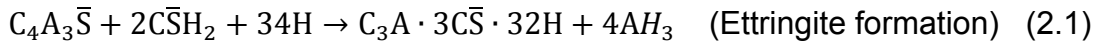
1. Reduced energy consumption during manufacture. The clinker temperature for producing CSA cement is ~200°C lower than those for Portland cement manufacture. On the other hand, the resultant clinker is very soft and has higher clinker porosity that requires lower grinding energy.
2. Lower CO₂ emission during manufacture due to reduced limestone utilization in raw materials.
3. High early strength development. Rapid hydration of calcium sulfoaluminate within the first few hours produces large amounts of ettringite formation, which are conducive to a higher strength development at early age.

2.2 Chemical compositions

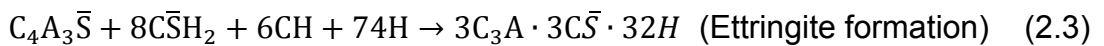
CSA cement presents a wide range of phase assemblages, but its main mineral (more than 50 wt.%) is calcium sulfoaluminate $C_4A_3\bar{S}$ (also known as Ye'elimite). Depending on the raw materials, belite or aluminate or ferrite phases may also be present (Quillin, 2001; Chen and Juenger, 2011; García-Maté *et al.*, 2014; Adolfsson *et al.*, 2007; Li *et al.*, 2014).

2.2.1 Calcium sulfoaluminate

In the pure CSA cement hydration system, calcium sulfoaluminate starts to hydrate rapidly within 15-20min after mixing (García-Maté *et al.*, 2014). It exhibits the formation of ettringite crystals (present as prismatic or needle-like shapes) together with amorphous alumina gels, providing enough gypsum is present (Eq. 2.1). Large amounts of ettringite formed are highly responsible for the quick setting of CSA cement and most of the strength development in the first few days (Glasser and Zhang, 2001; Liao *et al.*, 2011). Afterwards, formation of monosulfate initiates quickly with the depletion of gypsum (Winnefeld and Lothenbach, 2010) (Eq. 2.2).



If CSA cement is used as an alternative addition to Portland cement, CH is then produced from the reactant hydration of C_3S and C_3A in Portland cement. However the resultant CH is soon involved in the hydration of calcium sulfoaluminate, leaving ettringite as the main hydration product (Eq. 2.3). After the depletion of gypsum and CH, monosulfate starts to generate as shown in Eq. 2.2.



2.2.2 Belite

Hydration reaction of belite in CSA cement has been reported to be slightly different from that in the OPC cement (García-Maté *et al.*, 2012; Scrivener *et*

al., 2004). Belite hydrates at a much slower rate in the ordinary OPC pastes (Eq. 2.4), usually consuming 30% in the first 28 days and 90% after one year. However it exerts an irreplaceable role in improving cement strength at later ages.



In the pure CSA cement systems, crystalline calcium hydroxide produced from the relatively slow hydration of belite (Eq. 2.4) is soon consumed by calcium sulfoaluminate, with continuous formation of ettringite (see Eq. 2.3). On the other hand, belite becomes reactive with the remnants of aluminium hydroxide gel hydrated from calcium sulfoaluminate, leaving the formation of stratlingite C_2ASH_8 (Telesca *et al.*, 2014) (Eq. 2.5).



2.3 Durability

2.3.1 Carbonation

Concerns have been proposed for the poor carbonation resistant capacity of hydrated CSA-based materials due to the predominant presence of ettringite (Quillin, 2001). Mortars made by CSA cement with different w/c ratios and curing regimes have been studied (Mechling *et al.*, 2013). The results showed that CSA mortars exhibited greater sensitivity to carbonation relative to the reference Portland cement mortar, particularly at high w/c ratios (i.e. w/c 0.78 and 0.58); but with lower w/c ratios (i.e. of 0.45), comparable carbonation resistant capacities can be observed.

Chapter 2- Literature review on calcium sulfoaluminate cement

In-service examples of CSA based concretes have also been examined by removing samples from service conditions after 10-15 years (Glasser and Zhang, 2001). The investigated samples demonstrated well-performing engineering properties, none of them showed serious signs of fatigue or demands for repair. Carbonation depth tested was almost similar to those OPC concretes, eliminating the concerns that prominent ettringite presence in the matrix may cause detrimental carbonation with ageing.

2.3.2 Corrosion resistance

In terms of the corrosion resistance in steel reinforced CSA-based concrete, controversial opinions still exist. Glasser (Glasser and Zhang, 2001) reported that the embedded steel reinforcement in CSA matrix stayed fresh and passivated after 14 years of service, attributed to its self-desiccation properties which therefore provides less bleeding water available in the vicinity of steel. However, Kalogridis (Kalogridis *et al.*, 2000) reported that the less alkaline pore solution within the CSA concrete exposed the reinforcing steel to a higher corrosion risk, revealed by a more negative potential than those for the OPC samples in half-cell potential measurements. Half-cell potential value for OPC specimens varied between -100 to -300mV during 13 months in 3.5% NaCl solution, whereas it remained at about -500 to -600mV for CSA-based specimen under the same testing condition. The result suggests a higher risk of reinforcement corrosion in CSA-based matrix, particularly at the intermittent exposure to 3.5% NaCl solution, oxygen is able to contact with the reinforcing bars besides a high concentration of Cl⁻ in the vicinity of steel. The ingress of

Chapter 2- Literature review on calcium sulfoaluminate cement

detrimental Cl^- and oxygen, together with the low alkalinity in the pore solution, may consequently destroy the passivation of reinforcement and fail to protect steel from corrosion any more.

Studies on the mortars made by pure CSA cement (Janotka *et al.*, 2002; Janotka and Krajci, 1999; Janotka *et al.*, 2003) showed that steel embedded in CSA matrix had lost their passivation after 90 days of wet curing, suggested by a potential dynamic curve. In contrary, blended CSA cement with an addition of 15 wt.% OPC provided a considerable desirable environment for the steel reinforcement to stay passive, comparable to the reference OPC concretes (Janotka *et al.*, 2002; Janotka *et al.*, 2003).

Chapter 3- Literature review on GRC composites

Degradation mechanism of GRC composites made by OPC is discussed in this chapter; also the microstructural reasons at the interface and interfilamentary space are discovered. Accelerated ageing for the durability study of GRC is discussed. Improvement of GRC by modifying matrix (e.g. pozzolanas and CSA cement) is also summarised. At the end, evolution at the interface between glass fibre and cement on the durability (e.g. bonding strength and failure mode) is discussed.

3.1 Introduction

A prominent weakness of cement paste is its brittle behaviour with a low tensile strength and poor resistance to crack initiation and propagation (Brandt, 2008; Majumdar and Laws, 1991), as shown in Table 3.1.1. The concept of combining cementitious materials with dispersed reinforcing fibres dates back to about 1900, and at that time the development of asbestos cement obtained extensive success. It was originally expected to improve the brittle performance of cement pastes by providing post-peak toughness and bridging the crack opening and propagation. However, health concerns on the carcinogenic hazard of asbestos were reported soon and this terminated the engineering applications of asbestos cement in most developed countries (Hughes and Weill, 1991; Coutts, 2005; Pacheco-Torgal and Jalali, 2011). Afterwards a level of interest was sustained to find out alternative fibres for cement reinforcement; different types of fibres have

Chapter 3- Literature review on GRC composites

been investigated, e.g. natural fibres, carbon fibres, glass fibres, steel fibres and synthetic fibres.

Table 3.1.1 Properties of hardened cement paste, from reference (Majumdar and Laws, 1991)

Elastic modulus (GPa)	7-28
Compressive strength (MPa)	14-140
Tensile strength (MPa)	1.4-7
Modulus of rupture (MPa)	2.8-14
Tensile failure strain (%)	0.02-0.06
Poisson ratio	0.23-0.30
Thermal expansion (per °C × 10 ⁶)	12-20
Volume shrinkage on drying (%)	0.2-0.3
Density (mg/m ³)	1.7-2.2

Glass fibre reinforced composite (GRC) is a versatile construction material that has been widely used in engineering over the last four decades. It is normally made in the form of thin sheet and is particularly suited on many semi-structural applications e.g. architectural cladding panels, roofing, permanent formwork, floor surfaces and façade renovation (Majumdar and Laws, 1991; Pera and Ambroise, 2004; Enfedaque *et al.*, 2011).

To make the composite, small amounts of chopped glass fibres (usually $V_f \sim 5\%$) are incorporated as rovings of up to 64 strands and each strand is normally made up of ~200 filaments with a standard diameter of ~14 μm . Different production methods have been developed for the manufacture of fibre reinforced concrete, i.e. pre-mix, spray-up, automated process or in the knitted fabric form. The addition of glass fibre strands is designed to imbue

Chapter 3- Literature review on GRC composites

the composite with toughness and enhance its brittle behaviour by post-peak toughness and enhanced failure strain. Typical mechanical performances of normal GRC composites is summarised in Table 3.1.2. It shows that the tensile strength of GRC has been improved to 8-18MPa, compared to an averaged value of 1.4-7MPa for cement pastes (Table 3.1.1). Considerably enhanced strain to failure value of 0.8-1.7% reflects a much more ductile and flexible behaviour of this cementitious material with the reinforcement of glass fibres. It is essential to understand the potential factors affecting the mechanical performances of GRC composites prior to any specific materials design. Cement matrix formulations, curing and service conditions, plus type and volume of glass fibre reinforcements (e.g. fibre content, fibre length and orientation) are all significantly relevant to the macro-performances of GRC to various degrees.

Table 3.1.2 Typical properties of unaged GRC composites

Property	Range
Tensile strength, MPa	8-18
Flexural strength, MPa	12-50
Initial modulus, GPa	8-25
Post-cracking modulus, GPa	0.6-1.0
Strain to failure, %	0.8-1.7

3.2 Historical

The first systematic research on GRC composites was launched by Biryukovich and his colleagues in former USSR in 1964, using low-alkali cements and the reinforcement of E-glass (Majumdar and Laws, 1991; Biryukovich and Yu, 1964). It was particularly designed for electrical

Chapter 3- Literature review on GRC composites

insulation. However, E-glass showed severe chemical corrosion in the highly alkaline Portland cement solution over time (Brandt, 2008) and thus special glass fibres with greater degree of alkaline resistance than that of borosilicate E-glass was required in order to apply GRC in engineering.

Further project was undertaken by Majumdar and Ryder in 1966 at Building Research Establishment (BRE) and the preliminary results showed that several glass compositions, particularly those based on a $\text{Na}_2\text{O-SiO}_2\text{-ZrO}_2$ system exhibited sufficient potential capability of alkaline resistance for an advanced GRC system (Biryukovich and Yu, 1964). Based on this work, first commercial AR fibres containing about 16% zirconia were produced by Pilkington Brothers PLC in collaboration with the National Research Development Corporation and BRE in 1971, trademarked as Cem-FIL. This was a breakthrough, marking the beginning of the GRC industry. With the advent of AR glass fibres, interest in GRC as a new generation of construction material was immediate and it soon reached extensive applications in engineering. Chemical comparison of AR glass fibre and E-glass was summarised by Majumdar (Majumdar and Laws, 1991) as shown in Table 3.2.1. Significant reduced amount of Al_2O_3 and CaO can be observed in commercial Cem-FIL, which is also renewed by the addition of 16.7% ZrO_2 and minor amounts of TiO_2 .

Table 3.2.1 Chemical compositions of various glass fibres (wt.%) from reference (Majumdar and Laws, 1991)

	SiO_2	ZrO_2	TiO_2	Al_2O_3	B_2O_3	CaO	MgO	Na_2O	K_2O	F_2
E-glass	54.0	–	–	15.0	7.0	22.0	0.5	0.3	0.8	0.3
Cem-FIL	62.0	16.7	0.1	0.8	–	5.6	–	14.8	–	–

Chapter 3- Literature review on GRC composites

However, detrimental degradation still occurs in aged GRC composites reinforced by AR glass fibre, without totally eliminating the tendency of considerable reduction in tensile strength and ductility as service time develops (Butler *et al.*, 2010; Nourredine, 2011). Therefore attempts continued to produce much more alkali resistant glass fibres, which are expected to offer better chemical compatibility with alkaline cement matrix in the long term. Development of surface treatment of fibres by the incorporation of polyhydroxy-phenols consequently leads to the commercial production of second generation of AR glass fibre, e.g. Cem-FIL2 AR glass fibres. This coating is gradually released into the alkaline matrix around the glass fibres, not only reducing the possibility of glass/cement reaction to a significant degree, but may also modify the hydration products near fibre surfaces (Bentur *et al.*, 1985; Majumdar and Laws, 1991). Majumdar (Majumdar and Laws, 1991) compared the mechanical performances of GRC made from Cem-FIL and Cem-FIL2 respectively. The results showed considerable improvements in GRC performance using Cem-FIL2 under natural weathering at BRE, and it still retained most of the initial strength and toughness after at least 9 years of natural weathering. Detailed information is shown in Table 3.2.2.

Chapter 3- Literature review on GRC composites

Table 3.2.2 Comparison of mechanical properties of GRC composites reinforced by both Cem-FIL and Cem-FIL 2 under natural weathering at BRS, from reference (Majumdar and Laws, 1991)

Age	Cem-FIL 2/OPC GRC						Cem-FIL/OPC GRC					
	MOR ¹	LOP ²	IS ³	UTS ⁴	E ⁵	FS ⁶	MOR ¹	LOP ²	IS ³	UTS ⁴	E ⁵	FS ⁶
180d	-	-	-	-	-	-	35	17	18	13	38	5500
1y	-	-	-	-	-	-	31	16	12	10	38	-
2y	36	11	20	13	39	8000	28	18	8	10	37	430
4y	33	15	14	13	36	7310	22	15	5	8	41	240
9y	30	14	13	11	44	4710	18	16	6	6	39	160

Note: Matrix formulations are 70 wt.% OPC and 30 wt.% sand

¹ Modulus of rupture, unit in MPa; ² Limit of proportionality, unit in MPa; ³ impact strength, unit in kJ/m²; ⁴ ultimate tensile strength, unit in MPa; ⁵ elastic modulus, unit in GPa; ⁶ failure strain, unit in microstrain.

3.3 Theoretical mechanism of GRC composite

Fig. 3.3.1 shows an idealized stress-strain curve for theoretical 2-D reinforced composite (with sufficient glass fibre reinforcement) and the curve is clearly divided into four regions:

In the pre-cracking region (region I), tensile behaviour of young GRC composites demonstrates a linear elastic relationship in the stress-strain curve, where both cement matrix and fibres are performing together in a normal composite manner. The composite modulus E_c can be calculated based on the mixture rule:

Chapter 3- Literature review on GRC composites

$$E_c = E_m V_m + \eta E_f V_f$$

E_m and E_f is the modulus of matrix and fibre respectively. Efficiency factor η ($0 < \eta < 1$) is generally applied in composites where fibres are short and not aligned with the direction of stress. The mostly widespread manufacture process (i.e. spray-up method) distributes short fibres in a random way. For composites with a 2-D random fibre layout, η is calculated to be 0.375; with a random 3-D fibre alignment, η is 0.2 (Purnell, 2007).

Region II refers to the multiple cracking region. After reaching the limit of proportionality (LOP) point, stress increases at a decreased rate and composites behave as less stiff materials. This acts as a transitional process to transfer load from matrix to fibre progressively due to the development of series of multiple cracks within the matrix. A corresponding serrated curve is displayed in the stress strain curve because stress increases if one crack is arrested and strength decrease would occur if the crack propagates.

In the following post-cracking region (region III), stress continues to increase linearly at an extremely slow rate with a growing elongation while the visible crack keeps opening. Glass fibre strands are carrying the load alone in this single process during the pull-out procedure, and thus the cracks are bridging by the fibres to some extent to prevent further propagation.

Region IV – the post-peak region – is a process when the maximum stress capacity of the composite has been exceeded before subsequent catastrophic failure occurs.

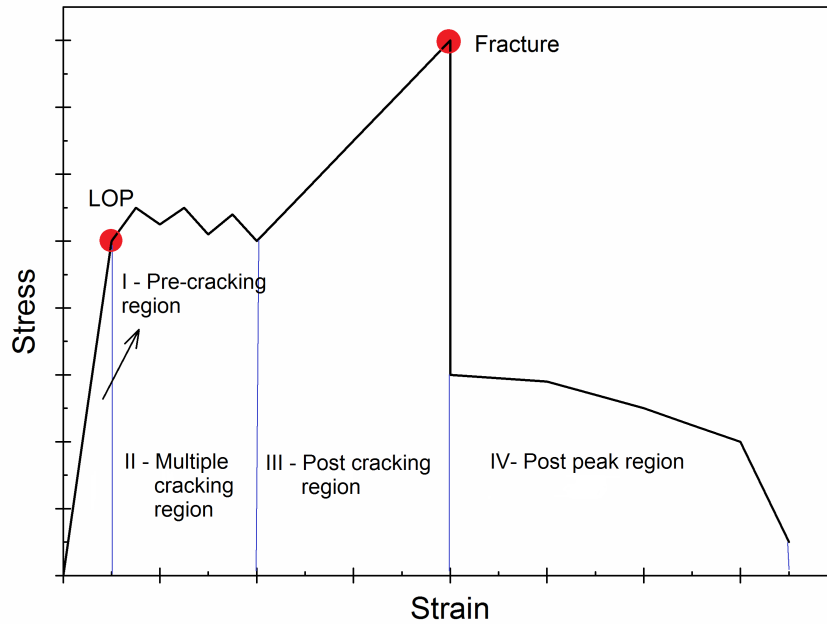


Figure 3.3.1 Typical stress-strain curve for GRC composite reinforced by short fibres with high fibre content ($V_f > V_{f,crit}$, $l \leq l_c$), from reference (Purnell, 2007)

3.4 Durability

Long-term durability of GRC composites has been a major concern in limiting the widespread application of this versatile material. GRC made by normal Portland cement demonstrates significant reductions in both tensile strength and ductility as time develops, particularly under humid environments (Butler *et al.*, 2009a; Orłowsky and Raupach, 2008; Peled *et al.*, 2005; Enfedaque *et al.*, 2012). The long-term properties of a typical spray-dewatered GRC composite reinforced by 5 wt.% Cem-FIL AR glass fibres are shown in Table 3.4.1, summarised from data in literature (Majumdar and Laws, 1991). Those investigated GRC composites have exhibited tensile strength reductions from 14-17MPa at 28 days to as little as 4-7MPa gradually after 17 years UK weathering. The corresponding bending

Chapter 3- Literature review on GRC composites

strength at early age is within a range of 35-50MPa but a residual value of only 13-18MPa is observed after ageing for 17 years.

Table 3.4.1 Examples of the measured strength properties of spray-dewatered OPC/GRC reinforced by 5 wt.% Cem-FIL AR glass fibre) with ageing, from reference (Majumdar and Laws, 1991)

Age	28d	1y	5y	10y	17y
Tensile strength (MPa)	14-17	11-14	7-8	7-8	4-7
Bending strength (MPa)	35-50	30-36	21-23	15-19	13-18
Failure strain (%)	1	0.5	0.05	-	-
Young's modulus (GPa)	20-25	20-25	25-32	27-30	25-36
Impact strength (kJ/m ²)	17-31	13-16	4-7	2-6	2-5

3.4.1 Mechanisms

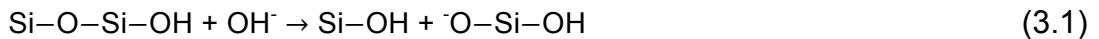
Mechanisms underlying the degradation process of GRC composites are still under debate, but it is generally considered to associate with fibre corrosion by the alkalinity attack from the matrix (Orlowsky *et al.*, 2005; Orlowsky and Raupach, 2006; Cuypers *et al.*, 2006; Cohen and Peled, 2012) and/or loss of fibre flexibility by the CH precipitation within and around glass fibre strands (Bentur, 1985; Orlowsky *et al.*, 2005; Cohen and Peled, 2012; Butler *et al.*, 2010).

Besides this, static fatigue of the embedded glass fibres under sustained load in the highly alkaline environment is also reported to have an influence on the ageing of GRC composites (Michalske and Freiman, 1983; Purnell *et al.*, 2001; Purnell and Beddows, 2005; Orlowsky *et al.*, 2005; Orlowsky and Raupach, 2006; Orlowsky and Raupach, 2008).

Chapter 3- Literature review on GRC composites

3.4.1.1 Fibre corrosion

Inorganic silicate glasses are not intrinsically immune to alkali attack in the alkaline pore solution of Portland cement matrix. Its main structure (silicon-oxygen-silicon network) can be destroyed by the hydroxyl ions (see Eq. 3.1), leading to significant fibre structure breakdown.



With the addition of 16-20 wt.% ZrO_2 in AR glass fibres, this destructive reaction is supposed to be suppressed to some degree as Zr-O bonds are more alkaline resistant than the Si-O in alkaline solutions (Paul, 1977; Butler *et al.*, 2010). Despite of this improvement, AR glass fibres embedded in the alkaline cementitious matrix are still reported to suffer from considerable chemical attack with ageing (Nourredine, 2011; Hempel and Butler, 2007; Butler *et al.*, 2010; Enfedaque *et al.*, 2012). Such corrosion can be delayed effectively by the application of organic polymer sizes on fibre surface. This leads to the advent of the second generation of AR glass fibres, which is a breakthrough in GRC industry (Gao *et al.*, 2004; Liu *et al.*, 2011; Gao *et al.*, 2007; Butler *et al.*, 2010).

3.4.1.2 Matrix densification and interfilamentary precipitation

For the newly made GRC, the interface between fibre and cement tends to be much more porous than that in the surrounding matrix (Bentur and Mindess, 1990; Cohen and Peled, 2010). This is beneficial for the composite overall in subject of improved toughness properties, as cracks travelling through the brittle matrix are prone to be diverted along the porous interfacial zone rather than propagate further through the glass fibres (Barhum and

Chapter 3- Literature review on GRC composites

Mechtcherine, 2013). Besides this, spaces between fibres also remain almost empty at early age, as penetrated hydrated matrix and/or hydration products are absent at this stage (Bentur *et al.*, 1985; Bentur, 2000). This guarantees a considerably flexible fibre behaviour, which helps to adjust or re-distribute their locations in a rope-like manner when forces apply, which favourably adds a magnitude of post-peak toughness to the composite material.

With the progress of hydration process, solid hydration phases (predominantly crystalline CH) tend to densify the interfilamentary spaces (Majumdar and Laws, 1991; Proctor *et al.*, 1982; Cohen and Peled, 2010). A consequence of this is the increase in bond strength between filaments, resulting in a rather rigid and integrated composite structure. It leads to catastrophic losses of flexibility and glass fibres fails to fulfil its original expectations to imbue toughness to the composite, changing failure mode gradually from fibre pull-out to fibre breakdown (Bartos and Zhu, 1996; Bentur, 1985; Yilmaz and Glasser, 1991; Glinicki and Brandt, 2007).

Formation of hydration products (particularly CH) also directed towards the interfacial zone and fills most of the empty spaces in the region. This increases the bond strength between fibres and cement matrix and forms an intimate contact layer at the interface (Zhu and Bartos, 1997; Glinicki and Brandt, 2007; Cohen and Peled, 2010). Therefore propagation of cracks tends to be more likely to become sporadic as ageing continues and resultantly increases the possibility of crack growth through glass fibres, thus limiting the bridging capacities of fibres to a significant degree.

Chapter 3- Literature review on GRC composites

Incorporation of nano-particle fillers (i.e. silica fume particle or polystyrene-based polymers) between fibre filament has been indicated as an efficient way to reduce the matrix penetrability problem (Cohen and Peled, 2010; Cohen and Peled, 2012). The magnitude of efficiency is highly dependent on the type, structure and properties of the filler.

3.4.2 Accelerated ageing

The introduction of any novel construction material in industry requires a pre-investigated knowledge on its long-term durability performances before a widespread adoption could occur. However, it is time-consuming to expose the tested specimens under natural weathering for expected long time period before any statistical data can be achieved.

Accelerated ageing mechanism is then introduced, by immersion of investigated GRC specimens in hot water at elevated temperatures (typically over 50°C) for different periods to induce ageing thermally. Hot water accelerated ageing technique exhibits full potential for the estimation of time-dependent behaviour of GRC composites by a variety of accelerated ageing models proposed in literature (Purnell *et al.*, 2001; Litherland, 1981; Van Itterbeeck *et al.*, 2009; Purnell *et al.*, 2008; Van Itterbeeck *et al.*, 2012; Purnell *et al.*, 1999). Accelerated ageing tests make it possible to correlate shorter periods of accelerated ageing (at specified accelerated temperature) with longer periods of in-service weathering in a quantitative relationship.

Proctor and his colleagues (Proctor *et al.*, 1982; Litherland, 1981) first developed an accelerated ageing model in the late 1970s, by using OPC matrices reinforced by the first generation AR glass fibres. In the study, a

Chapter 3- Literature review on GRC composites

small block of cement reinforced by a single glass fibre strand was cast (see Fig. 3.4.1 below) and specimen was cured at room temperature in the first 24h prior to be immersed under elevated temperatures. After specified ageing periods, direct tensile strength of the embedded fibre strand was measured and the original results are shown in Fig. 3.4.2.

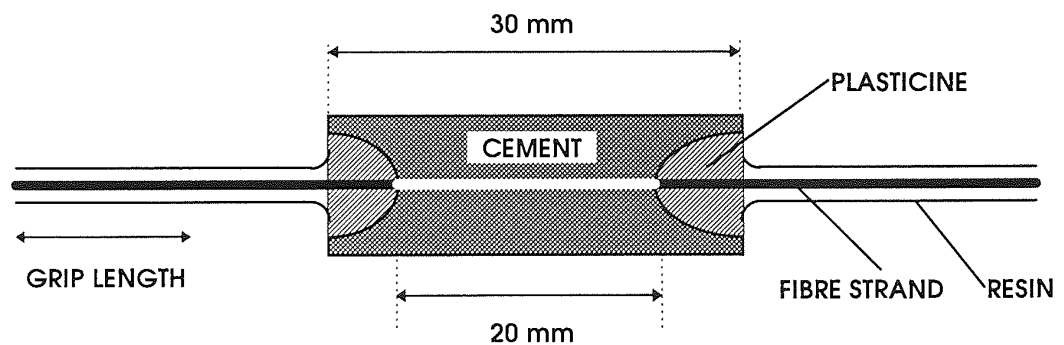


Figure 3.4.1 Illustration of strand-in-cement tensile specimen test

Accelerated ageing model proposed by Litherland (Litherland, 1981) was based on the assumptions that (a) chemical reaction between glass and cement is directly relative to the rate of loss in the glass fibre strength, (b) time taken for the SIC strength to fall to any given value σ_{sic} can be regarded as an inverse measure of the rate of strength loss, and (c) GRC composite strength is dependent on fibre volume, $\sigma_c = \sigma_f V_f$. It was assumed that there was an Arrhenius relationship between strength reduction with ageing time and the ageing temperature, as shown in Fig. 3.4.3, which corresponded to activation energy of $\sim 90\text{kJ/mol}$. The temperature coefficient given in Fig. 3.4.3 can be applied for making quantitative predictions using time transpositions. Therefore it can be suggested that under UK weathering:

1 day at 50°C in water = 101 days in natural weather

Chapter 3- Literature review on GRC composites

1 day at 60°C in water = 272 days in natural weather

1 day at 70°C in water = 693 days in natural weather

1 day at 80°C in water = 1672 days in natural weather

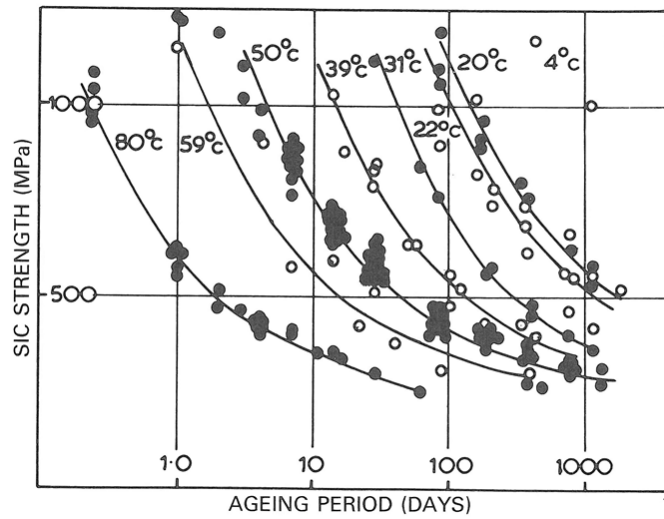


Figure 3.4.2 SIC strength retention in water at various temperatures, from reference (Litherland, 1981)

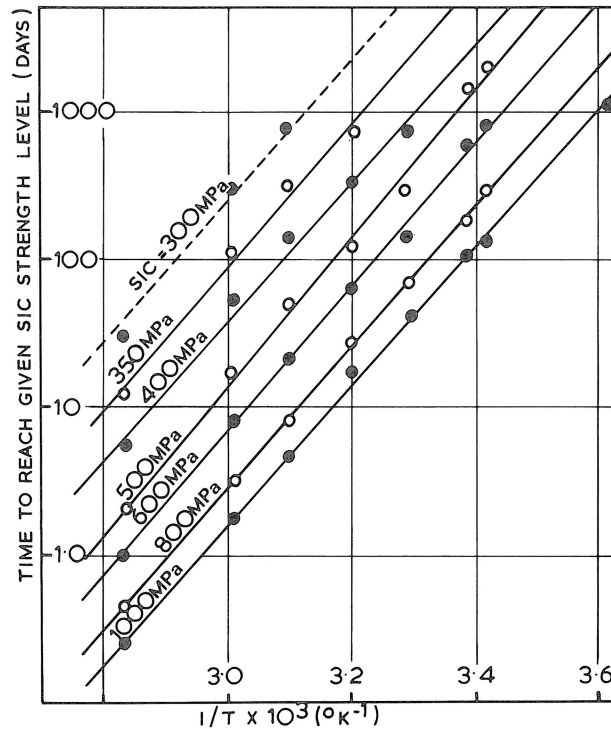


Figure 3.4.3 Arrhenius graphs from SIC tests, from reference (Litherland, 1981)

However, with the introduction of second generation AR glass fibres as well as the development of various modified matrix formulations by non-Portland cement matrix (e.g. calcium sulfoaluminate cement) and/or Pozzolanic materials, long-term ageing characteristics of those modified composites may differ from the composites made by Cem-FIL used in the Litherland's ageing model (Litherland, 1981). Therefore the accelerated ageing model suggested by Litherland may not be applicable to these new materials and further modification is necessary. It was found that Cem-FIL2 composites had the same acceleration factors as the original composite made by Cem-FIL (Proctor *et al.*, 1982).

Purnell (Purnell *et al.*, 2001; Purnell *et al.*, 2008; Purnell and Beddows, 2005) proposed a new static fatigue model to explain the losses in strength

Chapter 3- Literature review on GRC composites

of accelerated aged GRC composites; modified matrix with the addition of metakaolin and calcium sulfoaluminate-based materials were used respectively in the study. It concentrated on the static fatigue caused by the enlargement of fibre flaws on a surface under hydrothermal and mechanical loading, as a substantial degradation mechanism instead of fibre corrosion with ageing. Under this circumstance, strength failure could occur with subtle applied surface stress, which is likely to aggravate the flaw growth. Besides this, weathering temperature and the chemical environment within the matrix (e.g. pH and moisture) also has the potential to deteriorate flaw size, which could result in shrinkage or expansion thermally. GRC modified by Pozzolanic metakaolin and sulfoaluminate cement based materials both showed improved ageing-resistant ability, possessing similar activation energy of 57-59 kJ/mol, lower than that of 94-97 kJ/mol for the OPC matrix.

3.5 Improvement of GRC from matrix modification

Matrix formulations are primary factors controlling the durability properties in GRC systems. Modified matrix by different pozzolanas or non-Portland cement matrix is an advisable solution for producing more durable GRC composites. Pozzolanic additions of metakaolin, pulverised fuel ash (pfa), silica fume or micro silicon, with contents ranging from 10% to as high as 70%, have been reviewed extensively (Sabir *et al.*, 2001; Enfedaque *et al.*, 2010; Enfedaque Diaz *et al.*, 2010; Purnell *et al.*, 1999; Hayashi, 1985; Bartos and Zhu, 1996; Leonard and Bentur, 1984). Non-Portland cement such as calcium aluminate cement (Purnell *et al.*, 2000; Purnell and

Chapter 3- Literature review on GRC composites

Beddows, 2005; Pera and Ambroise, 2004) is a popular subject in GRC studies and encouraging results have been obtained.

3.5.1 GRC from Pozzolanas additives

3.5.1.1 Metakaolin

Potential attention has been drawn for the employment of metakaolin in GRC composites (Purnell *et al.*, 1999; Enfedaque *et al.*, 2010; Enfedaque Diaz *et al.*, 2010; Peled *et al.*, 2005). It is processed from calcination of kaolin clay at moderate temperatures (650-850°C). General agreement has been reached by researchers that 20-25% addition of metakaolin could confer remarkable composite properties improvement under both UK natural weathering and accelerated ageing (Zhu and Bartos, 1997; Enfedaque Diaz *et al.*, 2010; Purnell *et al.*, 1999). This advantageous effect can be attributed to the readily pozzolanic reaction, which helps reduce the CH amount considerably and consequently leads to reduced alkalinity within the pore solution. Regarding to the changes of microstructure at interfaces in the metakaolin-based GRC, Purnell (Purnell *et al.*, 2000) reported the ingress of small amounts of matrix into the interfacial zone at early age. However for the unaged OPC composites, spaces between filaments remain almost vacant at this stage. After ageing for 56 days at normal temperature, a continuous CH layer, intermixed with small amount of carbonate, is formed at the interfacial zone. But the layer does not penetrate into fibre bundles with ageing. In this way fibres could remain flexible and this is beneficial for composite to retain most of the tensile strength and ductility with ageing.

Chapter 3- Literature review on GRC composites

3.5.1.2 GGBS

Using Portland cement matrix with the addition of 20% ground granulated blast furnace slag and with the reinforcement of Cem-FIL AR glass fibres, the modified GRC composites exhibited similar strength retention and durability trends with ageing, as in the case of ordinary GRC composites (Majumdar and Laws, 1991; Purnell, 2007; MUTHUPRIYA, 2013; Butler *et al.*, 2010). Cement matrix with 70% GGBS replacement is less vulnerable for the embedded glass fibres and a large proportion of tensile strength and toughness is retained with time under natural weathering, e.g. ultimate tensile strength is 14MPa after 1 year and a retain of 11MPa is reached after 9 years ageing (Majumdar and Laws, 1991).

3.5.1.3 Silica fume

It has been reported that GRC with up to 20% silica fume addition has a similar initial strength to those without silica fume addition, but this advantage does not maintain with ageing and considerable durability improvement in GRC has not been achieved as expected (Hayashi, 1985; Yilmaz and Glasser, 1991; Marikunte *et al.*, 1997). Similar study by Enfedaque (Enfedaque *et al.*, 2010) revealed an insignificant effect of the 10-20% silica fume addition on the improvement of durability of GRC composites, suggested by tensile test and failure mode from the microstructure of fractures surface; it exhibited gradual breakdown of fibre bundles in hot water accelerated ageing tests for 80 days.

However, if silica fume fillers are incorporated to the glass fibre bundles directly, improved GRC performances can be obtained particularly with relatively larger 200 nm particle (Cohen and Peled, 2010). This improvement

Chapter 3- Literature review on GRC composites

can be attributed to the filling effect of particles in the empty space between filaments and thus contributes to more efficient stress transfer to inner fibre and also limits the available spaces for the penetration and growth of solid hydration products, therefore eliminating the potential fibre corrosion caused by notch effect.

3.5.2 GRC from non-Portland cement

High alumina cement (HAC) and super-sulfated cement (SSC) used to be popular matrix formulations for producing GRC composites with improved performances, which exhibited better retention of properties with ageing than that for those OPC/GRC composites at ambient temperatures (Majumdar and Laws, 1991; Purnell, 2007). However, a deleterious conversion reaction took place in HAC system at high temperatures and high carbonation rate of SSC lead to significant composite strength reductions.

Over the past two decades, extensive investigations has been reached for the study of calcium sulfoaluminate cement as a new non-Portland cement binder, which is expected to produce more advanced GRC composites (Purnell *et al.*, 1999; Purnell and Beddows, 2005; Pera and Ambroise, 2004). Degradation rate of the calcium sulfoaluminate cement-based composites was considerably reduced as suggested by hot water accelerated ageing tests (see Fig. 3.5.1); most of its pseudo-ductility and toughness were retained after 316 days at 50°C, and bridging effect carried out by the glass fibres could still be observed in the curve, although accompanied with a slight tensile strength reduction. For the ordinary GRC reference, the material became very brittle after 28 days.

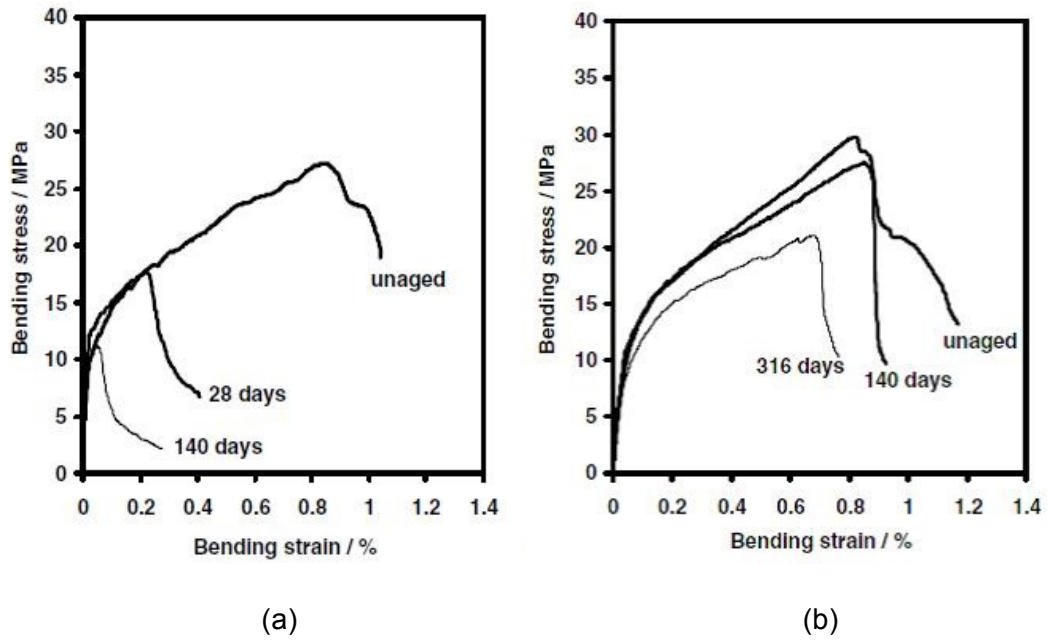


Figure 3.5.1 Stress-strain performance of (a) OPC/GRC and (b) CSA-based GRC composites aged at 50°C, from reference (Purnell and Beddows, 2005)

The significantly improved durability benefits of GRC composites modified by calcium sulfoaluminate-based materials have been attributed to its low alkalinity in pore solution with a pH value lies between 10 and 11.5, which provides a less aggressive chemical environment for the embedded glass fibre bundles. And more importantly it is because of the absent of CH formation during hydration, thus reduces the possibility of severe bundle filling and notching effect on the filament surface (Purnell *et al.*, 2000; Purnell and Beddows, 2005; Zhou *et al.*, 2006).

3.6 Role of interface

The role of the glass/cement interface, particularly its microstructural evolution and chemical development as service life increases, has been considered to be of vital importance in controlling the mechanical behaviours of GRC composites (Hempel and Butler, 2007; Butler *et al.*, 2010).

Chapter 3- Literature review on GRC composites

Severe densification at the fibre/cement interface with the infill of progressively formed hydration products, particularly under moist, can lead to enhanced bond strength (Katz and Bentur, 1996; Bentur, 2000; Hempel *et al.*, 2007; Butler *et al.*, 2010). As a result of this densification, filament becomes less flexible and increases the stress transfer from the bulk matrix to the fibre bundle (Cohen and Peled, 2010), thus limiting the favourable energy dissipation through the porous interfacial region when matrix cracks propagate.

Moreover, precipitation and growth of massive hydration, particularly large crystalline CH plates, were reported to gradually penetrate into bundles as time develops (Cohen and Peled, 2010; Cohen and Peled, 2012; Butler *et al.*, 2010). These penetrated phases significantly increase the bond between filaments and reduces the flexibility of fibre bundles accordingly. Thus sliding between filaments is restricted to great extent if stress is transferred from the matrix to the bundle (Butler *et al.*, 2010), leading to detrimental fibre breakdown. On the other hand, adherence and growth of the solid hydration products on the filament surface, i.e. dominant crystalline CH, can lead to pronounced notching effect of the filaments (Butler *et al.*, 2010; Cohen and Peled, 2010; Yilmaz and Glasser, 1991). Consequence of this local stress concentration is the reduction in fibre tensile strength and composite behaviour may change from ductile to brittle (Cohen and Peled, 2010).

Therefore, evolution of the microstructure at the interface between fibre and cement with ageing is a very important aspect in deciding the bond strength between them and the failure mode of reinforcements; both of which are intrinsically responsible for the durability and mechanical performances of

GRC composites. As a consequence, it is necessary to investigate into the microstructural changes at this interfacial region in the long term, which can be correlated to the composite mechanical performances prior to a full knowledge on the degradation mechanisms of aged GRC composites can be achieved.

3.7 Discussion

Long-term performances of the composites can be predicted in consideration of a compromise between time factor and the side effect that higher curing temperature could bring for the intrinsic nature of the hydrated matrix. Accelerated ageing tests may not only simply accelerate the fibre/cement hydration as expected, but can also have a substantial influence on the intrinsic nature of hydrated matrix to some extent (e.g. different hydration products may form with elevated ageing temperature), which is a key factor deciding the degradation mechanism; different mechanisms may apply at high temperatures, limiting the usefulness of the procedure (Purnell and Beddows, 2005). This could lead to overestimations or underestimations on the durability properties of those investigated GRC composites (Purnell *et al.*, 1999). Debate is still under discussion on whether hot water accelerated ageing test is valid for the durability studies of GRC composites, but it is generally accepted that this is useful in comparing the time-dependent behaviours of GRC made by different modified matrices. In addition, an alternative accelerated ageing method, i.e. combining freeze-thaw cycles and wet-dry cycles, is also proposed for durability studies of GRC composites (Enfedaque *et al.*, 2012).

Chapter 3- Literature review on GRC composites

Due to a lack of consensus on the validation of hot water accelerated ageing tests, long-term durability and mechanical performance data of aged GRC composites under normal weathering temperature is thus extremely valuable in the process of understanding the real degradation process of GRC composites.

Chapter 4- Literature review on interfaces in steel reinforced concrete

This chapter mainly concentrates on the nature of the interface between steel and concrete in steel reinforced OPC concrete, which is significantly relevant to corrosion resistance capacity. Major achievements for imaging analysis technique in literature is summarised for quantitative analysis at the interface.

4.1 Introduction

Reinforcement corrosion is one of the main causes of deterioration of reinforced concrete structures, arising as a worldwide concern in the construction industry. Among the parameters, the nature of the interface between steel and concrete has been considered to play an important role in governing the corrosion resistance of embedded reinforcements. It is particularly linked to the buffering action of solid hydration products precipitated in the vicinity of reinforcement and the formation of water-filled voids at the interface (Castel *et al.*, 2003; Nasser *et al.*, 2010; Zhang *et al.*, 2011).

In general, steel reinforcement embedded in concrete is protected by a thin film of passivating iron oxide adhered on its surface, which can be attributed to the high alkalinity in Portland cement pore solution. However, progressive carbonation of hydration phases is likely to cause a localised pH reduction at the steel/concrete interface, increasing the possibility of passive layer breakdown. Chloride-induced attack is another mechanism associated with

Chapter 4- Literature review on interfaces in steel reinforced concrete

reinforcement corrosion; chlorides act as a catalyst to corrosion once there is sufficient chloride concentration at the rebar surface to disrupt the passive layer (Medeiros and Helene, 2009). It has been pointed out that in order to maintain the passive state of embedded steel in concretes, a pore solution pH value above 8.5 is necessary (Glass *et al.*, 2000).

If corrosion initiates, the growth of corrosion products at the steel/concrete interface is prone to exert substantial internal stress on the surrounding concrete, therefore may lead to deleterious volume expansion and subsequent cracking, spalling as well as potential loss of structure integrity. This eventually facilitates the build-up of multiple connected channels for the further movement of detrimental Cl^- , O^{2-} and CO_3^{2-} ions in aqueous solutions (Cabrera, 1996; Koleva *et al.*, 2006; Amleh and Ghosh, 2006), thus aggravating the reinforcement corrosion process. As well as causing internal stress, corrosion may disrupt the bond between steel and concrete. Effects of corrosion level on the bond strength have also been studied, with a general conclusion that rapid decrease of bond strength occurs with an increased level of corrosion (Fang *et al.*, 2004; Cabrera, 1996; Vidal *et al.*, 2007).

4.2 Reinforcement corrosion

The main mechanisms underlying the breakdown of passivity on steel surface can be attributed to two aspects:

- Introduction of chloride ions
- Depletion of alkalinity in pore solution due to carbonation

4.2.1 Chloride-induced corrosion

Introduction of chloride ions into concrete is either from mix contaminants or from external environments, such as seawater or de-icing salts. The minimum chloride concentration value (or called chloride threshold level) necessary to breakdown the local film is usually presented as a ratio of chloride to hydroxyl ions, free chloride content, or percentage of total chloride relative to weight of cement (Ann and Song, 2007).

Assessment of chloride threshold value is an important step to predict the serviceability of reinforced concrete. However, previous studies indicated a significant discrepancy of chloride threshold level ranging from 0.2% to 2.5%, expressed as free chloride content (Alonso *et al.*, 2001; Alonso *et al.*, 2000; Mohammed and Hamada, 2001; Alonso and Sanchez, 2009; Zhang *et al.*, 2011). This large variability of chloride threshold level from different authors (0.2-2.5%) can be attributed to the variances in parameters applied in different experimental work, e.g. type and content of cement, type of steel, experimental exposure conditions, corrosion initiation assessment methods, the form used to represent CTL and the condition of the steel/concrete interface etc. (Alonso and Sanchez, 2009).

In the case of chloride ingress, a proportion of the chloride ions react with cement paste, generating the formation of chloro-aluminate complexes, e.g. $3\text{CaO} \cdot \text{Al}_2\text{O}_3 \cdot \text{CaCl}_2 \cdot 10\text{H}_2\text{O}$ (Friedel's salt). Accumulation of corrosion products in the vicinity of reinforcement can cause spalling or cracking in the concrete, which in turn facilitates the transportation and ingress of chloride, moisture and oxygen towards the rebar and therefore aggravates the reinforcement corrosion (Shi *et al.*, 2012; Glasser *et al.*, 2008). The

Chapter 4- Literature review on interfaces in steel reinforced concrete

remaining chloride ions remain in the pore solution as free chloride, which may gradually permeate towards the reinforcement through porosity structure and initiate subsequent reinforcement corrosion.

4.2.2 Corrosion by carbonation

Carbonation of the alkaline constituents in cement owing to reaction with atmospheric carbon dioxide can lead to significant local pH reduction in the pore solution to a near-neutral level, which may result in insufficient alkalinity at the interface to maintain the passive film and then cause steel corrosion to initiate (Page, 2007; Anstice *et al.*, 2005). Natural atmospheric carbonation is a very slow process but for aged structures, carbonation-induced reinforcement corrosion can become an important cause for serviceability failures.

A secondary effect of carbonation on corrosion activation is that it can lead to the release of bound chloride ions progressively into the pore solution by dissolution of Friedel's salt (Suryavanshi and Narayan Swamy, 1996; Csizmadia *et al.*, 2001; Page, 2007; Saillio *et al.*, 2014). This in turn aggravates the corrosion to some extent. When the amount of free chloride ions are at above the chloride threshold level, depassivation of reinforcement and severe pitting corrosion may occur even under the condition of high alkaline pore solution.

4.3 The role of steel/concrete interface

The nature of steel/concrete interface plays an important role in influencing the overall performance and durability of reinforced concretes, particularly

Chapter 4- Literature review on interfaces in steel reinforced concrete

the resistance of embedded reinforcement to depassivation under chloride ingress (Castel *et al.*, 2003; Soylev and Francois, 2003; Page, 2009; Neff *et al.*, 2011; Zhang *et al.*, 2011; Horne *et al.*, 2007). For example, a high-quality steel/concrete interface reduces the risk of corrosion initiation and may restrict the corrosion rate after the onset of corrosion.

A systematic correlation has been investigated between the quality of steel/concrete interface and the potential corrosion rate of the embedded reinforcements, on both macroscopic and microscopic levels (Yonezawa *et al.*, 1988; Glass *et al.*, 2000; Vidal *et al.*, 2007; Angst *et al.*, 2009; Soylev and Francois, 2003). It was found that the corrosion rate of reinforcement was prone to increase if, in the vicinity of the steel, there was considerable presence of air voids (Glass *et al.*, 2001; Nasser *et al.*, 2010; Horne *et al.*, 2007), by providing enhanced availability of oxygen to support the cathodic oxygen reduction reaction. On the other hand, the interfacial influence on corrosion is also linked to the formation of solid hydration phases on the steel surface, predominantly the crystalline CH, which can supply a buffering effect to help retain a high alkalinity in the pore solution, thus is useful to maintain the passive state of reinforcement (Pourbaix, 1974; Nasser *et al.*, 2010).

Therefore, it is of vital importance to investigate both the microstructural and compositional nature of the steel/concrete interface, before better-performed and more durable steel reinforced concretes can be created.

4.4 Microstructure at steel/concrete interface

Early research on steel/concrete interface was pioneered by Page (Page, 1975). The study aimed to characterize the topographical morphology at the steel/concrete interface. Fractured surfaces of reinforced concrete were reviewed by SEM using secondary electron imaging mode. Results generally concluded that the metal was in contact with a CH rich layer, and much more CH was located at the interfacial zone than that in the bulk concrete. This insoluble CH layer has led to a general assumption of enhanced pH buffering capacity at the interface, which is able to protect the reinforcement from corrosion for longer periods. A updated description of CH rich layer was soon proposed (Alkhalaf and Page, 1979), stating that SEM results showed a non-continuous CH layer with variable thickness on mild steel surfaces, also with inclusions of C-S-H gel that were finely intermixed with the crystalline CH deposits.

Similar conclusions were reached by studying the fractured surfaces on ordinary Portland concrete reinforced by stainless steel wire (Pinchin and Tabor, 1978). The obtained results revealed CH-enriched interfacial zone after curing for 7 days, and microstructure at the steel/cement interface seemed to change very little afterwards. X-ray diffraction analysis was undertaken to quantify the concentrations of CH within a distance of 10 μ m away from the wire surface. As expected, an increased amount of CH concentration was found in the vicinity of steel, 20-40% higher CH concentration than that in the bulk matrix.

Efforts continued towards elucidating more profound knowledge on the microstructural characteristics at the steel/concrete interface as well as the

Chapter 4- Literature review on interfaces in steel reinforced concrete

chemical compositions at the region. It was found that large amounts of CH and ettringite co-existed at the interface between steel and ordinary Portland cement paste at early age, according to X-ray diffraction analysis (Li and Hu, 2001). This was explained by the water film formed on steel surface at early age, which was caused by the inner bleeding of cement pastes owing to the wall effect of reinforcement. And shrinkage of the hydrated cement paste away from the steel was able to provide much more space for the rapid diffusion of chemical ions, such as Ca^{2+} , SO_4^{2-} and Al^{3+} , towards the interfacial zone. Once these ions reached the oversaturation conditions, they would crystalize and grow to form large crystals. Further EDX analysis presented a generalized local chemical composition at the interface (Table 4.4.1); it demonstrated a dominance of Ca and Si to be as high as over 80 wt.% and ~10 wt.% respectively for up to 28 days, only with minor precipitation of Al and S.

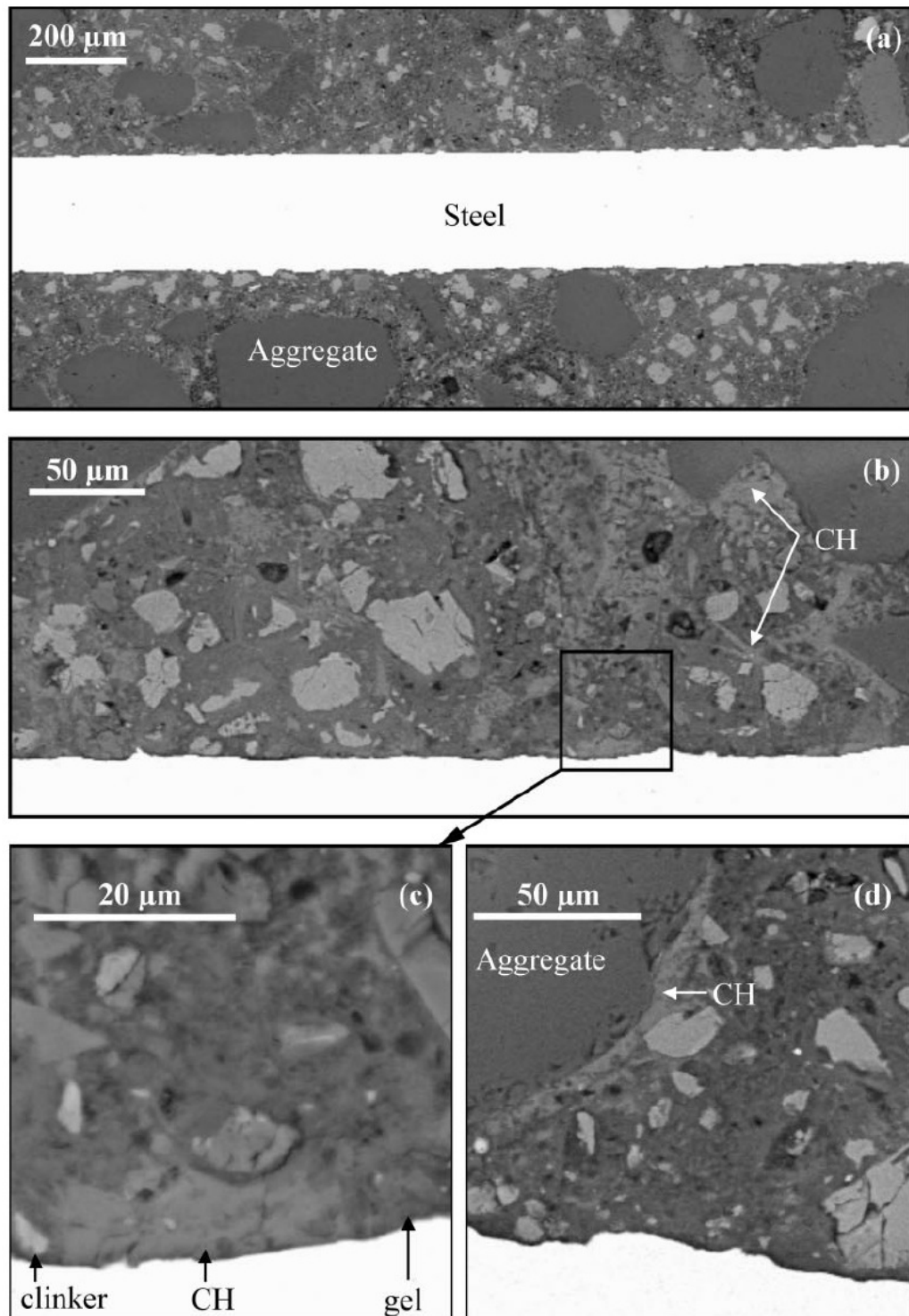
Table 4.4.1 Chemical compositions at the interface between steel disc and ordinary cement paste (wt.%), from reference (Li and Hu, 2001)

	Al	Si	S	Ca
3 days	3.62	13.74	2.23	80.41
28 days	2.96	10.87	2.27	83.90

While the examination of fractured surface on reinforced concrete can be successfully achieved by secondary electron imaging mode, it can only provide qualitative information on the characterization of the interfacial zone, but unable to obtain quantitative chemical analysis at the interface.

Chapter 4- Literature review on interfaces in steel reinforced concrete

A detailed study on backscattered electron images of polished reinforced concretes was conducted by Glass for the first time under low-vacuum conditions (Glass *et al.*, 2001). However, unlike the early lime layer hypothesis proposed, findings in this study showed that CH was often absent from the interfacial zones while unhydrated cement clinker and potential C-S-H gel had been recognised to co-exist with CH at part of the local interfacial region (Fig. 4.4.1). There was no general indication of preferential CH formation at the steel/concrete interface and interfacial zones were highly representative of the bulk matrix chemically.



KEY




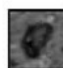
 unhydrated clinker	 CH (with some gel)	 gel (mainly C-S-H)	 pore/void
--	--	--	---

Figure 4.4.1 Microstructure images shown that CH is often absent at the steel/concrete interface, from reference (Glass *et al.*, 2001)

Chapter 4- Literature review on interfaces in steel reinforced concrete

Later research was studied by Horne (Horne *et al.*, 2007) to examine the microstructural features of polished reinforced concretes in respect of many aspects parameters, e.g. different w/c ratios (0.49 and 0.7), steel orientation (horizontal and vertical to the casting direction), state of the steel surfaces (with mill scale and wire-brush cleaned) as well as the hydration age (1 days, 7 days, 28 days and 365 days). It indicated a non-continuous layer of CH build-up in contact with the steel surface (within 5 μ m away from steel) and increased levels of CH and porosity were found to be presented in the vicinity of steel rebar, an order of magnitude higher than that in the matrix (detailed information in section 4.5.3).

4.5 Quantification analysis

4.5.1 Overview

Investigation of the microstructure of concretes by backscattered electron microscopy has become a common technique nowadays; it is a powerful tool for the study of cementitious materials. This technique is able to provide useful information on the porosity (Wong *et al.*, 2006), pore structures (Werner and Lange, 1999) and phase distribution within the cement system. These beneficial advantages lead to extensive studies on developing useful image analysis programs to add quantitative information to the analysis of the interface (Horne *et al.*, 2007; Diamond, 2001; Diamond and Huang, 2001; Glass *et al.*, 2001; Yang and Buenfeld, 2001; Werner and Lange, 1999; Deschner *et al.*, 2013; Stutzman, 2004), which is expected to achieve the following two tasks.

Chapter 4- Literature review on interfaces in steel reinforced concrete

- Phase segmentation by morphological features and/or arithmetic process
- Quantitative measurements on the area fraction of each segmented phase

4.5.2 Phase segmentation

Automated image analysis of polished cement-based materials was first introduced in 1995 (Darwin and Abouzeid, 1995), with three matrix formulations prepared with different w/c ratios and admixtures of silica fume. In this study, phases were identified based on grey level segmentation and detailed information on specific grey scale range of each phase (unhydrated cement, CH, inner product of C-S-H, undesignated product and voids) was also presented. After curing for 28 days, CH area percentage was calculated as 24.6% for the w/c 0.5 cement pastes, 22.0% for the w/c 0.3 cement paste and 13.5% for the w/c 0.3 cement pastes with silica fume addition (based on the average data on up to 640 BSE images). These data was generally comparable with the results obtained from the corresponding thermogravimetric analysis, accounting for 20.1%, 20.7% and 13.5% respectively.

Detailed procedure for phase segmentation of hydrated phases was described by Wang and Diamond (Wang and Diamond, 1995). In the study, backscattered electron images of cement pastes (with w/c ratios of 0.45 and 0.3, with or without super-plasticizer addition) cured for 100 days were obtained. It was found out that area fraction of CH, porosity and unhydrated cement could be easily achieved using grey scale threshold method. However for the segmentation of hydrated C-S-H gel, a series of computer-

Chapter 4- Literature review on interfaces in steel reinforced concrete

based programs (e.g. erosion, dilation and hole-filling) were necessary in order to create a binary image, eliminating the problems caused by the overlapped grey scales at the boundaries between two hydrated phases.

Direct segmentation of aggregate in a concrete or mortar system from the complex bulk matrix was difficult because of its wide range of overlapped boundaries with C-S-H gel and CH phases. A macro program was then developed by Werner and Lange in 1999 (Werner and Lange, 1999), using a series of image filtering process e.g. smoothing, saturation and edge effect.

X-ray elemental mappings were first applied in image analysis process by Stutzman (Stutzman, 2004) in combination with the corresponding BSE image, which successfully separated belite, tricalcium aluminate, ferrite, alkali sulfate and gypsum by arithmetic process (Fig. 4.5.1).

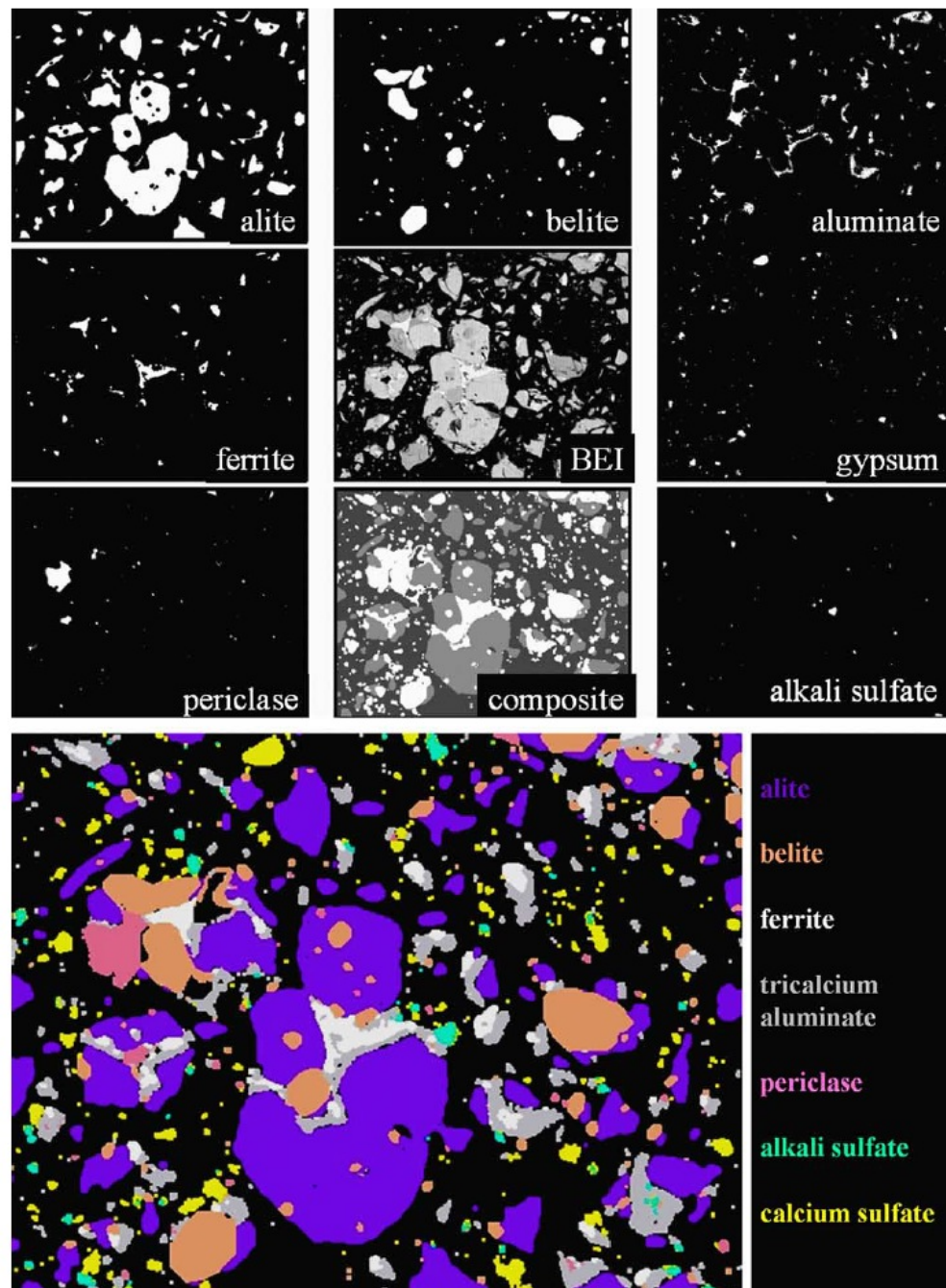


Figure 4.5.1 Phase segmentation in cement paste and a combined image used for area analysis, from reference (Stutzman, 2004)

4.5.3 Quantification at the steel/concrete interface

Quantitative analysis at the steel/concrete interfacial zone has been achieved (Horne *et al.*, 2007) in order to have a further understanding on the chemical composition at this region. In the study, region growing was applied

Chapter 4- Literature review on interfaces in steel reinforced concrete

as a method to produce a band of pixels, which are within equal distances from steel surface. Each strip has a width of $1.86\ \mu\text{m}$, growing from the surface of steel and generating a region which is within $\sim 120\ \mu\text{m}$ away from the steel surface (Fig. 4.5.2).

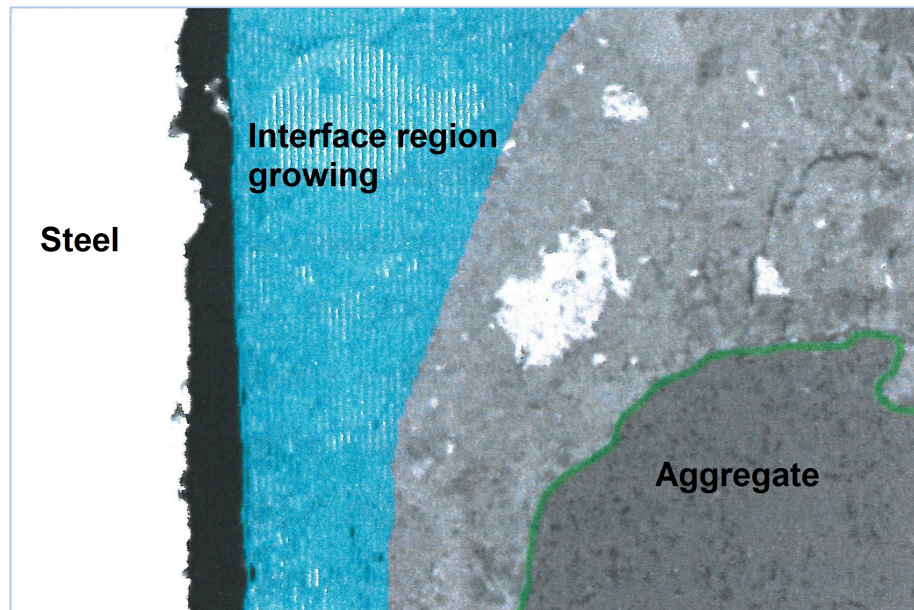


Figure 4.5.2 An example for regional growing at the interface from reference (Horne, 2004)

The quantitative results of different phases at various ages are shown in Fig. 4.5.3. Increased levels of CH precipitation as well as porosity and decreased levels of unhydrated cement were presented at this interfacial region in comparison to the bulk matrix. As curing age increased, the porosity percentage at interface decreased significantly from 35% at 1 day to 5% after curing for 365 days while CH concentration increased to as high as 30% at 365 days.

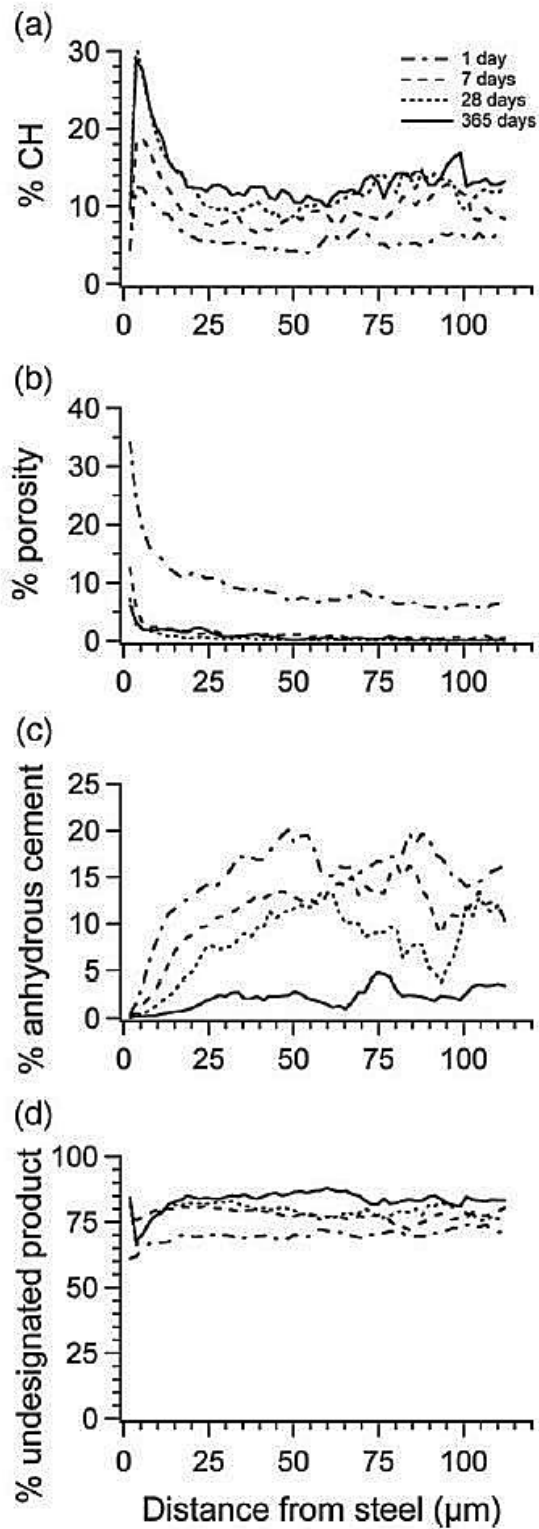


Figure 4.5.3 Microstructural gradients in the interfacial region between cement paste and vertically cast steel in a concrete with a w/c ratio of 0.49; from reference (Horne *et al.*, 2007)

4.6 Discussion

Although the achieved quantification at the steel/concrete interface can provide useful information on the microstructural and compositional features of this region, there are no standard procedures established for the phase segmentation. Different methodologies applied in different studies can cause user-bias. Moreover, the existed image analysis techniques are not productive and they are unique for one specific cementitious material, e.g. the threshold values for phase segmentation need to be adjusted for different concrete mixing designs. Therefore an updated image analysis technique with a wider range of applications (i.e. varying mixing designs for both hydrated Portland cement and non-Portland cement systems) becomes very imperative to reflect increases in image processing power, consequently giving much more accurate results on quantitative analysis.

Microstructure at the steel/concrete interface in Portland cement system has not been fully understood so far and debate still continues over the nature of the interfacial region. Whether or not preferential accumulation of different ions is occurring at the interface still remains unknown. And it is necessary to further investigate the distribution of different atomic ratios such as Ca/Si, Al/Ca, S/Ca as a function of certain distance away from steel; this useful information facilitates the straightforward interpretation of the chemicals present at the interface and can also reflect the ion transport properties at this region over curing, thus is eventually responsible for the corrosion resistance of reinforcement embedded in Portland cement systems.

The popularity of CSA cement, used as a potential low-carbon binder, encourages the studies on steel reinforced CSA concrete systems,

Chapter 4- Literature review on interfaces in steel reinforced concrete

particularly focusing on the corrosion resistant capability of the reinforcement embedded in this newly modified CSA-based material. Microstructure at the steel/CSA cement interface has not been studied in detail; this need to take place in order to provide confidence in the likely durability performances of the proposed steel reinforced CSA concrete.

Chapter 5- Experimental

This chapter introduces the materials and methodology used in this research. Analytical techniques (e.g. thin section imaging, SEM/EDX, DTA/TG and XRD) are described with settings. Detailed procedures to produce thin section petrographic samples are also present.

5.1 Materials and mix design

5.1.1 GRC composites

Two matrix formulations were used in this project, namely OPC (CEM II 32.5R, 'O' for short) and a blend of OPC and calcium sulfoaluminate cement (commercially called Nashrin¹, 'N' for short). Both of the matrices were reinforced by chopped and randomly orientated AR glass fibres, with a volume fraction of 4.5-5%. Incorporation of sand in those two GRC mixes (with a sand/cement ratio of 1:1) was designed to reduce composite shrinkage. Water to cement ratio for both types of GRC composites was ~0.31. Specimens were cast in the form of thin sheet in a previous project, with a slab size of 225mm × 55mm × 10mm. After curing for 10 years at 25°C under water, the composites were removed from the tanks and dried in lab air for ~24h. In this way, hydration stop was expected to be finished and the composites were wrapped in plastic bags for storage prior to a series of laboratory tests.

¹ Nashrin formulation: Blue circle Mastercrete 12 kgs, blast furnace slag 12 kg (w/w SiO₂ 32.4%, Al₂O₃ 12.9%, CaO 42.3%, MgO 6.5%, SO₃ 2.0%), NSR sulfoaluminate additive 6 kg (w/w Al₂O₃ 19.6%, CaO 39.0%, SO₃ 34.7%, R₂O 0.15%), set controlling agent Sette D-400 0.6 kg.

Chapter 5- Experimental

Comparative specimens made by hot water accelerated ageing were also produced in order to compare accelerated ageing with low-temperature ageing. In this study, accelerated ageing at 50 °C for 140 days was undertaken, which is equivalent to 46 years ageing for OPC/GRC and ~7.7 years for Nashrin/GRC under typical UK weathering conditions (Purnell and Beddows, 2005; Purnell *et al.*, 2008). Chemical compositions of those two types of GRC composites are given in Table 5.1.1.

Table 5.1.1 XRF results of OPC and Nashrin modified GRC aged for 10 years at 25°C

Compound	Unit	O	N
SiO ₂	%	51.03	51.91
CaO	%	25.08	19.35
Na ₂ O	%	0.64	0.55
MgO	%	0.38	1.70
Al ₂ O ₃	%	2.82	5.05
P ₂ O ₅	%	0.04	0.02
SO ₃	%	1.94	4.99
K ₂ O	%	0.47	0.61
TiO ₂	%	0.26	0.28
Cr ₂ O ₃	%	0.01	0.00
Mn ₃ O ₄	%	0.03	0.13
Fe ₂ O ₃	%	1.12	0.68
ZnO	%	0.01	0.01
SrO	%	0.05	0.03
ZrO ₂	%	0.82	0.56
BaO	%	0.03	0.04
LOI	%	15.27	14.09

5.1.2 Steel reinforced concrete

The commercial CSA cement used in the study of steel reinforced concrete system was provided by Hanson Heidelberg Cement Group. The fine

Chapter 5- Experimental

aggregates used in this study were natural sand with a particle size 0–3mm and the coarse aggregates were siliceous crushed stone with a diameter up to 20mm. Detailed information on particle size distribution for the fine aggregate and coarse aggregate is presented in Fig. 5.1.1. Tap water was used in this experiment and the water to cement ratio was 0.69. A mixing design of cement: water: fine aggregate: coarse aggregate 1: 0.69: 2.4: 3.6 was applied to produce both CSA concrete and corresponding OPC concrete as a reference. Details on mixing design are listed in Table 5.1.2.

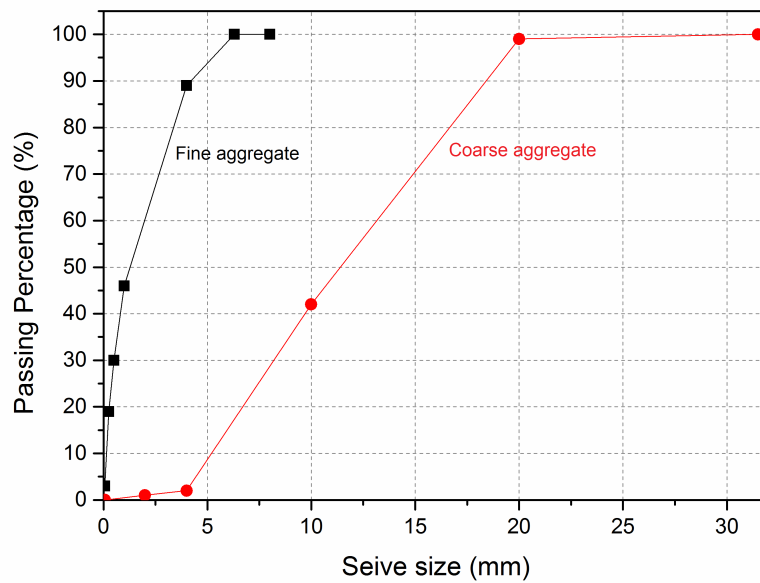


Figure 5.1.1 Particle size distribution of aggregates used in the project

Table 5.1.2 Mix design of C35 CSA concrete

Mixture	
CSA cement, kg/m ³	309
Water, kg/m ³	213
Fine aggregate, kg/m ³	740
Coarse aggregate, kg/m ³	1100
w/c, %	0.69

Round bright steel bars with a diameter of 10mm were chosen as reinforcements, trying to simulate the real in-service engineering as much as possible while taking considerations into the potential difficulties involved in sample preparation (e.g. the extreme hardness of steel bar during precision cutting and grinding process). Embedded steel bars were cleaned by acetone first in order to remove any loose rust or grease on the surfaces. The freshly mixed concrete was firstly placed in 100mm × 100mm × 100mm cubic moulds and vibrated on a vibrating table. Four bars (each with a length of ~ 150mm) were then inserted vertically into each concrete cube along the casting direction (Fig. 5.1.2). Cast cubes were vibrated again for two minutes to make sure that appropriate compaction was applied, minimizing the possibility of air entrapment near the rebar surfaces. After setting for 24 hours, cast reinforced concrete specimens were demoulded and exposed to a 100% relative humidity atmosphere at 20±2°C until testing at given ages (28 days and 1.5 years). During curing, a small amount of Vaseline was applied on the exposed rebar surface to restrict superficial corrosion of the steel.



Figure 5.1.2 An example of the arrangement of four reinforced bars in CSA concrete

Cement paste samples with the same w/c of 0.69 as the steel reinforced concrete were prepared for bulk chemical analysis, this aims to eliminate the interference of aggregates and thus avoid complicating chemical analysis of the hydrating cement matrix. Deionized water was used and small amounts of mixes were prepared by gentle stirring for at least two minutes. The mixed paste was then cast into small plastic cylindrical tubes with a diameter of 10mm and height of 50mm. The moulds were rotated at 12 rpm for a period of 24 hours to prevent segregation. Afterwards the paste samples were then sealed in a plastic bag and water-cured at $22\pm 1^{\circ}\text{C}$ for 7 days, 28 days, 90 days and 1.5 years respectively. At the end of each curing period, pastes were demoulded and the central portion was crushed into smaller fragments and then ground into fine powder for immediate bulk analysis.

Chemical compositions of the CSA cement and Portland cement are listed in Table 5.1.3. According to Bogue calculation, OPC cement contains 70.1% C_3S , 2.8% C_2S , 9.5% C_3A and 5.9% C_4AF . Estimation of the clinker

Chapter 5- Experimental

compositions in CSA is based on stoichiometric calculations: Ye'elimite 71.3%, belite 25.8% and very small amount of gypsum 2.9%.

Table 5.1.3 Chemical composition of CSA cement and OPC cement by XRF analysis

Compounds	Unit	CSA	OPC
CaO	%	42.33	62.14
SiO ₂	%	9.00	19.42
Al ₂ O ₃	%	33.82	4.83
SO ₃	%	8.83	4.81
Fe ₂ O ₃	%	1.35	1.95
MgO	%	2.29	2.13
K ₂ O	%	0.22	0.75
Na ₂ O	%	0.12	0.24
P ₂ O ₅	%	0.06	0.10
TiO ₂	%	1.61	0.24
V ₂ O ₅	%	0.02	0.01
Cr ₂ O ₃	%	0.02	0.01
Mn ₃ O ₄	%	0.03	0.07
ZnO	%	0.01	0.04
SrO	%	0.07	0.07
ZrO ₂	%	0.04	0.00
BaO	%	0.02	0.02
LOI	%	0.16	3.17

5.2 Experimental design

XRD and DTA/TG were used for the chemical study of the bulk matrix in both the GRC and steel reinforced concrete systems. Thin section petrography specimens of both composite systems were prepared for microstructural observations i.e. thin section images and SEM/EDX analysis. Bending tests were carried out for the aged GRC composites. Finally image analysis at the steel/concrete interface was performed in the steel reinforced concrete system. Detailed information on experimental design for GRC

Chapter 5- Experimental

composites and steel reinforced concretes are presented in Table 5.2.1 and Table 5.2.2 respectively.

Table 5.2.1 Design of the experimental work on GRC part

Tests used	Nashrin/GRC		OPC/GRC	
	0d	10y	0d	10y
XRD	x	✓	x	✓
DTA/TG	x	✓	x	✓
Bending test	x	✓	x	✓
Thin section images	✓	✓	✓	✓
Microstructure on fractured surfaces	x	✓	x	✓
Microstructure on polished surfaces	x	✓	x	✓
Microanalysis	x	✓	x	✓

Table 5.2.2 Design of the experimental work on steel reinforced concrete part

Tests used		CSA concrete				OPC concrete			
		7d	28d	90d	1.5y	7d	28d	90d	1.5y
Bulk analysis	XRD	✓	✓	✓	✓	✓	✓	✓	✓
	DTA/TG	✓	✓	✓	✓	✓	✓	✓	✓
Microstructure at the interface	BSE images		✓		✓		✓		✓
	Mappings	N/A	✓	N/A	✓	N/A	✓	N/A	✓
	Microanalysis		✓		✓		✓		✓
EDX analysis at the interface	Ca/Si		✓		✓		✓		✓
	Al/Ca	N/A	✓	N/A	✓	N/A	✓	N/A	✓
	S/Ca		✓		✓		✓		✓

5.3 Thin section petrography (TSP) production

5.3.1 Overview

Thin section petrographic specimens of both GRC composites and steel reinforced concretes were produced for the microstructural analysis. Steel reinforced concrete cubes were first sectioned into four even parts along the casting direction, ending up with each part containing a vertical bar in the middle on a transverse section, surrounded by bulk concrete. After a series of cutting and grinding procedures (detailed description in section 5.3.2-5.3.10), thin section petrographic specimen on a transverse section of reinforced concrete was finished with a longitudinally bar located in the middle of glass slide.

Specimen thickness was about 30 μ m after several cutting and grinding procedures. Slides were covered by a cover slip immediately after finishing and were kept in a low-CO₂ desiccator for later SEM analysis. There are several procedures involved to produce a thin section petrography specimen as presented in Fig. 5.3.1. This technique is highly dependent on user's technical experience and each step should be taken with extreme care. Detailed information on the process of each procedure is listed in the following sub-sections.

Chapter 5- Experimental

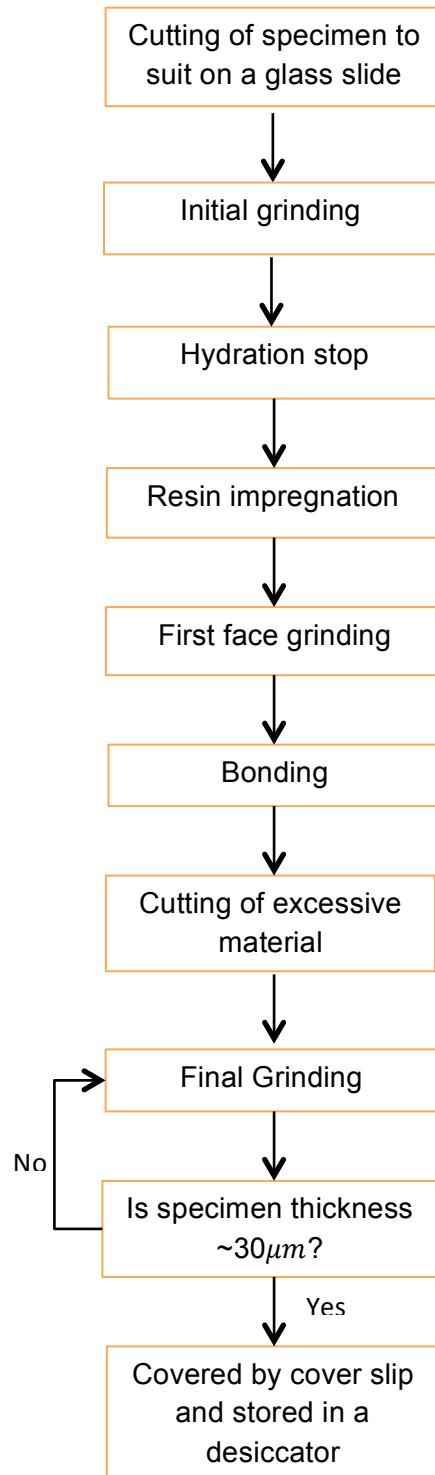


Figure 5.3.1 Flowchart of the sequences to produce a thin section petrography specimen

5.3.2 Initial cutting

Reinforced concrete cubes (100mm × 100mm × 100mm) and GRC slabs (225mm × 55mm × 10mm) need to be trimmed into proper sizes in order to be bonded with glass slide (48mm × 28mm) later. They were firstly cut into smaller concrete blocks (50mm × 50mm × 25mm) and GRC blocks (55mm × 20mm × 10mm) by a coarse cutting machine in casting shop. Precision cutting was followed then by using an automatic controlled cutting machine (Accuton-50 by Struers), trimming the excessive materials in order to fit on a glass slide (48mm × 28mm). Special cut-off wheel (E0D15 produced by Struers) with electroplated diamond was used to cut the steel reinforced concrete due to extreme hardness difference between steel (with a diameter of 10mm), cement paste and aggregate. At the end of this cutting process, a trimmed concrete block was supposed to be finished with an estimated size of 22mm × 16mm × 15mm and estimated GRC sample sizes were 25mm × 30mm × 10mm.

5.3.3 Initial grinding

Initial grinding aims to create a flat surface that is prepared to bond with a glass slide. Manual grinding on a silicon carbide paper P500 was conducted, together with a visual check if the surface was flat enough. This procedure was an important prerequisite to ensure a satisfied complete finish of the TSP specimen with even thickness.

5.3.4 Hydration stop

Hydration stop of specimens in a controlled manner is necessary to arrest the cement hydration before any microstructural and chemical studies commence after given curing periods. There are several methods to stop cement hydration in cementitious materials, e.g. oven heating, solvent exchange and freeze drying (Gallé, 2001; Collier *et al.*, 2008; Zhang and Scherer, 2011; Snoeck *et al.*, 2014). Oven heating is a fast drying technique but it damages cement microstructure significantly as excessive shrinkage is likely to be introduced; and decomposition of C-S-H, AFm and Aft phases may also happen with over-heating over 60°C. It has been reported that solvent exchange may possibly cause additional reaction with hydration products or through strong adsorption (Day, 1981; Snoeck *et al.*, 2014).

In this project, freeze drying was chosen to remove any moisture from the materials. Specimens were first immersed in liquid nitrogen (at a temperature of ~196°C) for few minutes, during which process moisture present in the specimen was frozen rapidly forming ice due to the temperature difference. Afterwards specimens were placed in a freeze drier immediately, ice formed within the porosity would then sublime directly, and causing less capillary stress compared to other drying techniques e.g. oven heating and solvent exchange. The freeze dryer was set up at constant temperature of -40°C with the vacuum maintained at $\sim 1.5 \times 10^{-1}$ mbar. Removal of the free water can thus be finished until a constant weight of sample was maintained. After finishing of hydration stop, the specimens were stored in a desiccator containing dried silica gel in order to avoid the take-up of atmospheric moisture before resin impregnation.

5.3.5 Resin impregnation

Resin impregnation of specimens is a very important step to reinforce the brittle structure of cementitious materials prior to grinding and polishing processes. After resin hardening, penetrated resin within the pore structure strengthens the concrete microstructure and greatly improves its ability to withstand the stresses caused by grinding and polishing during the sample preparation (Kjellsen *et al.*, 2003).

A low-viscosity resin and hardener (EpoFix Kit) was mixed at a weight ratio of 25:3 by gentle stirring for at least two minutes. Each specimen was placed in one polyethylene holder, with the flat surface facing down to the bottom of holder. Mixed resin and hardener was de-gassed first in a vacuum chamber to remove air bubbles, and then the mixture flowed into the holder slowly until it could cover the entire specimens. When air bubbles stopped generating on the top, vacuum could be released then and it further facilitated longer penetration lengths of resin into the pore structure. Finally, specimens were left overnight for hardening and demoulded after this.

5.3.6 First face grinding

After de-moulding, excessive resin needs to be trimmed in order to ensure that the sample can sit squarely on a glass slide. Excessive resin was cut off using cutting machine Accurom-50, followed by a gentle manual grinding by hand on SiC500 paper to remove the excessive resin layer on bonded surface and expose the sample surface. Over-grinding should be avoided because it is likely to remove the impregnated resin that is supposed to reinforce the microstructure. For steel reinforced concrete, a very thin layer

Chapter 5- Experimental

of resin cover must be left on the bonded surface in order to help subsequent bonding with glass slide. Otherwise after bonding, there may be insufficient bond strength between the totally exposed steel surface and glass slide, causing the steel to possibly peel off from the glass slide during the cutting or final grinding process. A microscope observation was a supplementary way to check the flatness of surface after a quick visual check.

5.3.7 Bonding

Before bonding, glass slide was cleaned with acetone to remove any grease left on the surface. An araldite epoxy-based resin was used in the bonding process. To reduce the viscosity of resin and improve the depth of resin impregnation, glass slides and concrete specimens were warmed up on a hotplate (set up at 38°C) for about 10 minutes. At the same time, a very small amount of the Epothin epoxy resin and hardener (according to a weight ratio of 5:2) were mixed gently in a glass sample vial for two minutes. Then the mixture was vacuumed down in a vacuum chamber until bubble stops generating on the top. A small amount of the mixed resin was then applied on the bonded surface along one edge of the specimen. Finally, a warmed glass slide was placed onto the bonded surface in a rocking manner; gradually making resin flow over the first face and forces applied during the rocking manner could expel any air bubbles in the resin. Afterwards the reinforced concrete block bonded with a glass slide underneath was left on a flat table overnight for hardening, with heavy plate placed on the top, in order

to remove air bubbles from the bonding surface and thus ensures a rigid bonding strength.

5.3.8 Removal of excess material

Prior to final grinding process, the bonded specimens on glass slides need to be thinned in order to save the grinding work as much as possible. Cutting machine Accuton-50 was used to cut off the excessive materials, finishing with a specimen thickness of about 300 μ m.

5.3.9 Final grinding

Final grinding process was completed with a series of silicon carbide paper with different grit sizes, i.e. P200, P500, P1200 and P2400. When grinding on a grit paper, the fixed diamond grit knocks off tiny particles from the sample surface. The grit size can then be reduced progressively to remove smaller and smaller particles from the surface, ending up with a favourably smoother surface. A correlation of silicon carbide paper grade with its diamond size is shown in Table 5.3.1.

Table 5.3.1 Illustration of grit sizes and their corresponding grade standard

SiC grade	200	500	1200	2400
Diamond (μ m)	60	30	14	10
Force (N)	7.5	7.5	5.0	5.0

Chapter 5- Experimental

A grinding machine Rotopol 35 was used in this procedure (Fig. 5.3.2). Silicon carbide abrasives were bonded to self-adhesive disks on a lapping wheel, with a turntable speed at 60 rpm. There is always a compromise between time consumption used in the grinding process and the preservation of microstructure with less exposure time and less heat damage. Grinding force is one of the important factors controlling the total time used for grinding samples to a specific thickness; greater force leads to less grinding time but it will introduce more friction and heat thus may damage the microstructure. If a smaller grinding force is applied, it takes longer time to grind off the particles and more importantly, and ridges can be created. Therefore different grinding forces were chosen at different grinding stages, e.g. force of 7.5N applied in grinding with P200 and P500, 5N for grinding with P1200 and P2400 paper.

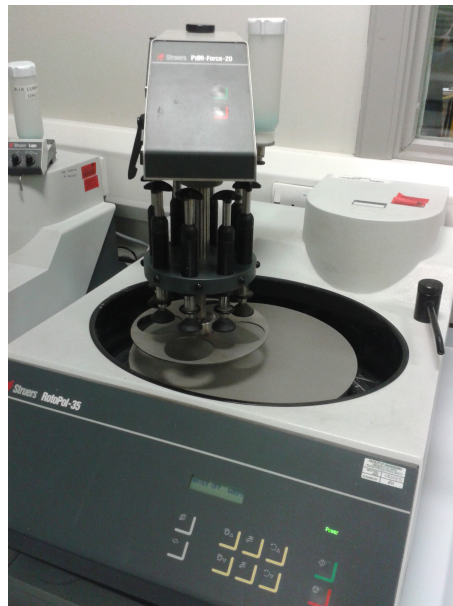


Figure 5.3.2 The grinding machine (Rotopol 35 by Struers) used in the final grinding process

Chapter 5- Experimental

During the grinding process, any debris entrapped under the grinding surface was likely to cause scratches on sample surfaces. So specimens were cleaned regularly during the grinding process with cotton wool. Lubricant was also applied on the grinding face to effectively cool down the sample surface, on top of which heat could be generated due to repeated friction with the coarse SiC paper. An outline of the whole grinding process is listed in Fig. 5.3.3 and detailed information is as below.

Chapter 5- Experimental

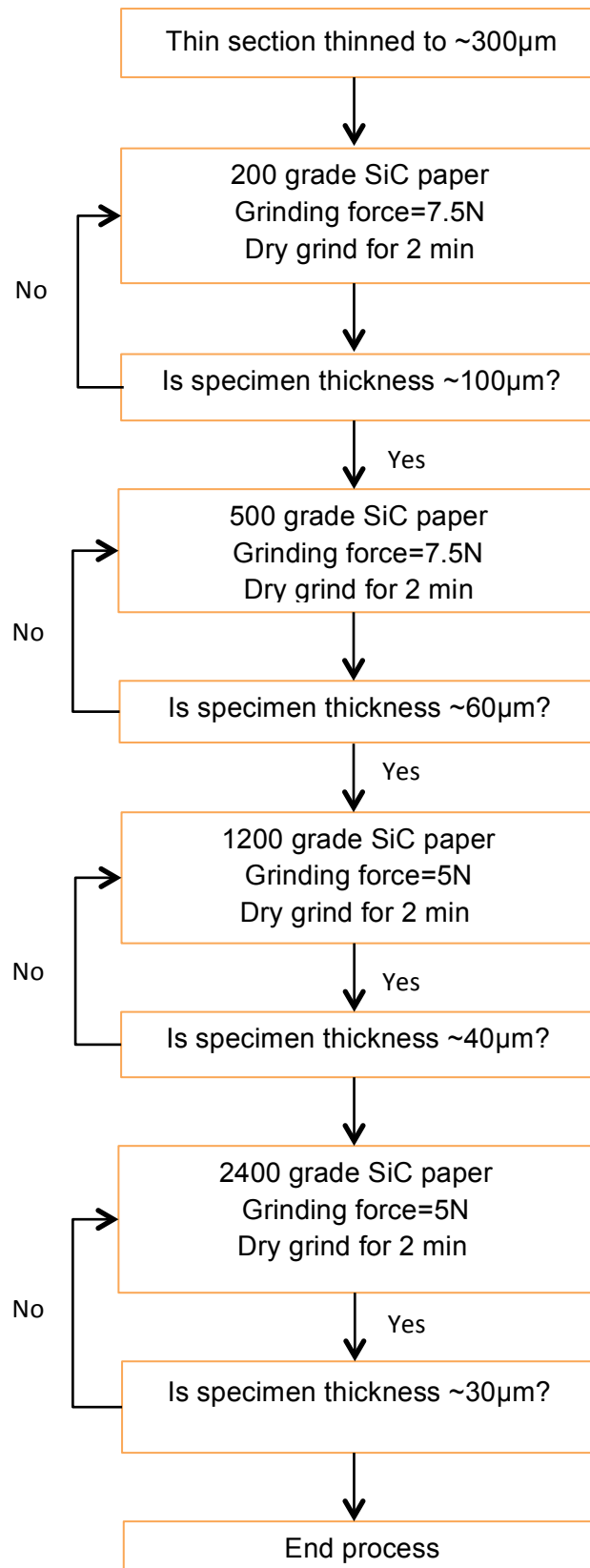


Figure 5.3.3 Sequence of the procedure of final grinding process

5.3.10 Storage

After the grinding process finishes, thin section petrographic specimens need to be covered with cover slips on top immediately, putting small amount of Vaseline on the four corners of the slides to help relatively firm covering. The specimens were then stored in a low-CO₂ desiccator. Prior to microstructure study, cover slips were removed gently by sliding. Any remaining Vaseline on glass slide was wiped off gently with tissue to prevent contamination of the vacuum system in the SEM chamber.

5.4 Bulk analysis

5.4.1 DTA/TG

Thermal analysis is widely used in research to analyse the presence and/or quantity of various compounds in hydrated cement paste by exploiting the fact that each compound will decompose (generally by dehydration or dehydroxylation) at a distinctive temperature. It includes techniques such as differential thermal analysis (DTA), thermogravimetry (TG) and differential scanning calorimetry (DSC).

TG mainly determines the weight changes when the substance is heated over at known intervals of temperature normally up to 1000°C. DTA records the differences in temperature between the investigated sample and the reference sample under the same heating program; during changes of sample state or crystal form, the latent heat of phase transition will be absorbed (or released) and the temperature of the sample will lag behind that of the reference material. It consequently correlates to an exothermal or

Chapter 5- Experimental

endothermal reaction occurring in the sample, which is recognised by the individual endotherm or exothermal peak in the DTA curve within a characteristic range temperature. Therefore DTA/TG can be used for qualitative and quantitative analysis to determine the relative quantity of hydrated compounds present in cement paste after different ageing periods.

Thermal analysis in this project was carried out using Stanton Redcroft Simultaneous Thermal Analysis STA-780. Different curing regimes of cement pastes were established in this project. A small amount of freshly ground powder (~18mg) of hydrated cement paste was packed into a platinum crucible with an inert reference sample alongside. They were heated in a furnace to 1000°C at a rate of 20°C/min under constant flow of nitrogen.

5.4.2 X-ray Diffraction (XRD)

X-ray diffraction (XRD) is a powerful technique for the study of crystalline materials in hydrated cementitious materials. X-rays are highly energetic photons generated from electronic transitions in the atoms of a targeted metal by an incident of accelerated electron beam. An incident accelerated electron hits the metal atom and knocks out an electron from the inner K-shell ($n=1$ shell), and a vacancy is therefore left in that shell. If an electron from another shell fills in the vacancy (electron transitions), X-rays are then emitted (Fig. 5.4.1).

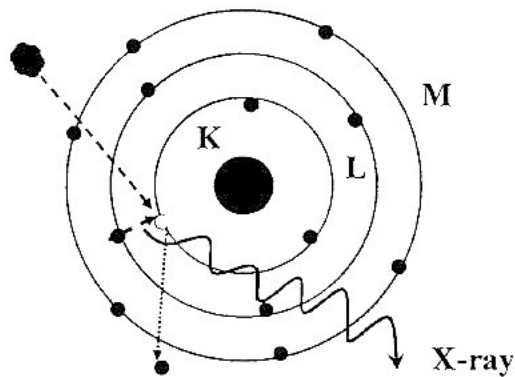


Figure 5.4.1 Illustration of X-ray generation

X-ray diffraction results from the diffraction of x-rays when interacting with a crystalline structure. Bragg's law shows the intrinsic relationship between interatomic spacing (d-spacing), the angle of diffraction (θ) and the wavelength of the incident X-ray radiation (λ):

$$2d \sin\theta = n\lambda$$

The d-spacing and λ are measured in angstroms, θ in degrees and n is an integer.

Powder X-ray diffraction patterns in this project were carried out by Bruker D8 using $\text{CuK}\alpha 1$ radiation. The working condition was 40kV and 30mA. Data of powder samples was collected in a 2θ -range from 5° to 80° with a step size of 0.02° and count duration was set to be 0.5s per step. The samples were freshly crushed and ground into fine powders in an agate mortar. Front loading was used to apply the powder samples into the sample holder, finishing with a flat surface by gently pressing with a glass slide.

5.5 Bending test

Mechanical performances of the aged GRC composites were assessed by four point bending testing. It was carried out on a Tinius Olsen bending machine according to BS-EN 1170-5:1997, with a span of 200mm and a loading rate at 1.8 mm/min. Detailed information on equipment setup is shown in Fig. 5.5.1. During the test, the load-deflection curve was displayed on the monitor and further stress-strain curve was calculated according to the acquired Microsoft Excel spread sheet.

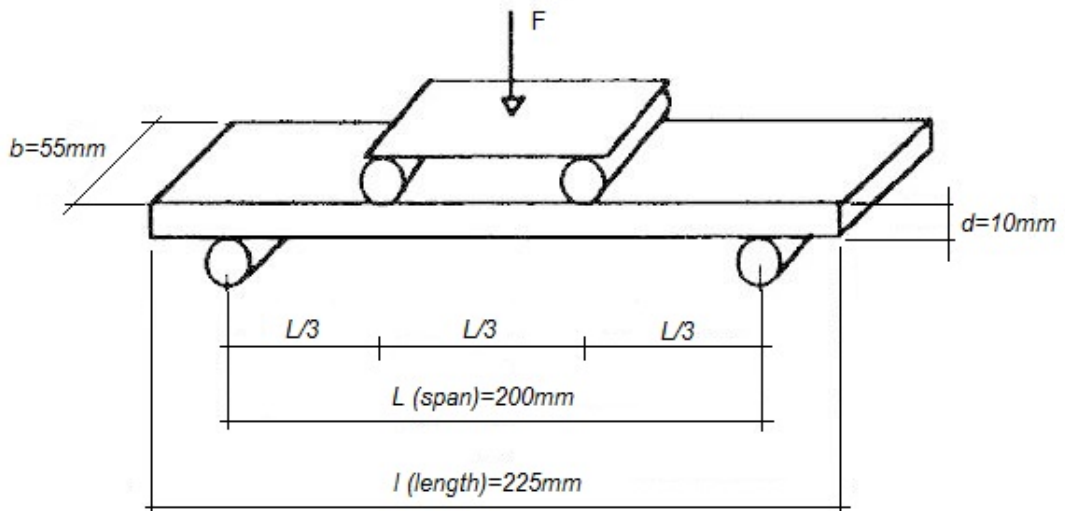


Figure 5.5.1 Experimental setup of four-point bending test on GRC slabs

5.6 Thin section (optical) microscope

Optical microscopy of resin-impregnated thin section slides is a traditional technique for microstructural studies of minerals and rocks, providing straightforward and qualitative identification of different components contained in the materials.

Chapter 5- Experimental

In the petrographic microscope, two polarising filters i.e. polariser and analyser (set at 90° to the polariser filter), are placed below and above the specimen stage respectively in an optic axis of the objective lens. Light passes through the polariser first and then it is resolved in an east-west plain. The polarised light is very interactive with the crystalline phases and it is refracted and split into two individual wave components, both of which are polarized in mutually perpendicular planes. Difference between the two refractive wave components is known as the birefringence for a crystalline phase. When the two wave components enter the analyser, only the rays vibrating at 90° to each other can interact with its birefringent crystals. Detailed information can be found in the reference (John *et al.*, 1998).

Crystals (e.g. CH, ettringite and calcite) existed in the thin-sectioned cementitious sample will exhibit unique interference colour that is highly dependent on the sample thickness. For example, CH crystals appears a colour of yellow in the middle but dark grey or even blue at the edge (John *et al.*, 1998). Silicon quartz is commonly very useful in indicating the estimated thickness of a thin section petrographic sample during sample preparation, by its interference colour according to the Michel-Lévi colour chart. For example, in a standard thin section petrographic concrete specimen ($30\mu m$ specimen thickness), maximum birefringence for quartz gives an interference colour of yellowish orange. Consequently at a regularly thickness of $30\mu m$, polarisation colours of each crystalline phase can be used to identify materials.

In this project, microscope was equipped with a digital camera that allows rapid image processing and acquisition of the thin section images. As glass

fibres are non-crystalline materials, therefore they will appear very dark under crossed polarised light in theory. In order to provide sufficient contrast in a thin section image, partially crossed polar at 75-80° was used for microstructural study of the thin-sectioned GRC composites. It mainly focused on the examination at the inter-filamentary spaces between glass fibres and also at the fibre/cement interfacial zones.

5.7 SEM/EDX

5.7.1 General introduction to SEM

SEM has been widely used to characterize the microstructure in hardened cementitious materials. A beam of high-energy electrons is scanned across the surface of a specimen and measures one of the signals resulting from the interaction between the beam and specimen. The main useful imaging methods are backscattered electron (BSE), secondary electron (SEI) and X-ray imaging with different interaction volumes (as shown in Fig. 5.7.1).

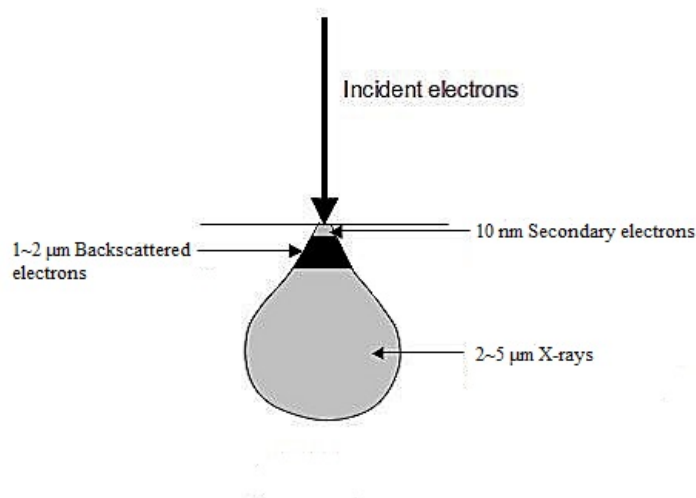


Figure 5.7.1 Overview of signal generation in SEM

Chapter 5- Experimental

Secondary electron is the most frequently used imaging mode in SEM due to its relatively high resolution. These electrons are less energetic ($<50\text{eV}$) than backscattered electrons and are originated within 10nm from the sample surface. It is a powerful technique to study the topographic features on the fracture surfaces of cementitious materials. In this project, secondary electron imaging was particularly employed for the studies of glass fibre reinforced composites; in particular it was introduced to examine the fracture surfaces by observing the failure mode of glass fibres and its surface smoothness, plus the quality at the interfacial zone between glass fibre and cement matrix.

Backscattered electrons are high-energy electrons ($>50\text{eV}$) that have undergone multiple elastic scattering events within the specimen. The greater energy results in a large interaction volume ($1\sim 2\mu\text{m}$ depth) and lower spatial resolution. Backscattering coefficient of a phase is primarily dependent on its physical density and the mean atomic number; accurately the higher the atomic number the brighter that region will appear and porosities appear as black in grey scales. Polished thin section petrographic specimens of both GRC composites and steel reinforced concrete were examined under backscattered electron imaging mode. A combined imaging of BSE images with thin section images at the same area of the sample was thus attempted to provide profound microstructural knowledge of the investigated samples.

Generated X-rays have a larger interaction volume ($2\sim 5\mu\text{m}$) and can be used as an analytical signal for qualitative and quantitative chemical analysis. Elemental mappings were acquired in this project to give

Chapter 5- Experimental

straightforward information on the distribution of elements within composites and spot analysis were also attempted to study the composition at the interfacial zone.

5.7.2 Coating

GRC specimens were fractured first with a sample height less than 15mm and were mounted on an aluminium stub with the fractured surface on the top. A layer of carbon paste was applied on the edges of the fractured surface in order to make it conductive through the stub. The same sample preparation method was applied for thin section petrographic samples, with a thin layer of carbon paste applied around the concrete sample in order to connect with the metal stub. Finally they were coated under vacuum, leaving a thin layer of carbon coating on the sample surface with a thickness of ~10 nm.

5.7.3 SEM set up

SEM work in this project was carried out using JEOL JSM-5900 LV. General SEM settings are listed in Table 5.7.1 below and detailed information will be explained in the sub-sections 5.7.3.1- 5.7.3.4.

Table 5.7.1 General SEM setup

Working distance (mm)	10
Accelerated voltage (keV)	15
Magnification	×400, ×1000
Spot size	25
Number of completed frames	5
Resolution width (pixel)	2048
Resolution height (pixel)	1536

5.7.3.1 Working distance

Working distance is one of the important parameters deciding the SEM image resolution. Smaller working distance leads to higher image resolution but a smaller depth of field may also be involved; increasing of the working distance is influential on obtaining a SEM image with lower resolutions. In this project, a working distance of 8-10mm was chosen to obtain good image quality regarding to a compromise between image resolution and depth of field.

5.7.3.2 Accelerated voltage

At higher accelerating voltages, SEM images with higher resolution can be obtained but the beam penetration and diffusion area can also become larger, resulting in unnecessary signals (e.g. backscattered electrons) being generated from within the specimen. These signals reduce the image contrast and veil fine surface structures. Besides this, higher accelerated voltage also leads to a higher possibility of charge-up and specimen damage.

Chapter 5- Experimental

In this project, a general accelerated voltage of 15kV was chosen to undertake the SEM work.

5.7.3.3 Magnification

Proper magnification is always a compromise between the field of areas studied and the SEM image resolution. A general magnification of $\times 400$ was used through this project, which was able to recognise the general interfacial characterisation with relatively large sampling area of the investigated samples. For some particularly interesting areas, SEM images were enlarged over a magnification of $\times 1000$ for both illustrative observations and/or EDX spot analysis.

5.7.3.4 Image resolution

SEM images in this part were collected using Aztec software package from Oxford Instruments. To give backscattered electron images or secondary electron images with high quality, resolutions of SEM images are set up at 2048 pixel \times 1536 pixel while collecting.

5.7.4 EDX

Energy-dispersive X-ray Spectroscopy (EDX) detector equipped with SEM allows the identification of the chemical composition at any region within the image. Only elemental mappings and spot analysis were performed in this project.

5.7.4.1 Elemental mappings

General settings of elemental mappings are shown in Table 5.7.2.

Table 5.7.2 General Mapping setup

Binning factor	1
Smoothing level	3
Number of completed frames	10
Dwell time (ms)	1.5
Energy range (keV)	10
Maximum pixel value (counts)	8.0
Total counts in element map (counts)	~37447

The corresponding elemental mappings were collected with a smaller image size of 1024 pixel \times 768 pixel compared to the corresponding BSE images, thus it took less acquisition time during mapping collecting. Different elements were selected for different cement systems. For the GRC composites, the following elemental mappings were collected:

- Calcium – Basic element in almost all the hydration phases in cementitious materials.
- Aluminium – Enriched in the aluminate phases, e.g. AFm, ettringite or alumina hydroxide gels in CSA-based materials.
- Silicon – Main composition of glass fibres and fine aggregates.
- Sulphur – present in ettringite and AFm phases.
- Sodium – To recognize of AR glass fibres as it is rich in silicon, zirconia and sodium.
- Zirconia – To recognize of AR glass fibres as it is rich in silicon, zirconia and sodium.

For microstructural studies of steel reinforced concrete, five elemental mappings were chosen:

Chapter 5- Experimental

- Silicon – Abundant in the aggregates and amorphous C-S-H gels.
- Calcium – The most common element in most hydrated cement phases.
- Aluminium – Found in aluminate phases such as ettringite, AFm and some amorphous aluminate phases (C-A-S-H).
- Sulphur – Existed in ettringite and AFm phases.
- Iron – Main composition of steel reinforcement.
- Oxygen – To reflect the rust layer in steel reinforcement.

5.7.4.2 Spot analysis

Spot analysis was performed on a flat thin section GRC slide, mainly focusing on the spaces between glass fibres. Owing to the relatively large interaction volume of X-ray signals, interference of glass fibre may possibly occur during the microanalysis. Therefore silicon signals originating from the glass fibre should be deducted from the total silicon content in microanalysis. Since ZrO_2 is present in glass fibres but absent from the hydrated cement, it could be used as a marker to calculate the proportions of silicon content of the spot analysis attributable to the glass fibres, by considering the composition of glass fibres (10% Na_2O - 22% ZrO_2 - 68% SiO_2 by weight).

For the thin-sectioned steel reinforced concrete specimen, spot analysis was carried out to study the chemical composition near steel surface. Atomic information of selected elements at each chosen spot were then collected and based on this, microanalysis plots of Si/Ca vs. Al/Ca and Si/Ca vs. S/Ca were calculated. They are found to be particularly helpful in determining compounds in cementitious materials, particularly at the interfacial region in this project.

5.8 Image analysis

In this project, quantitative image analysis technique is updated based on a combination of different elemental mappings within the same BSE image, instead of a series of phase segmentation and arithmetic calculations in the BSE images. In this study, image analysis is expected to be able to present different atomic ratios at the interfacial zone between steel and concrete, distributed as a function of the distance away from steel surface.

Different software package called Inca was used to collect SEM images and elemental mappings in the image analysis study, compared to the Aztec software in the qualitatively microstructural study. To obtain the most accurate quantification, elemental mappings used in the image analysis were obtained with much longer acquisition time (dwell time being 10 times longer than the qualitative elemental mappings). Preliminary experimental results conclude that aperture has a vital impact on the accuracy or density of the acquired mapping data, as shown in Fig. 5.8.1. Different settings on aperture (Aperture 2 and 3) and dwell time ($1000\mu\text{s}$ and $2000\mu\text{s}$) are compared to give the most accurate image analysis.

Chapter 5- Experimental

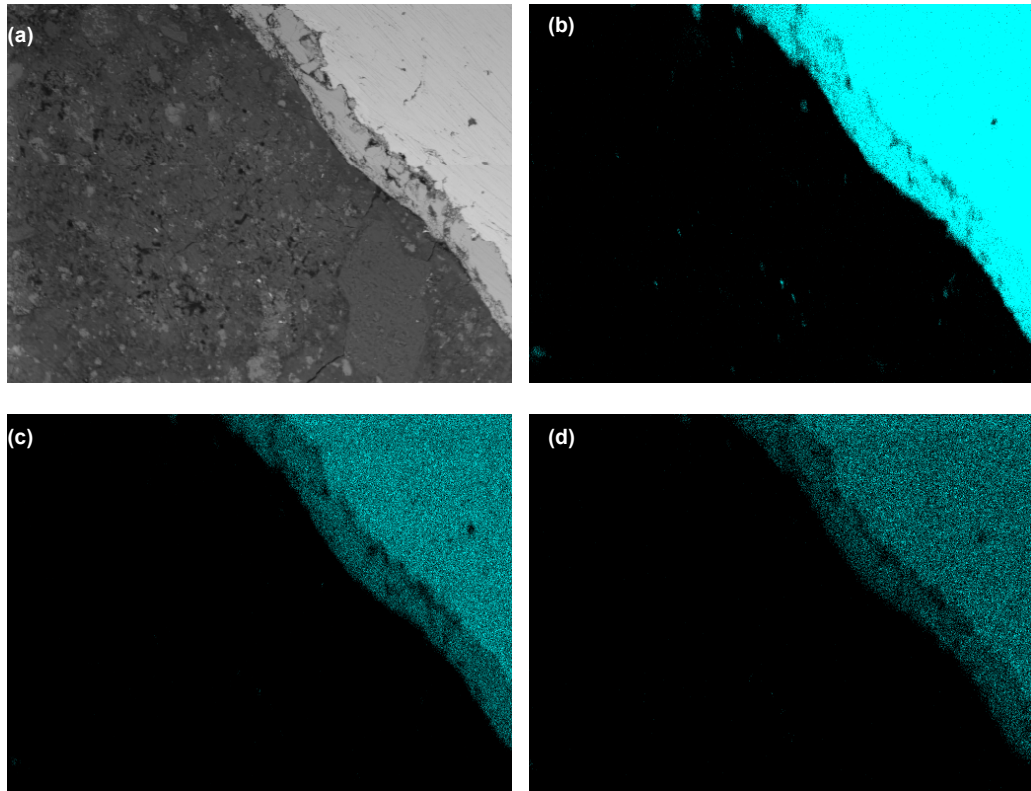


Figure 5.8.1 Different SEM settings for iron mappings in one of the examples of reinforced concrete sample

(a) Backscattered electron image of 28 days-cured steel reinforced CSA concrete, at a magnification of $\times 400$; (b) Iron mapping acquired by dwell time $1000 \mu\text{s}$ in Aperture 3, counts 28791769; (c) Iron mapping acquired by dwell time $2000 \mu\text{s}$ in Aperture 2, counts 10199096; (d) Iron mapping acquired by dwell time $1000 \mu\text{s}$ in Aperture 2, counts 5128775.

SEM settings with a larger aperture and reasonable dwell time of $1000 \mu\text{s}$ have been proved to create mappings with much more counts, thus providing much more precise data on the quantified elemental mapping. Ten frames were recorded for each mapping. BSE image and the corresponding elemental mappings were collected by Smartmap function in the Inca software (see Fig. 5.8.2) and backscattered electron images were collected at a smaller image size of $512 \text{ pixel} \times 384 \text{ pixel}$.

Chapter 5- Experimental

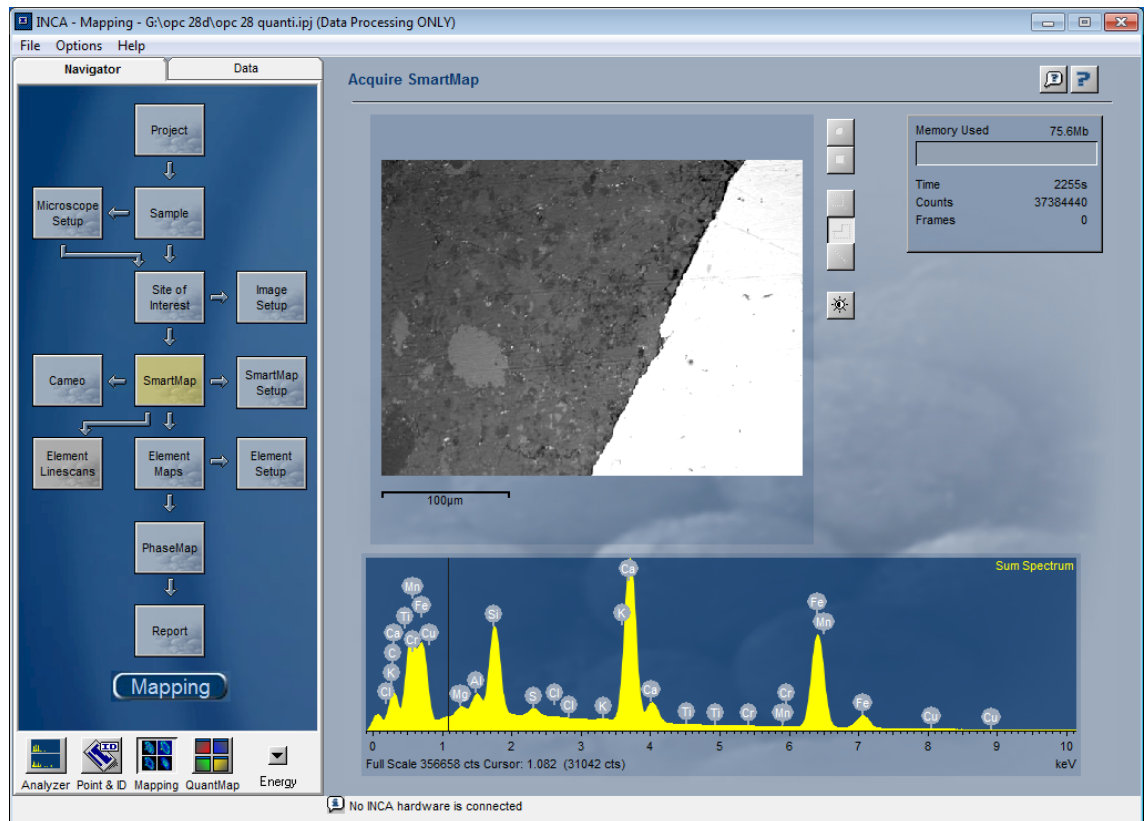


Figure 5.8.2 Smartmap in Inca used to collect elemental mappings for image analysis

The atomic information contained in each mapping was then read pixel by pixel by the QuantMap function in Inca (see Fig. 5.8.3), ending up with an Microsoft Excel spread sheet containing 384 rows and 512 columns (Fig. 5.8.4); each cell was representative of a specific atomic number of one pixel at exactly the same location in an element mapping.

Chapter 5- Experimental

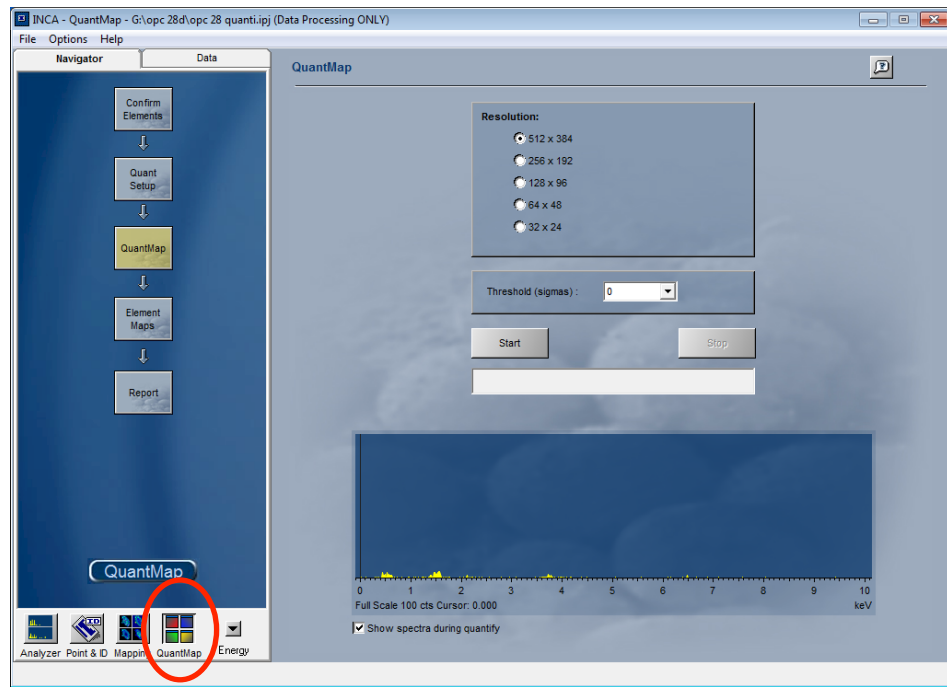


Figure 5.8.3 An example of reading elemental information pixel by pixel using Inca software

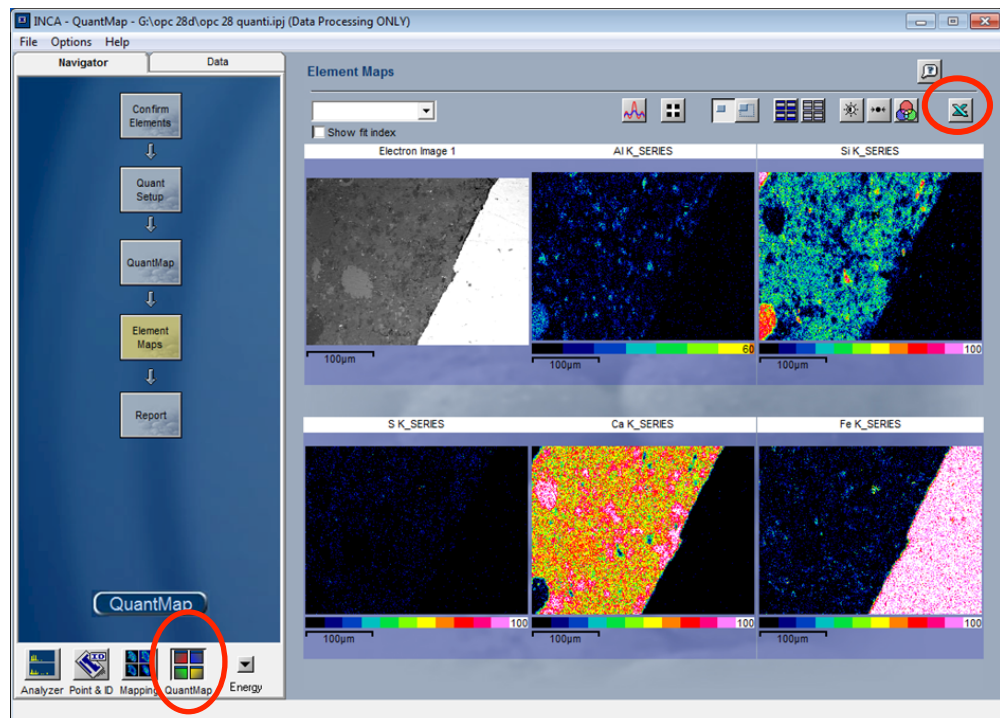


Figure 5.8.4 An example of obtaining the quantitative Microsoft Excel data on atomic information for each pixel

Chapter 5- Experimental

The Microsoft Excel sheet for iron mapping was used to extract the atomic data presented at the interfacial zone first. A macro written in MATLAB R2013b was established to find the edges of reinforcement first, indicated by a huge difference of atomic number between two pixels at the steel edges. Followed by this, the edge layer was expanded by extracting another 25 pixels data vertically, accumulating for about 30 microns in width which was supposed to be the interfacial information. If these cell locations were recorded in a MATLAB R2013b macro, the corresponding data for other elements i.e. Ca, Si, Al, S could be extracted in a new Microsoft Excel sheet. As a consequence, atomic ratios such as Ca/Si, Al/Ca and S/Ca can be calculated by average data with equal distance to steel. And relationship between the arrangement of atomic ratio and distance away from steel within 30 microns can be therefore built up.

This quantitative analysis methodology is highly reproducible and reliable as no user-bias is induced, compared to the image analysis technique based on phase segmentation in literature.

Chapter 6- Results and discussion: GRC

Aged GRC composites modified by CSA cement are compared with OPC/GRC in this chapter; the following results are presented: bulk analysis (DTA and XRD), thin section images, SEM on both polished and fractured surfaces, microanalysis at the space between fibres and microstructure observations on fibre surface. In the last part, bending performance of GRC are also compared with the corresponding unaged sample.

6.1 DTA

DTA curves of aged OPC/GRC and Nashrin/GRC are shown in Fig. 6.1.1. At lower-end temperature within the range of 100-180°C, DTA curves of both GRC materials appear to consist of three overlapping peaks, exhibited as a strong central endotherm at ~120°C and two broad shoulders on each side. This prominent triple endotherm is generally associated with (in the order of dehydration temperatures) the evaporation of weakly bound pore water, dehydration of C-S-H gels and dehydration of ettringite phases respectively. The low-temperature peak for Nashrin/GRC is significantly larger than that for OPC/GRC and the most prominent sub-peak is shifted towards higher temperature, suggesting a relative preponderance of ettringite over C-S-H gels. This is in agreement with the intrinsic hydration of the CSA-based materials, for which one of its main hydration products is ettringite, generated from the hydration of calcium sulfoaluminate phases within the cement clinker. Decomposition of CH occurs at the steps of 450-500°C and absence of CH endotherm is clear in Nashrin/GRC in comparison to the

Chapter 6- Results and discussion: GRC

dominant CH step for OPC/GRC. The importance of the absence of CH is in regard to the potentially improved durability of Nashrin/GRC composites as matrix densification and CH bundle filling remain as one of the degradation mechanisms of GRC composites. Steps between 650-780°C are indicative of the existence of calcium carbonate but very little seems to be apparent in either material. This curve includes another small endothermic peak at 573°C, which corresponds to $\alpha \rightarrow \beta$ transformation of the quartz crystals in the common fine aggregates.

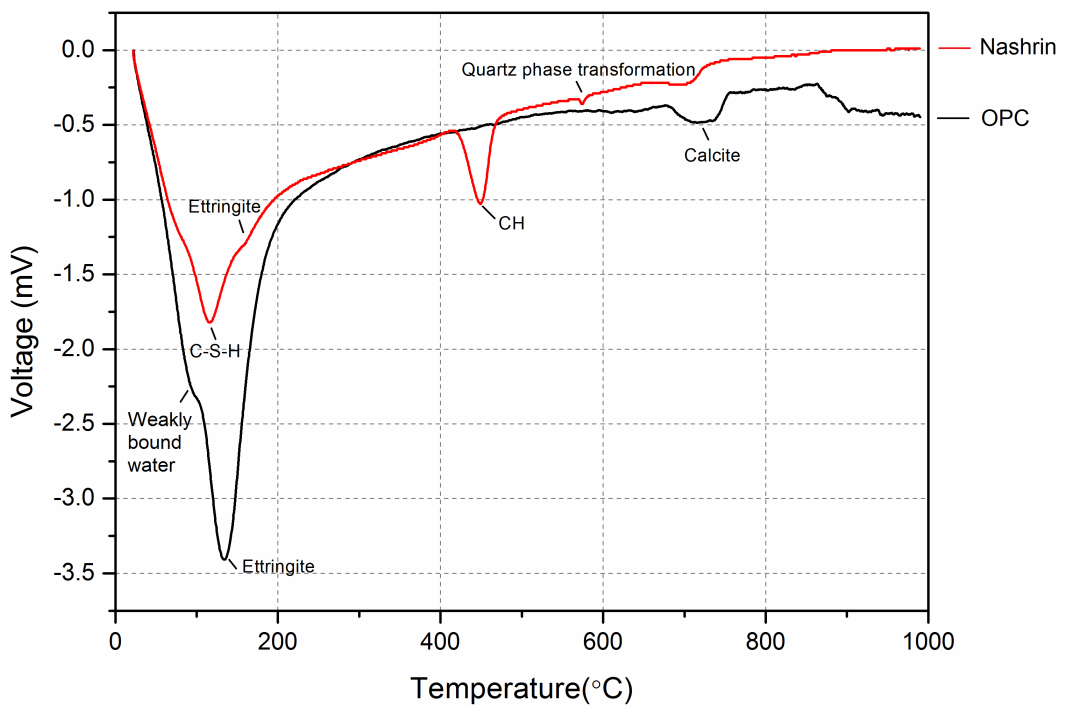


Figure 6.1.1 DTA results of 10y-aged OPC/GRC and GRC modified by Nashrin

6.2 XRD

XRD result for the OPC/GRC composite (Fig. 6.2.1) indicates that its main crystalline hydration product is CH, with minor amount of calcite and ettringite formation. This is generally consistent with the DTA data in section 6.1, except that C-S-H gels are not traced in XRD due to its poor crystallinity. XRD result of Nashrin/GRC composite clearly shows that CH is absent in the matrix, which agrees with the above thermal analysis results. The relatively large amount of ettringite shows that the hydrated Nashrin matrix is totally different from the OPC matrices. Minor calcite traced in both materials agrees with the DTA data above and indicated that little carbonation occurs during sample storage. A broad band between $2\theta = 32-33^\circ$ in both samples is indicative of the presence of remaining unreacted belite clinker; although aged for 10 years at normal temperature, complete hydration has not been achieved. Much more unreacted belite clinker remains in the Nashrin matrix, this can be explained that calcium sulfoaluminate reacts with water at an extremely rapid speed within the first few days, leaving limited amount of water available for the hydration of belite clinker at later ages. Abundant SiO_2 phases were traced in both samples due to the 50% sand addition to composites, which is added to counteract the drying shrinkage of cement matrix.

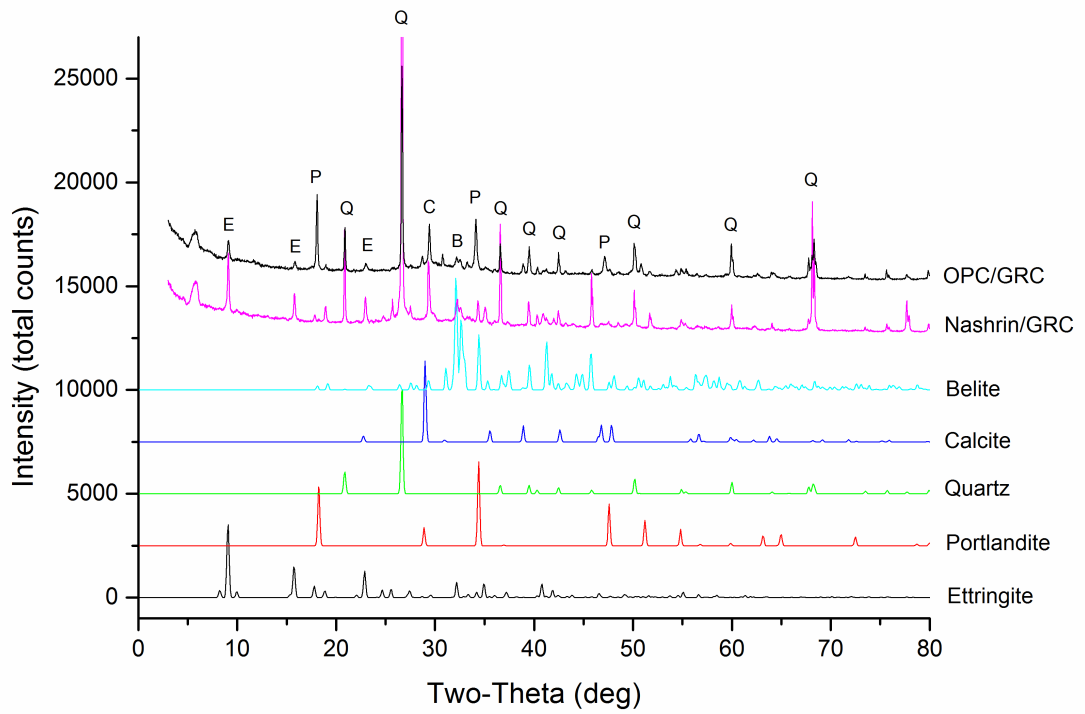


Figure 6.2.1 XRD results of 10y-aged GRC modified by Nashrin and OPC

(E: ettringite; P: Ca(OH)₂; Q: quartz; C: calcite; B: belite)

6.3 Microstructural study of Nashrin/GRC

6.3.1 Thin section image

Newly prepared samples from aged material were compared with unaged TSP specimens retained from the original study (Purnell and Beddows, 2005). They were observed under transmitted light microscopy to examine the general microstructure features in both glass/cement interface and interfilamentary spaces. Under crossed polarized light, glass fibres should appear black in colour theoretically as they are non-crystalline phases, making them rather difficult to be distinguished from the bulk cement matrix due to lack of contrast. It is found out that by slightly uncrossed polar at $\sim 75\text{-}80^\circ$, instead of crossing the polariser and analyser at 90° , a little light can transit through glass fibre bundles. Glass fibres then appear dark grey and can provide sufficient contrast to the hydrated cement matrix; this adjustment has insignificant influence on the diagnose of crystalline phases based on their interference colours.

At early ages, hydrated cement matrix has started to penetrate into the interfilamentary spaces between glass fibres in Nashrin/GRC as suggested by the presence of cementitious materials between fibres under partial plain polarised light, which appeared as light orange colour as showed in Fig. 6.3.1. This can be explained by the rapid hydration of calcium sulfoaluminate with water within the first few hours, generating large amounts of ettringite and aluminium hydroxide gels. The rapid formation of ettringite possibly results in significant internal tension, facilitating the matrix to penetrate further into the porous interfilamentary spaces (Chen *et al.*, 2012; Kasselouri

et al., 1995). The internal tension caused by ettringite crystal growth also possibly squeezes glass fibre bundles to some extent (Min and Mingshu, 1994; Valenti *et al.*, 2012), leaving a rather compact structure between the glass fibre strands.

For the aged Nashrin/GRC composite, two examples of thin section images chosen at different sites are illustrated in Fig. 6.3.2 and Fig. 6.3.3. The corresponding backscattered electron images are also studied with the same area as that in the thin section images, with common characteristic features (an aggregate particle in Fig. 6.3.2 and belite phase in Fig. 6.3.3) labelled in the images. Detailed qualitative and quantitative studies of these backscattered electron images are presented in section 6.4. Compared with the Nashrin/GRC at early age (Fig. 6.3.1), it was obvious that hydrated cement matrix penetration continues to occur into the spaces between fibres with ageing. Particularly in Fig. 6.3.3, a coincidence of vertical and horizontal fibres helps to examine the extent of bundle filling in the aged Nashrin/GRC composite. It was indicated that occasionally significant precipitation of crystal phases were observed at the interfilamentary spaces in a horizontal fibre bundle (in Fig. 6.3.3). Detailed chemical composition of these precipitated phases is investigated by microanalysis in section 6.3.2.

According to the thin section images of unaged and aged Nashrin/GRC composite, it can be concluded that there is almost no discernible microstructural changes during ageing process. This reveals a relatively stable microstructure evolution of GRC composites modified by Nashrin in the long term, which may be associated with significantly retained

Chapter 6- Results and discussion: GRC

composites mechanical performances with ageing (further discussed in section 6.5).

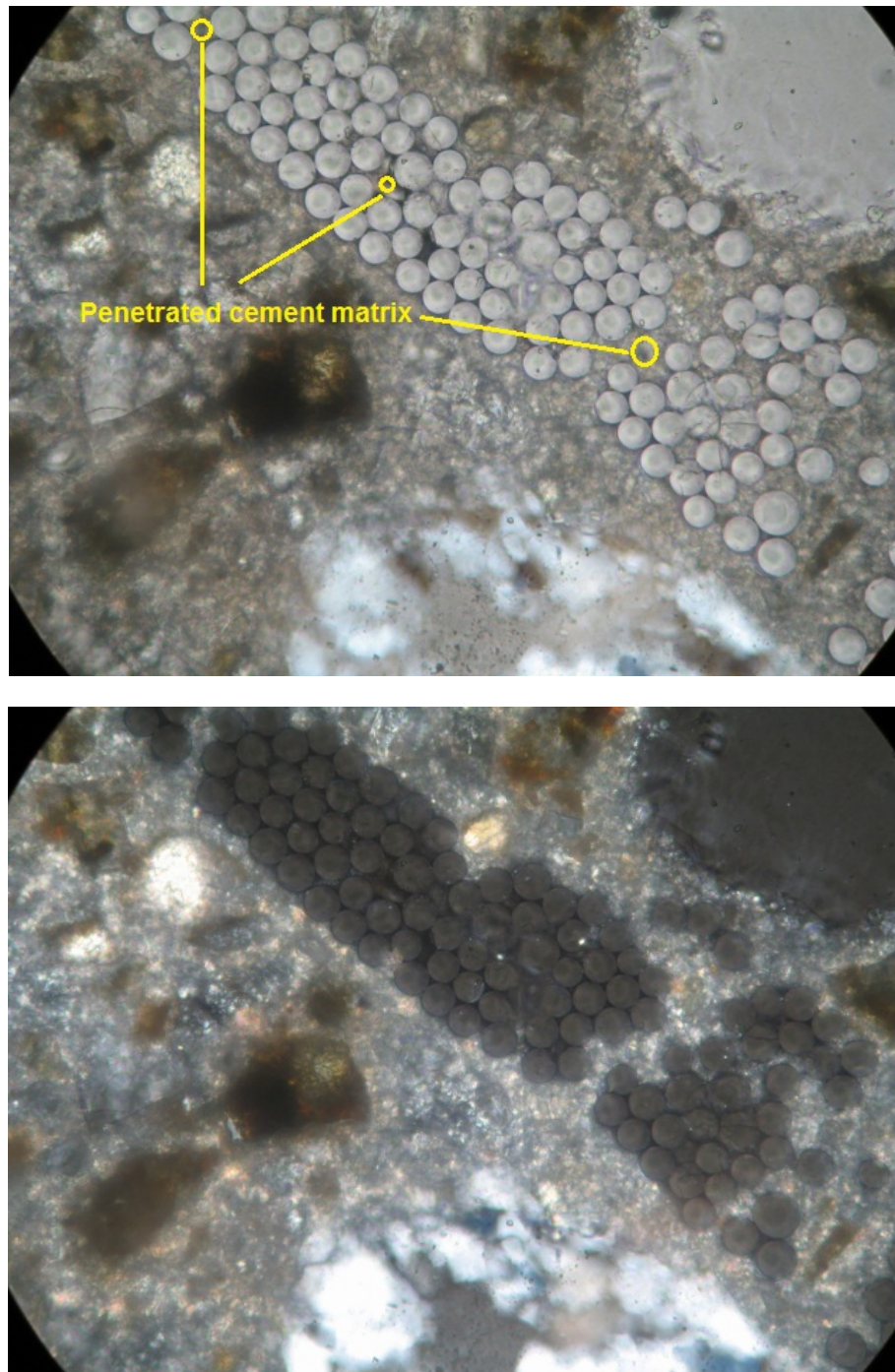


Figure 6.3.1 Observation of unaged Nashrin/GRC composite under plain polarised and uncrossed polarised light (polar at 80 degree), based on a thin section petrography sample made in a previous project; width of field 0.32mm

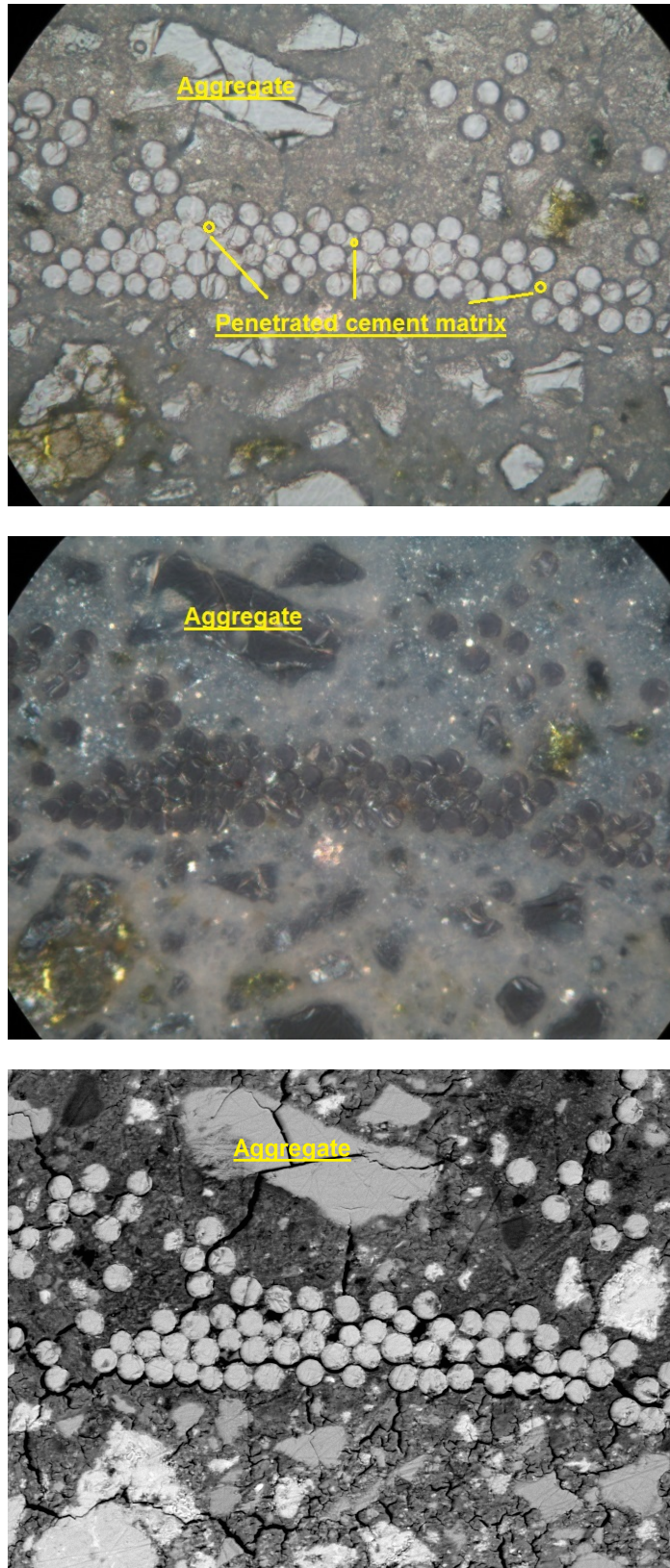


Figure 6.3.2 Observation of 10y-aged Nashrin/GRC composite under (a) plain polarised (b) uncrossed polarised light, polar at 78 degree and (c) backscattered image at the same location, width of field 0.32mm

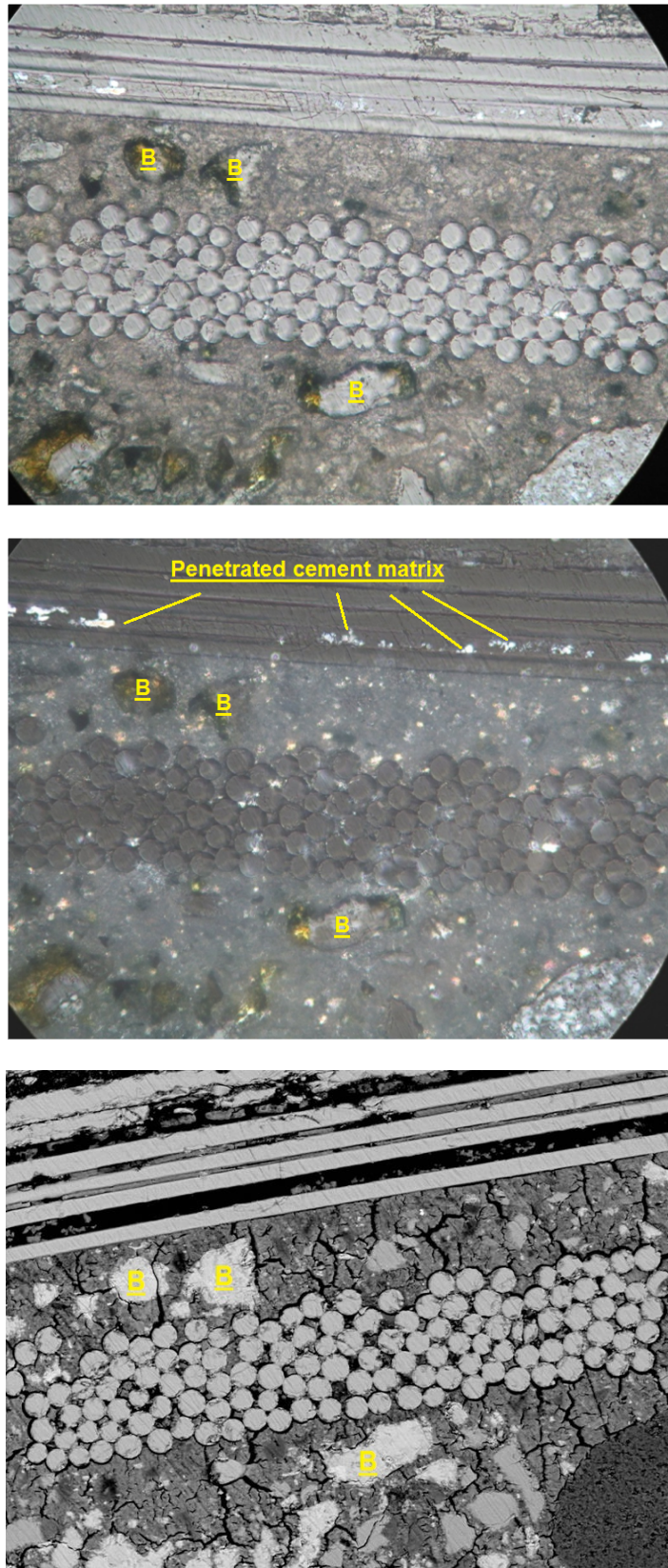


Figure 6.3.3 Observation of 10y-aged Nashrin/GRC composite under (a) plain polarised (b) uncrossed polarised light, polar at 75 degree and (c) backscattered image at the same location, width of field 0.32mm

6.3.2 SEM on polished sample

Ten sites were investigated for each sample with random selection and two representative examples were present in Fig. 6.3.4 and Fig. 6.3.5.

SEM observations on a transverse section of aged petrographic Nashrin/GRC are presented in Fig. 6.3.4. It provides further microstructural studies at the spaces between glass fibre bundle and at the fibre/cement interfacial zone.

A substantially dense microstructure around the glass fibre bundles was observed. It can be seen that matrix has not fully penetrated into the interfilamentary spaces yet after ten years ageing. Lots of those spaces still remained vacant and porous as suggested by the phases with very dark grey scales. At some regions a mixture of hydration products was adhering on the fibre surface intimately or fill the large air voids between fibres.

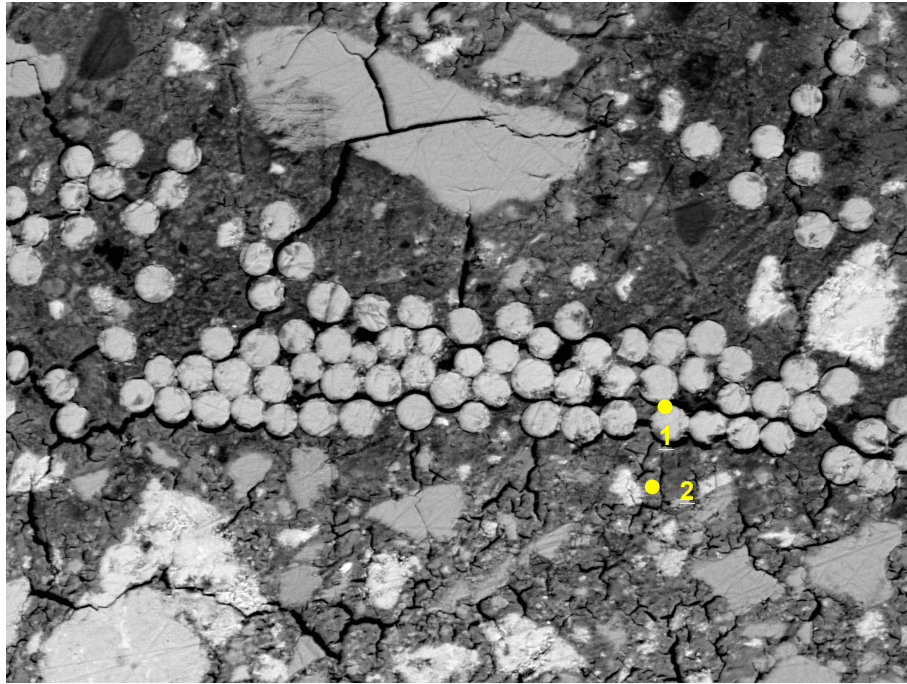
Chemical analysis from Point 1 (representative of the space between glass fibres) demonstrated a clustering of CaO and SiO₂ at the interfilamentary zone, accounting for 46.0 wt.% and 28.4 wt.% respectively, with small amounts of 13.7 wt.% Al₂O₃ and 7.5 wt.% SO₃ included as well. The Ca/Si ratio of Point 1 is 1.74 and the Al/Ca ratio was 0.33. Unhydrated cement clinker displayed as the lightest grey scale in the BSE image and further EDX analysis on Point 2 do confirm this.

Mapping of S showed that there was a sulphur layer along the fibre/matrix interface, also with the inclusions of Ca, Al and small proportions of Si. This proves the chemical composition of the matrix at the interface is different from the bulk. Accumulation of S, Ca, Al and minor Si can be observed in the

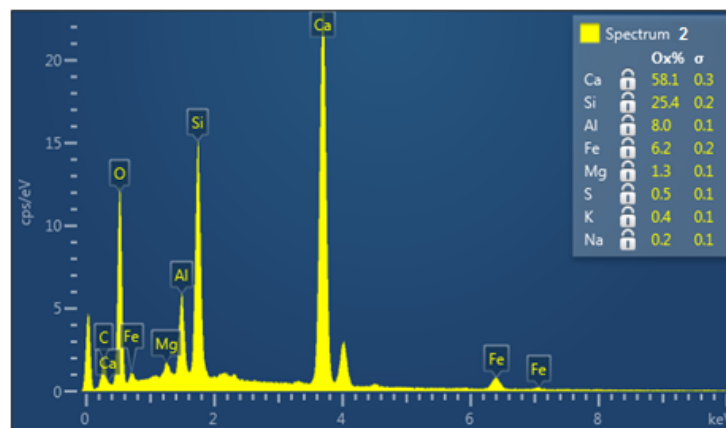
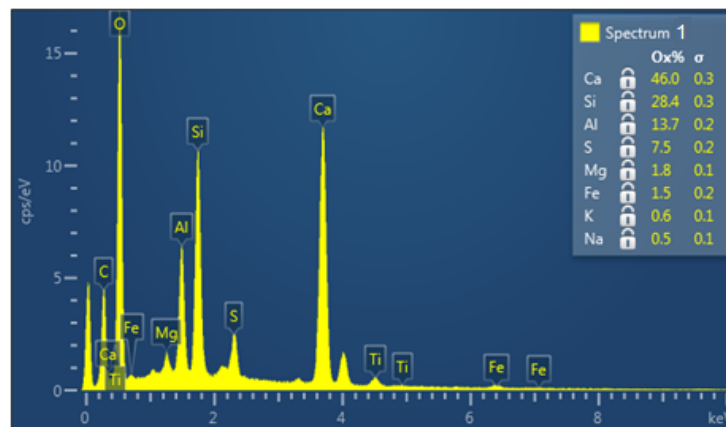
Chapter 6- Results and discussion: GRC

spaces between glass fibres. Detailed chemical information is presented in section 6.3.3. Mappings of Si, Na and Zr indicate their abundance on fibre surface and confirm that the glass fibres used in this project are in SiO_2 - Na_2O - ZrO_2 system.

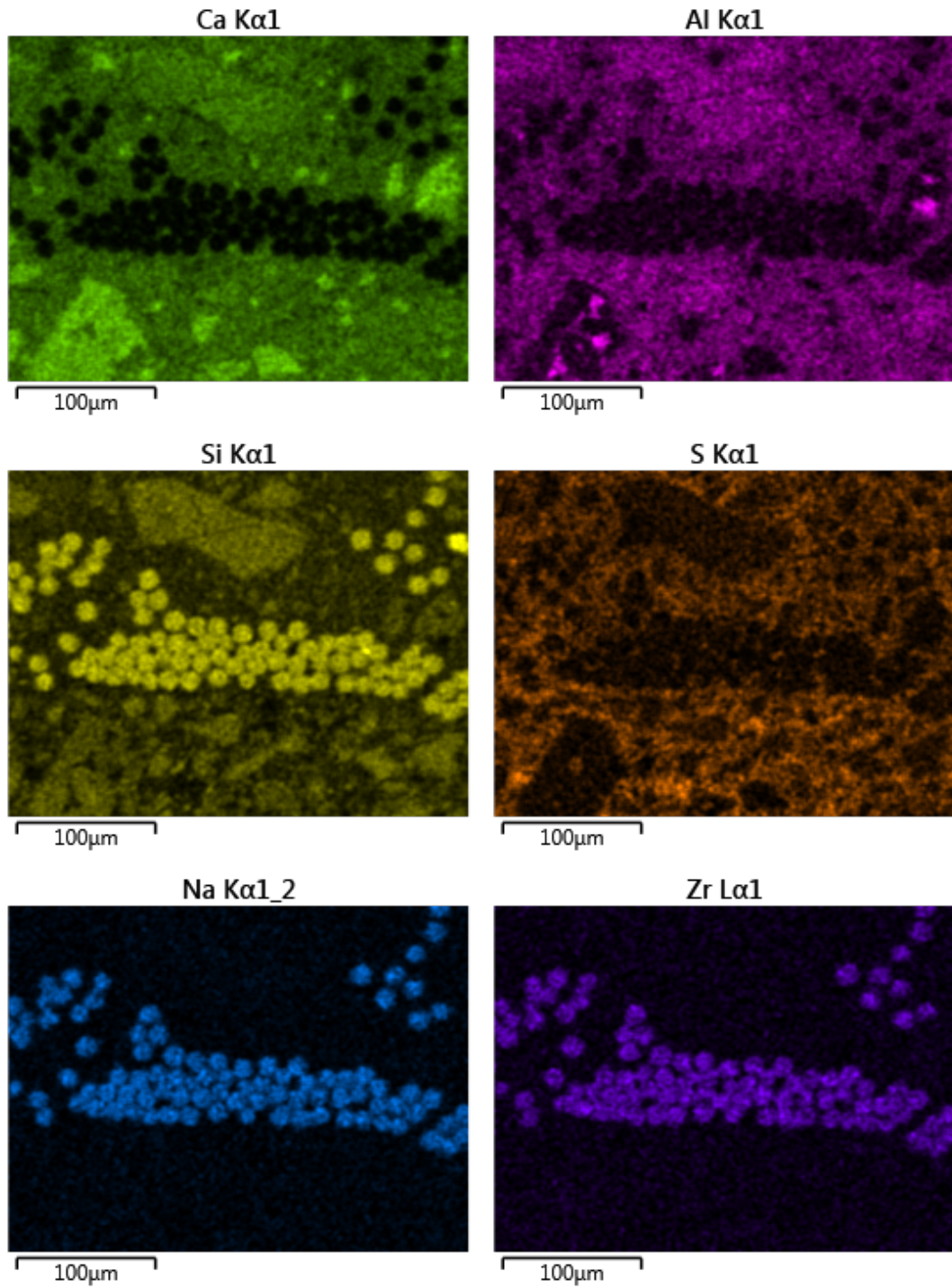
Chapter 6- Results and discussion: GRC



(a) BSE image (the same image as in Fig 6.3.2.c) at a magnification of x400; width of field $326\mu\text{m}$



(b) EDX spot analysis of Point 1 and 2



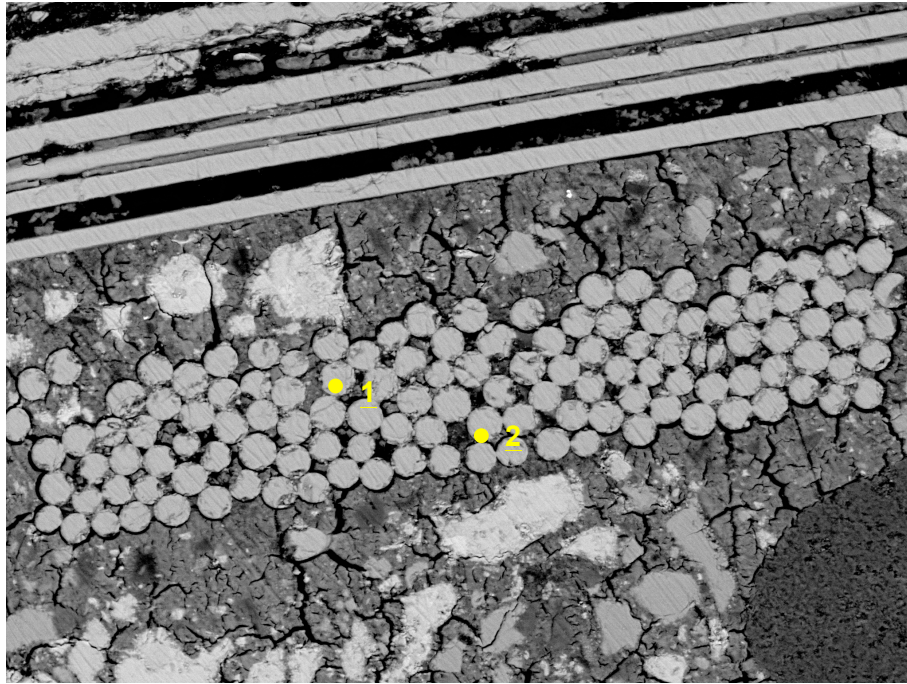
(c) Elemental mappings of Ca, Al, Si, S, Na, Zr

Figure 6.3.4 First example of microstructure of Nashrin/GRC aged for 10 years

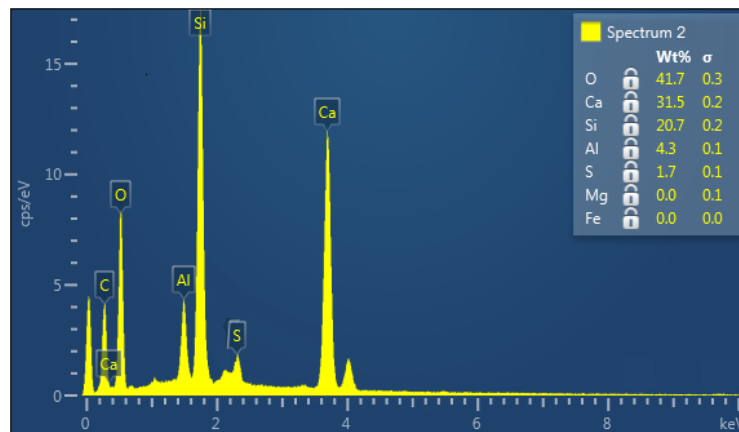
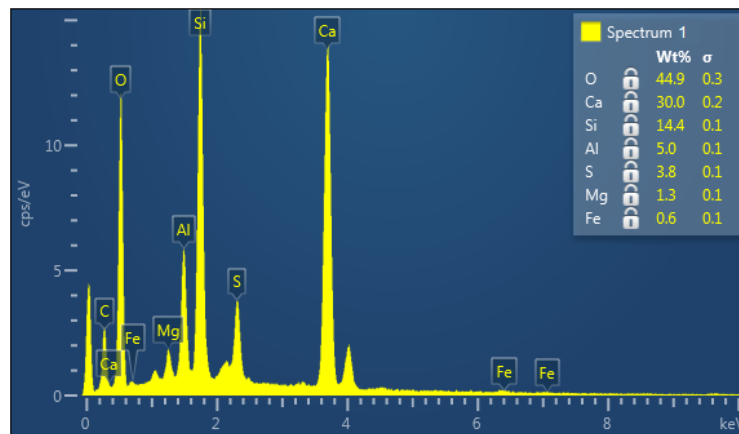
Chapter 6- Results and discussion: GRC

A BSE image containing both horizontal and vertical glass fibres were demonstrated in Fig. 6.3.5. Between the horizontal fibres, most of the spaces remained vacant but there were continuous or clustered hydration products precipitated occasionally, particularly within a limited interfilamentary space. Elemental mappings showed that there were significant amount of CaO, SiO₂ and SO₃ present in the interfilamentary space.

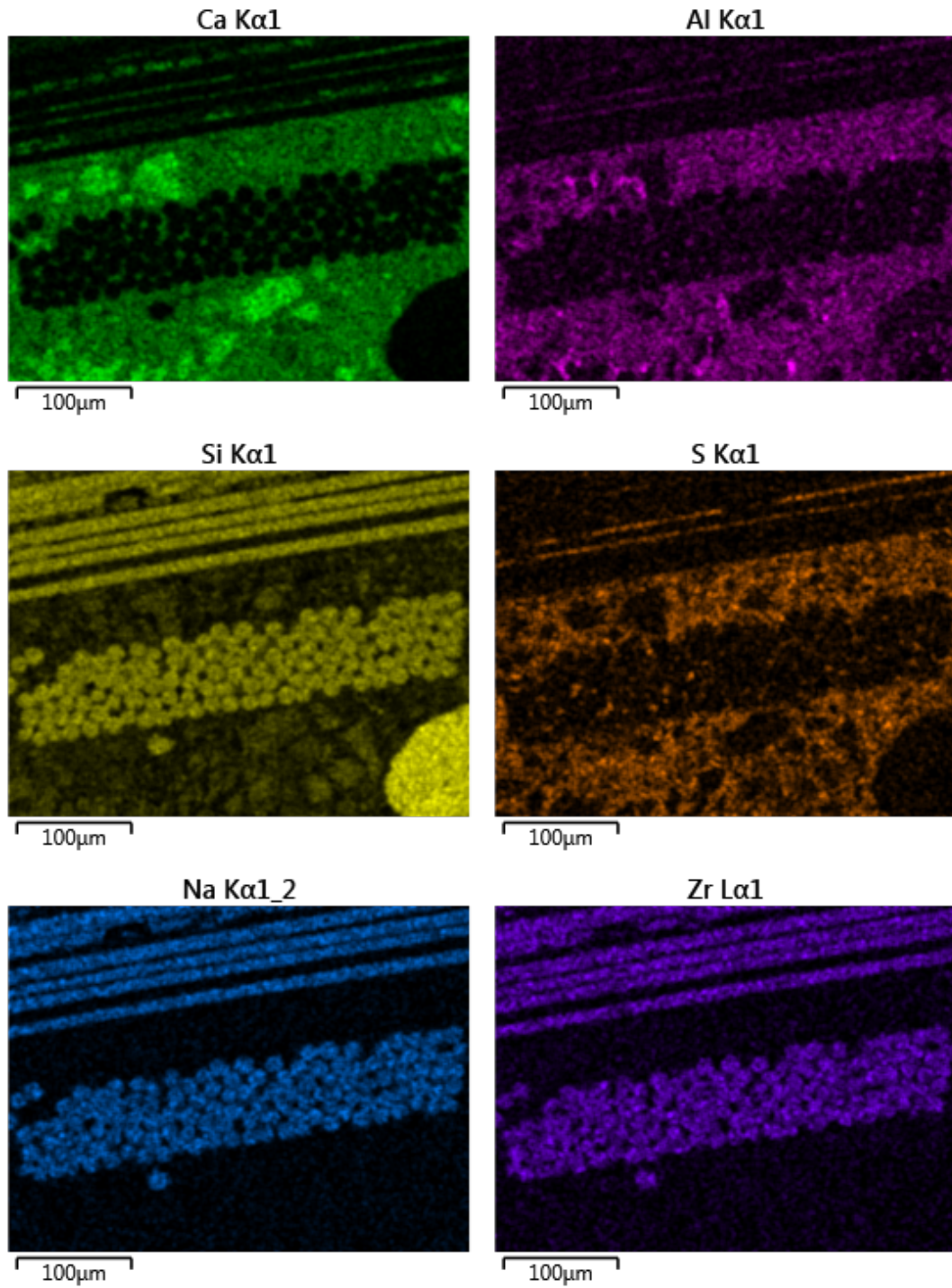
Spot analysis of two representative points was chosen to study the chemical composition of the precipitated hydration products between fibres in Nashrin/GRC. The Ca/Si ratio for Point 1 was calculated to be 1.5 and the Al/Ca was 0.3. For Point 2, a lower Ca/Si ratio of 1.0 and Al/Ca of 0.2 can be identified. Discussion on the spot analysis results is presented in section 6.3.3.



(a) BSE image (the same image as in Fig 6.3.3.c) at a magnification of x400; width of field $326\mu\text{m}$



(b) EDX spot analysis on Point 1 and 2



(c) Elemental mappings of Ca, Al, Si, S, Na and Zr

Figure 6.3.5 Second example of microstructure of Nashrin/GRC aged for 10 years

6.3.3 Microanalysis

The interpretation of interfilamentary phases is not straightforward because most microanalyses are of mixtures of up to four or even more phases admixed on a sub-micrometre scale. Plots of Al/Ca vs. Si/Ca and S/Ca vs. Al/Ca are chosen to investigate the chemical composition of these intermixtures. Owing to the relatively large interaction volume of X-ray signals compared to the narrow space between glass fibres, interference from the glass fibres may occur during microanalysis. This may result in unrealistically high proportions of silicon being recorded and therefore a similarly high Si/Ca ratio. Therefore during the microanalysis, SiO₂ signals originating from the glass fibre should be deducted from the total SiO₂ content. Detailed procedure is illustrated in the previous section 5.7.4.2.

Microanalysis of the interfilamentary space in 10y-aged Nashrin/GRC is shown in Fig. 6.3.6. In the Al/Ca ratio towards Si/Ca ratio plot, a trend line joining bulk C-S-H gel towards the AFt-type phases (Si/Ca=0, Al/Ca=0.33) can be clearly identified, along with some scattered data with slightly higher Al/Ca ratio. The plot of S/Ca towards Al/Ca ratio further indicates that there is a general trend line between the clusters of C-S-H gels towards AFt phases (Al/Ca=0.33, S/Ca=0.5), with a slight deficiency in sulfate. Therefore it can be concluded that the composition of the precipitated interfilamentary hydrated phases in aged Nashrin/GRC composites are mainly C-A-S-H gels finely intermixed with AFt phases at varying levels. The mean Ca/Si ratio of C-S-H gel is 1.1 (n=15, s=0.019), which is slightly lower than the normal range of the previously reported mean Ca to Si ratio 1.2-2.3 of outer C-S-H gel in neat Portland cement paste by Richardson (Richardson, 1999;

Chapter 6- Results and discussion: GRC

Richardson, 2008). The mean Al/Si ratio of the C-S-H data is 0.16 (n=15, s=0.013). This deficiency in calcium and higher Al/Ca ratio property in the C-S-H/AfT intermixture can be attributed to the intrinsic nature of the Nashrin-based materials, which is low in CaO and contains higher amount of Al_2O_3 in comparison to the traditional Portland cement.

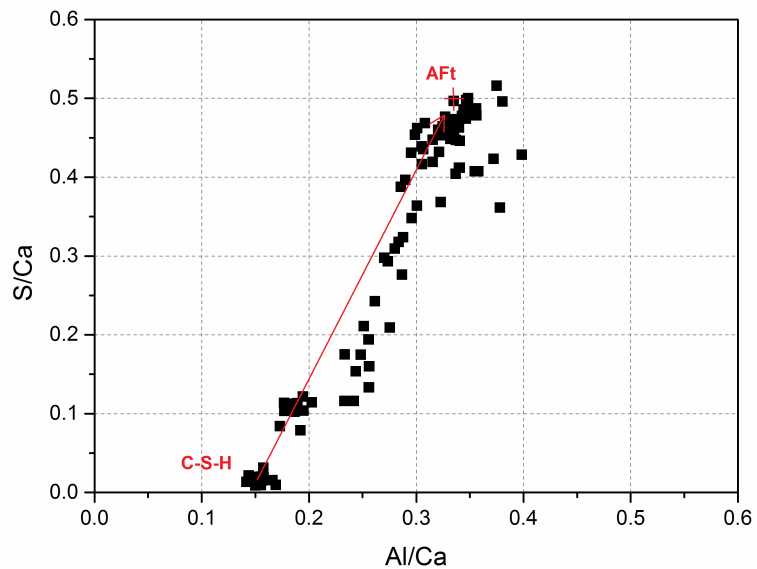
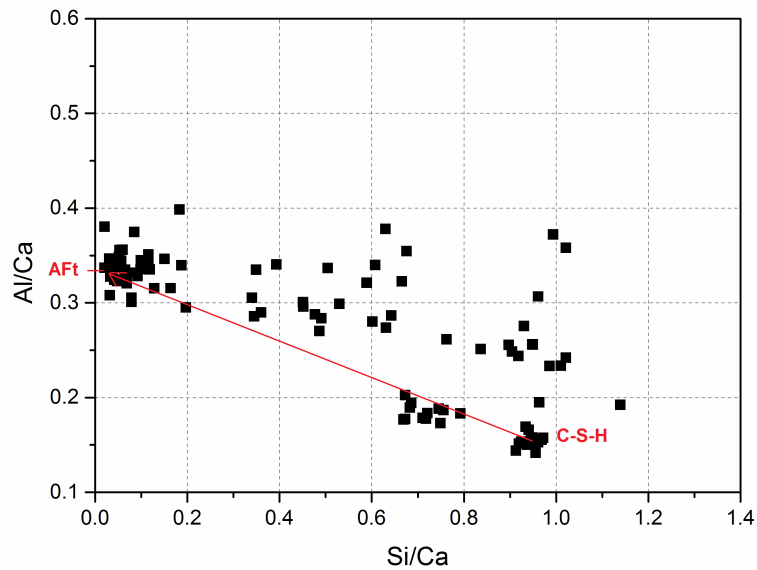
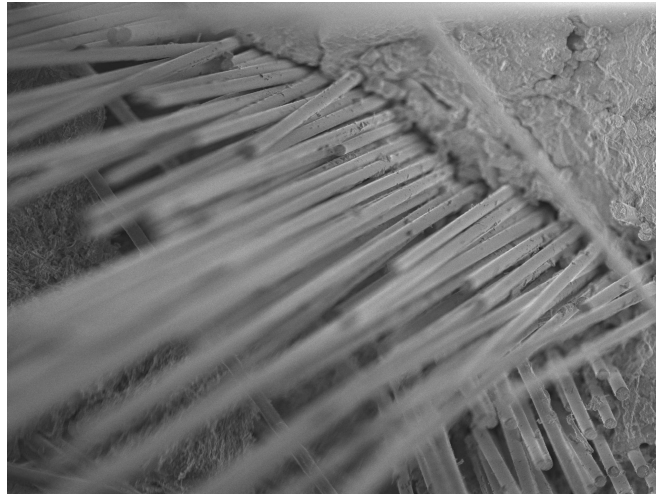


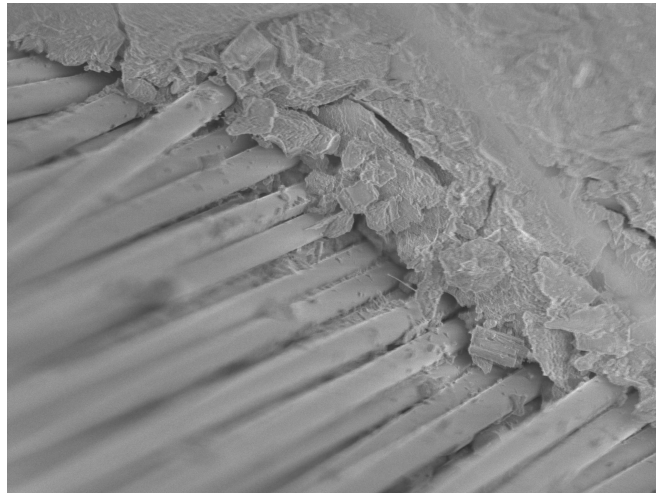
Figure 6.3.6 Scatter graphs of Nashrin-based GRC composites aged for 10 years at 25°C

6.3.4 SEM on fractured surface

Microstructural studies on the fractured surfaces of aged Nashrin/GRC are presented in Fig. 6.3.7. SEM images at different magnifications within the same site are illustrated to characterize the physical conditions at the fibre/cement interfacial zone. Fractured surfaces in Nashrin/GRC demonstrated well-preserved bundled feature of glass fibres after ten years ageing at 25°C. Most of the glass fibres were pulled out rather than fractured, piercing through the bonded bulk cement matrix. This indicates good mechanical properties of GRC composite modified by Nashrin are retained after 10 years. Furthermore, spaces between filaments remained almost vacant, only with small proportions of hydration products partly adhering on the fibre surfaces. The flexibility possessed by individual glass fibre within a bundle confers the ability of flexible movement after cracking of the composite has occurred, which would significantly increase the post-peak toughness of GRC composites. Interfacial zone between matrix and fibres also remains highly flexible, suggested by a porous layer near the surfaces of the outer fibres.



(a) $\times 200$, width of field $652 \mu m$



(b) $\times 500$, width of field $261 \mu m$

Figure 6.3.7 SEM images of fractured 10y-aged Nashrin/GRC at various magnifications

6.3.5 SEM on fibre surface

After ageing for ten years, fibre surfaces were still very smooth only with some layered or clogged hydration products adhering occasionally on the fibre (Fig. 6.3.8). Hardly any fibre weight loss or gross loss could be located on the fibre surface. Severe fibre corrosion cannot be observed on the fibre surfaces.

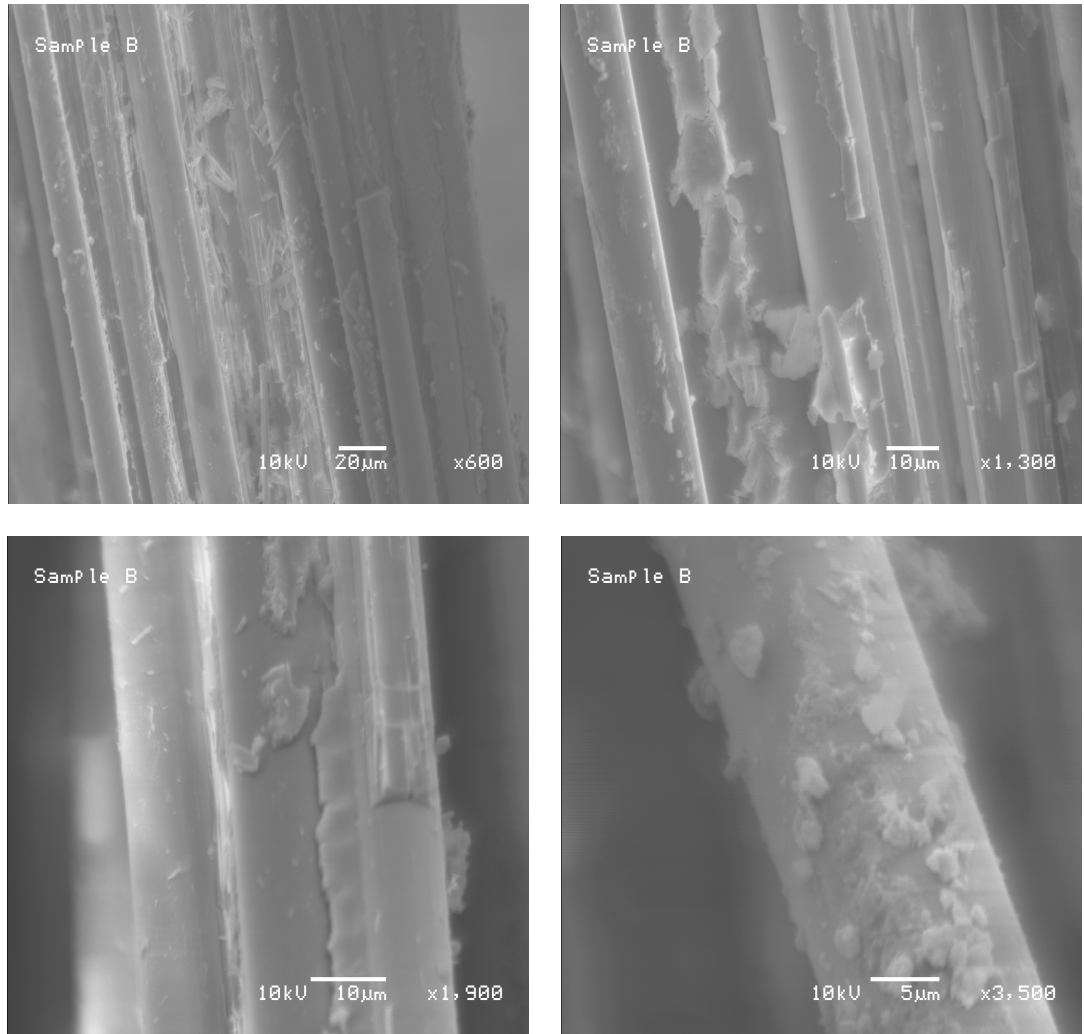


Figure 6.3.8 Microstructure of fibre surfaces in aged Nashrin/GRC composite

6.4 Microstructural study of OPC/GRC

6.4.1 Thin section image

Thin section petrographic specimen of the unaged OPC/GRC was produced in a previous project (Purnell and Beddows, 2005). Compared with the newly produced thin section slides of aged OPC/GRC, they were examined under the petrographic microscope to investigate the general microstructure changes at the interface and spaces between glass fibres.

Chapter 6- Results and discussion: GRC

At early ages the interfilamentary space of OPC/GRC samples (Fig. 6.4.1) was mainly filled with resin, suggesting that the spaces between glass fibres were quite empty at the beginning. When analysed under polarised light, OPC matrix shows crystal precipitation in a small scale near the interfacial zone. This means that matrix is beginning to penetrate into interfacial space partially along the perimeter of glass fibres.

After ageing for 10 years at 25°C, OPC matrix has significantly occupied the interfilamentary space (Fig. 6.4.2). And crystalline CH deposits, identified by its unique birefringence colour as yellowish orange, were accumulating at part of the interfacial zone. The microstructural changes with ageing are indicative of progressive hydration phase densification within the glass fibres and its impact on mechanical performances is further discussed in section 6.5.

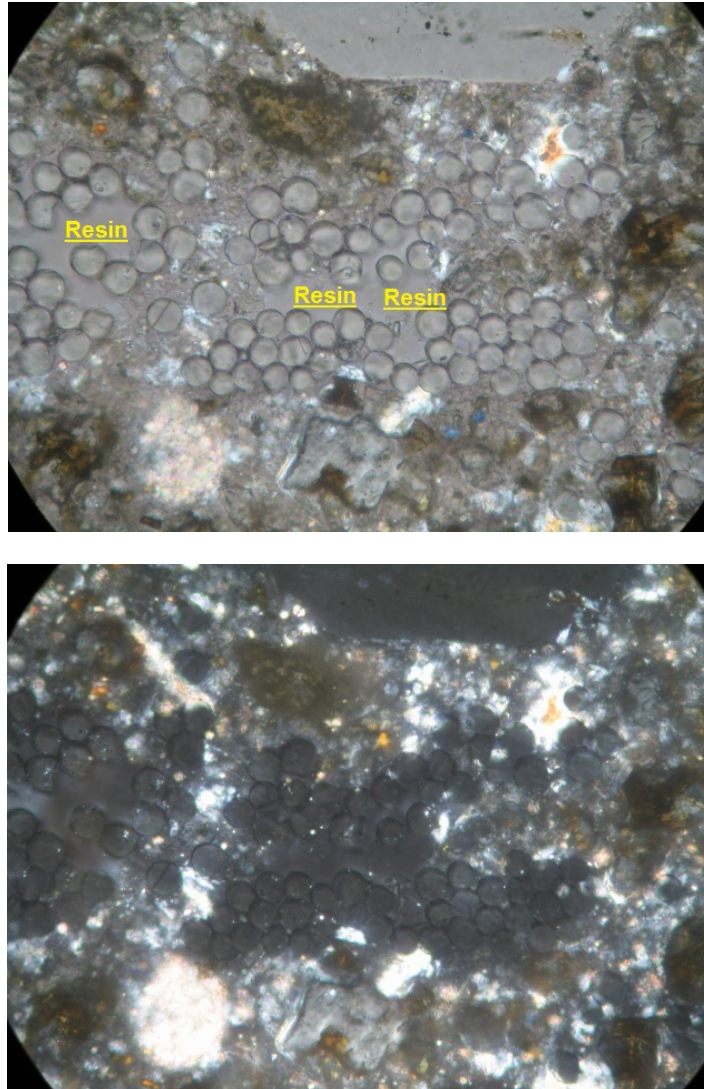


Figure 6.4.1 Thin section images of OPC-based GRC aged for 28 days at 25°C, under partial plain polarised and crossed polarised light, based on a thin section petrography sample made in a previous project; width of field 0.32mm

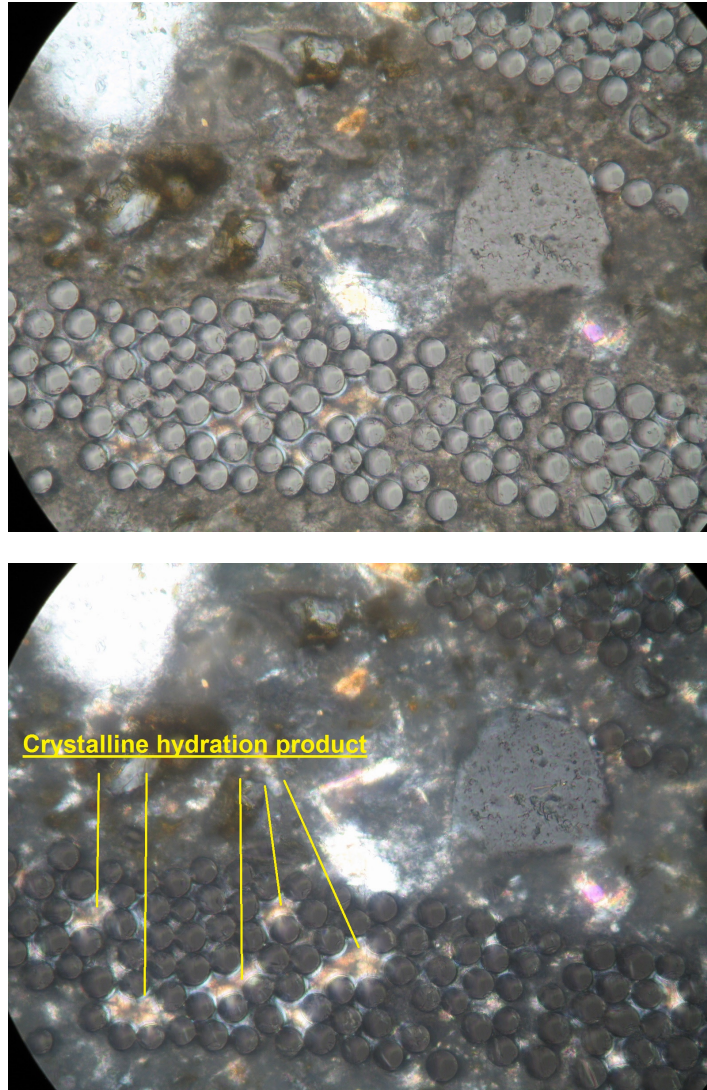


Figure 6.4.2 Thin section images of OPC-based GRC aged for 10 years at 25°C, under partial plain polarised and crossed polarised light, width of field 0.32mm

6.4.2 SEM on polished sample

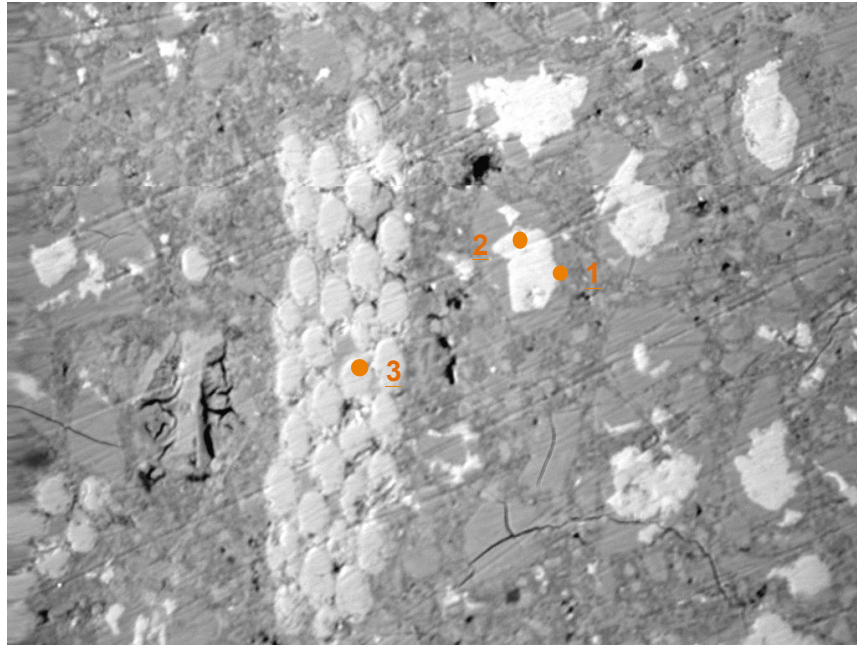
SEM observations were applied to study the microstructure in aged OPC/GRC; ten images were taken randomly and one representative example (in Fig. 6.4.3) was included below.

Microstructure of aged OPC/GRC composite (in Fig. 6.4.3) indicated that spaces between glass fibres were significantly densified with penetrated hydration products, with almost no porosity, significantly limiting the flexibility

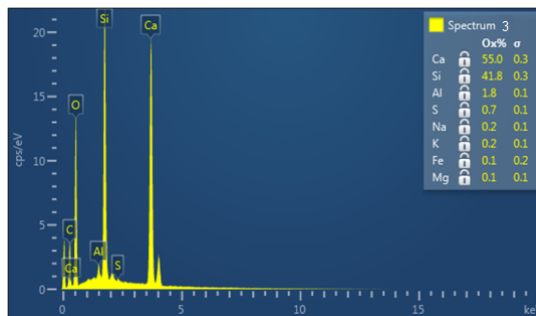
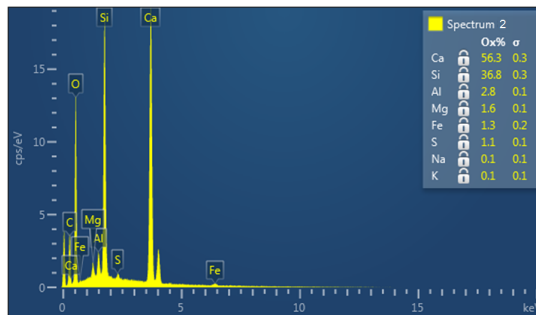
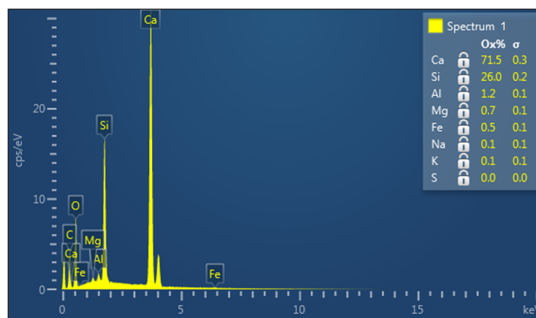
of the glass fibre bundles. It was mainly filled with massive hydration products of CH according to its light greyscale and it is mainly dominated by the elements of CaO, as suggested by the calcium elemental mapping. Large amounts of isolated unhydrated clinker was observed within the matrix (represented by Point 1), surrounded by inner products with various thickness ranging within few micrometres. EDX analysis of the inner product was studied by Point 2; its chemical compositions were dominated by CaO and SiO₂ with a Ca/Si ratio of 1.1. For these interfilamentary hydration products, the Ca/Si ratio was calculated to be 0.9 by EDX analysis (represented by Point 3). This is slightly lower than the Ca/Si ratio for inner product.

Traces of sulphur and aluminium were absent from the interfilamentary space according to elemental mappings; this eliminates the possibility of Aft and/or AFm phase formations at this interfacial zone. The calcium mapping reveals that calcium has penetrated far further into the interfilamentary spaces during ageing compared to Nashrin composites (see 6.3.4.c above), forming calcium-concentrated products, which could possibly be CH or CaCO₃ structures, and/or with the intermixture of C-S-H gels at various levels (further discussed in section 6.4.3). It leaves a considerably intimate contact between the embedded glass fibres. Abundance of sodium and zirconia observed on the fibre surface proves that these glass fibres involved in this project belong to AR glass fibres, which are based on the Na₂O-SiO₂-ZrO₂ systems.

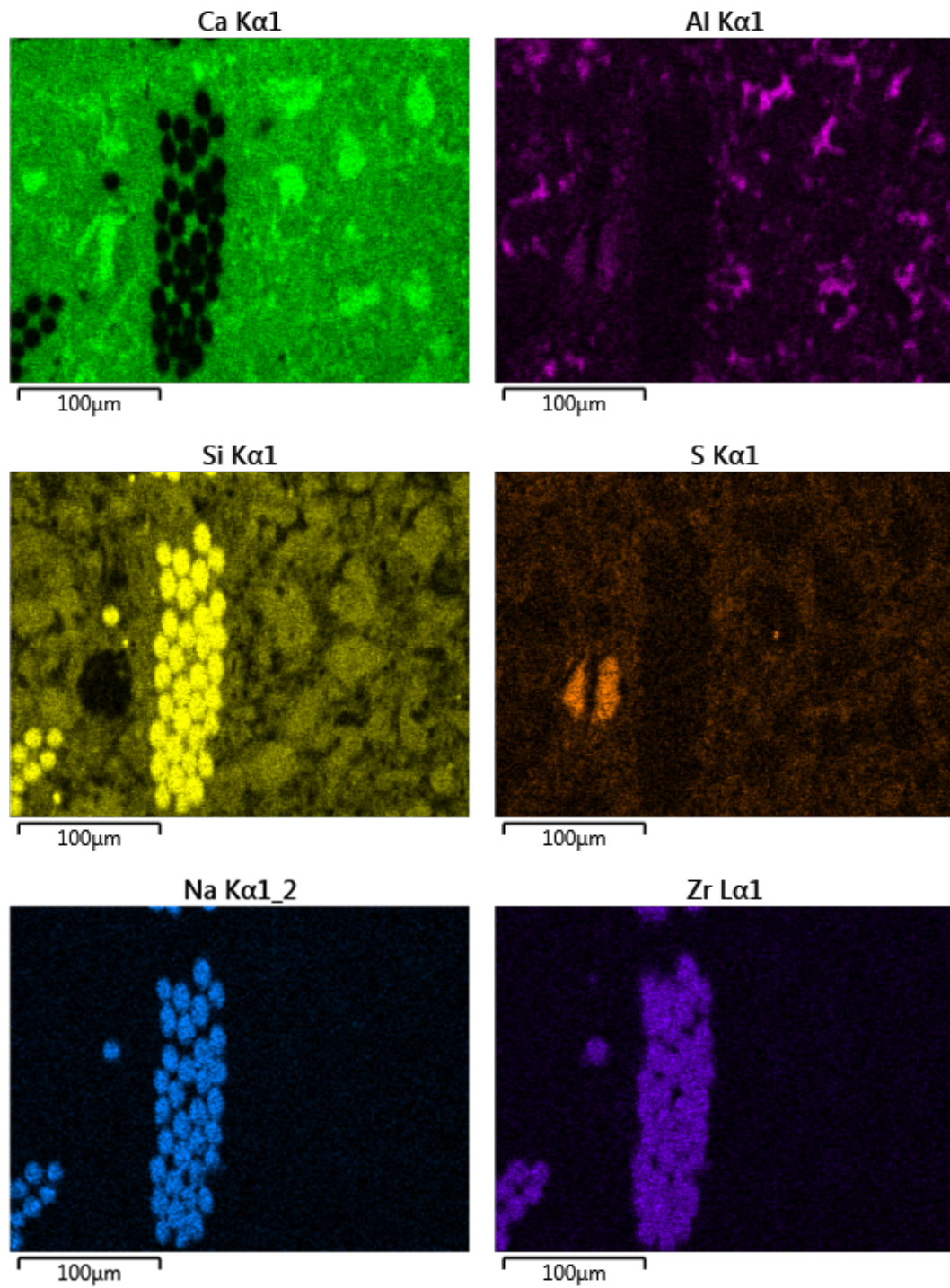
Chapter 6- Results and discussion: GRC



(a) BSE image at a magnification of x400; width of field 326 μ m



(b) EDX spot analysis on Point 1, 2 and 3



(c) Elemental mappings of Ca, Al, Si, S, Na and Zr

Figure 6.4.3 Microstructure of OPC/GRC aged for 10 years at 25°C

6.4.3 Microanalysis

As illustrated in section 5.7.4.2, SiO₂ content examined in EDX spot analysis has been corrected in order to remove the interference of SiO₂ that is originating from the glass fibres. Plots of Al/Ca vs. Si/Ca and S/Ca vs. Al/Ca are shown in Fig. 6.4.4.

The Al/Ca against Si/Ca plot indicated the existence of C-S-H gels at the spaces between glass fibres, and the data exhibited a tendency towards the origin of the plot, which represents the CH. The S/Ca against Al/Ca plot further confirmed the intermixture of CH and C-S-H, in which a cluster of data can be seen in the vicinity of the origin point with deficiency of sulphur and aluminium. Therefore a conclusion can be drawn that an intermixture of C-S-H gels and CH is precipitated at the spaces between glass fibre filaments. The mean Ca/Si ratio is 1.5 (n=8, s=0.017) and the Al/Si ratio is 0.03 (n=8, s=0.005). The mean Ca/Si ratio is in agreement with the reported value in literature in the range of 1.2-2.3 for neat Portland cement (Richardson, 2008; Richardson, 1999; Diamond and Bonen, 1995; Lecomte *et al.*, 2006; Famy *et al.*, 2002).

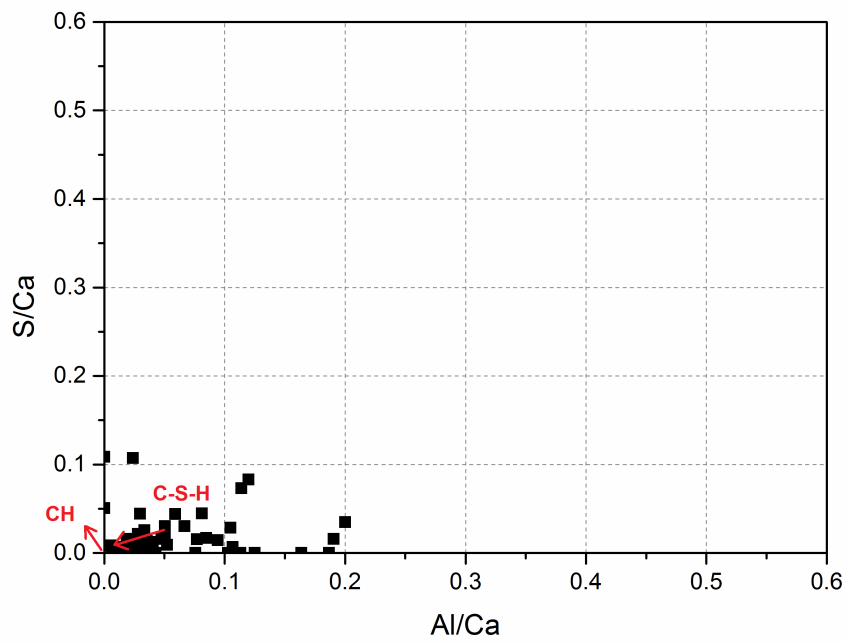
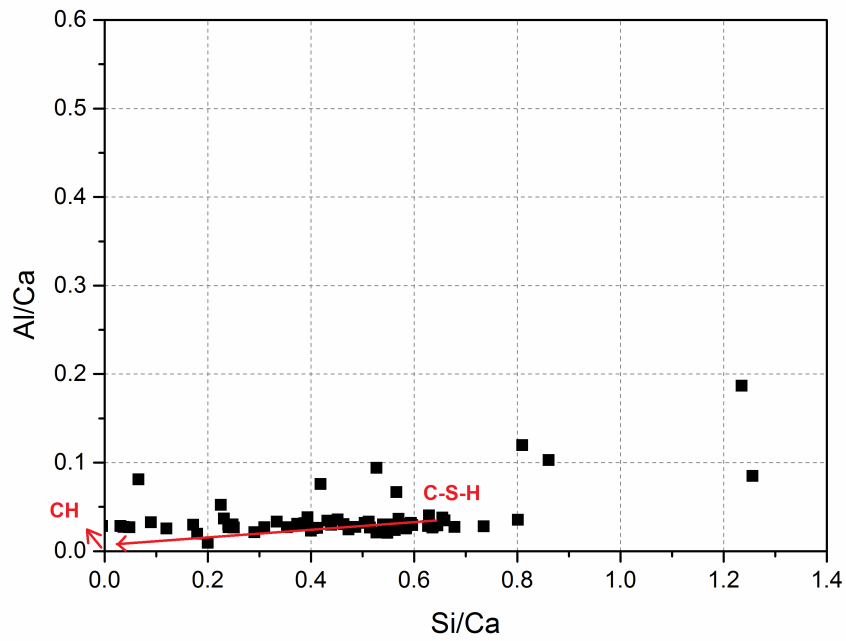
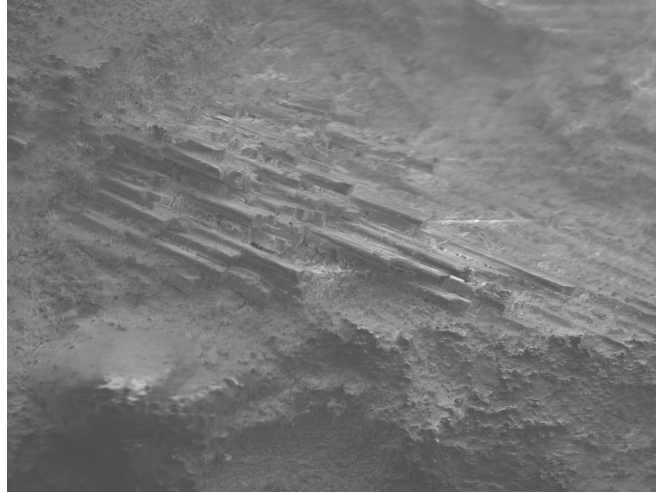


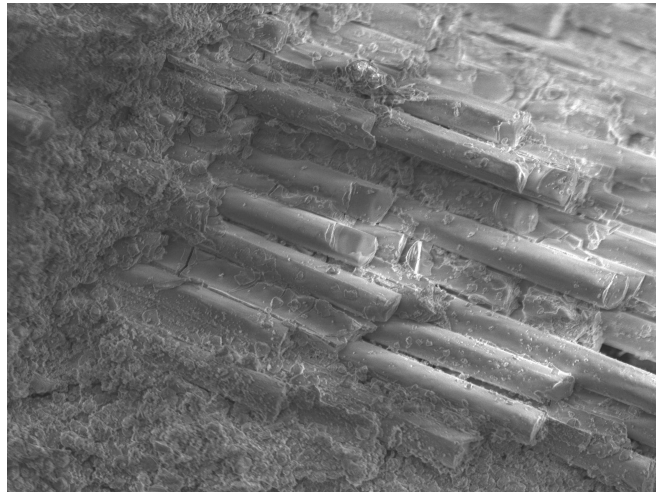
Figure 6.4.4 Scatter graphs of OPC/GRC composites aged for 10 years at 25°C

6.4.4 SEM on fractured surface

For the 10y-aged OPC/GRC composites, observation of the fractured surfaces (Fig. 6.4.5) showed significant fracturing of glass fibres, presenting in a quasi-conical array of glass fibres. Spaces between filaments were significantly densified by infilling with precipitated intermixtures of C-S-H gels and CH (see Fig. 6.4.4), making it an extremely rigid structure. Bundle filling may also lead to detrimental reinforcement embrittlement and fibre reinforcement would consequently lose its ability to provide toughness in GRC to some extent. There was an intimate contact between matrix and fibre bundle with almost no gap observed even at a higher magnification of $\times 500$. This dense interface would be less able to arrest cracks upon reaching the interfacial zone and cracks therefore would propagate quickly afterwards. Different magnifications at the same site are used to have a closer investigation of the interface morphology in the 10y-aged GRC non-modified composites.



(a) X200, width of field $652\mu\text{m}$



(b) X500, width of field $261\mu\text{m}$

Figure 6.4.5 SEM images of fractured 10y-aged OPC/GRC at various magnifications

6.4.5 SEM on fibre surface

Significant fibre corrosion can be observed in aged OPC/GRC composites (Fig. 6.4.6). Severe loss in smoothness happened at some regions along the fibre. In particular, considerable fibre volume loss can be observed and also portion of the coatings were peeling off from the fibre. This entire

Chapter 6- Results and discussion: GRC

phenomenon indicated that severe fibre corrosion happened in OPC/GRC composites after 10 years ageing.

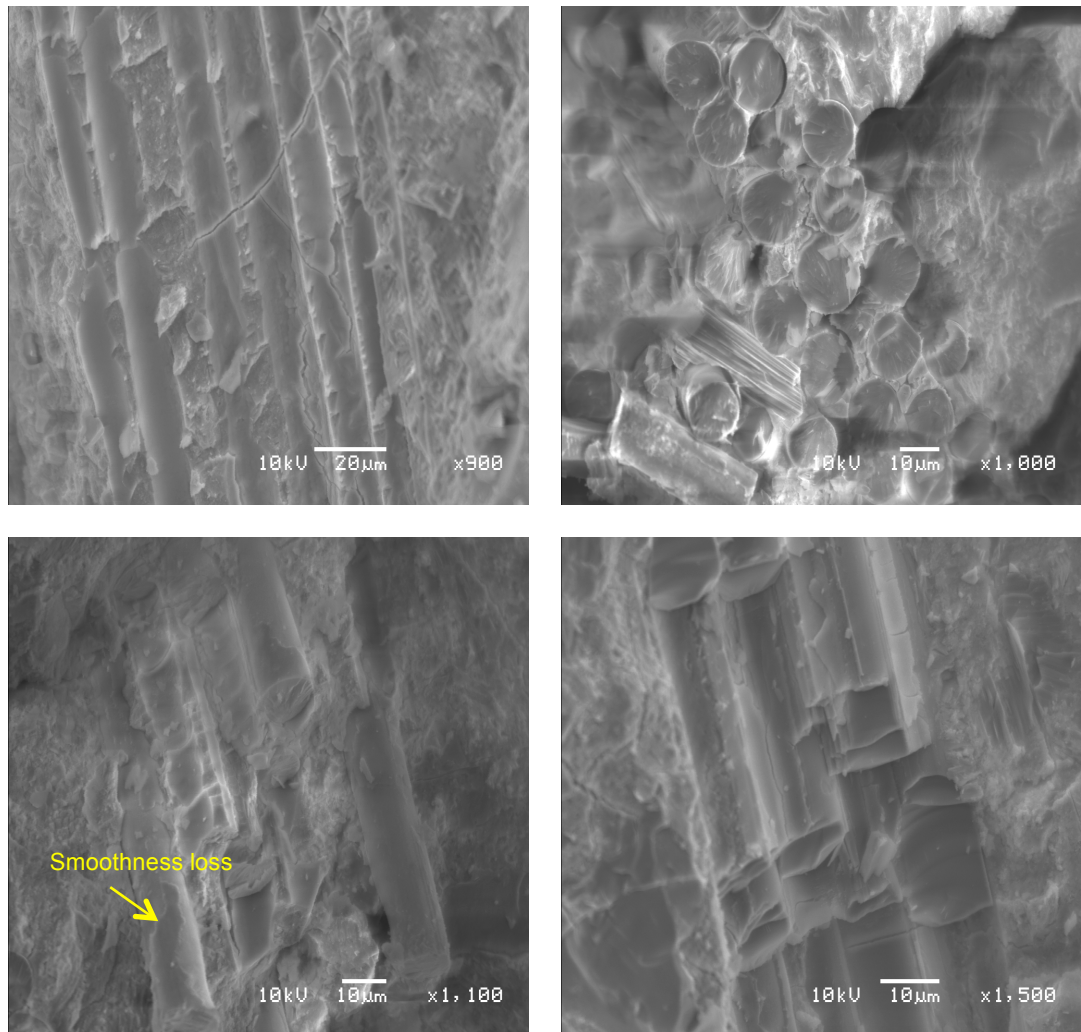


Figure 6.4.6 Microstructure of fibre surface in aged OPC/GRC composite

6.5 Bending tests

Two thin slabs of both aged OPC/GRC and Nashrin/GRC (225mm × 55mm × 10mm) were used for bending tests. Bending data for the unaged composites were extracted from a previous study (Purnell and Beddows, 2005).

Chapter 6- Results and discussion: GRC

Stress-strain properties of unaged GRC composites made by two formulations (i.e. OPC, Nashrin) are shown in Fig. 6.5.1. Comparable bending performances can be found in those two types of GRC composites, with MOR of 27MPa for OPC/GRC and 30MPa for Nashrin/GRC respectively. Both materials are significantly ductile, having an ultimate strain value of ~0.8%.

Fig. 6.5.2 shows the effects of long-term natural ageing (i.e. 10 years immersion at 25°C) on the flexural stress-strain relationship of the OPC and Nashrin-based composites. With ageing, the stress property of OPC/GRC remains almost unchanged only with a slight decrease in MOR from 27MPa to 26MPa. However, the composites have become extremely brittle, with an ultimate strain of only ~0.09%. Glass fibres therefore have lost their function to compensate the low toughness of cement mortar. Such stress variation with strain could be explained by the observation that a visible crack occurred immediately once the load was applied. But the fibres were weakened chemically and/or affected by interfacial deposition of CH physically, such that they cannot arrest the crack growth or bridge the growing crack. Consequently it led to the catastrophic loss of toughness in OPC composite. The microstructure observed on the fractured surfaces (Fig. 6.4.5) also confirms such mechanism causing the strength degradation of the OPC composite.

In contrast, Nashrin/GRC exhibited significantly less reduction in toughness after 10 years normal ageing. The ultimate strain value reduced to 0.55% after 10 years, an order of magnitude larger than that of 0.09% for the aged OPC/GRC. The fibres still showed considerable ability to carry load alone by

Chapter 6- Results and discussion: GRC

bridging cracks development. However, composite strength of the normal aged composite maintained almost the same as that in the unaged sample; MOR changed from 30MPa in the unaged to 32MPa after ageing for 10 years. This is inconsistent with the previous accelerated ageing testing, in which medium composite strength reduction was observed (further discussed in section 8.3). These results improved confidence in the widespread application of CSA cement modified matrix in GRC industry.

Chapter 6- Results and discussion: GRC

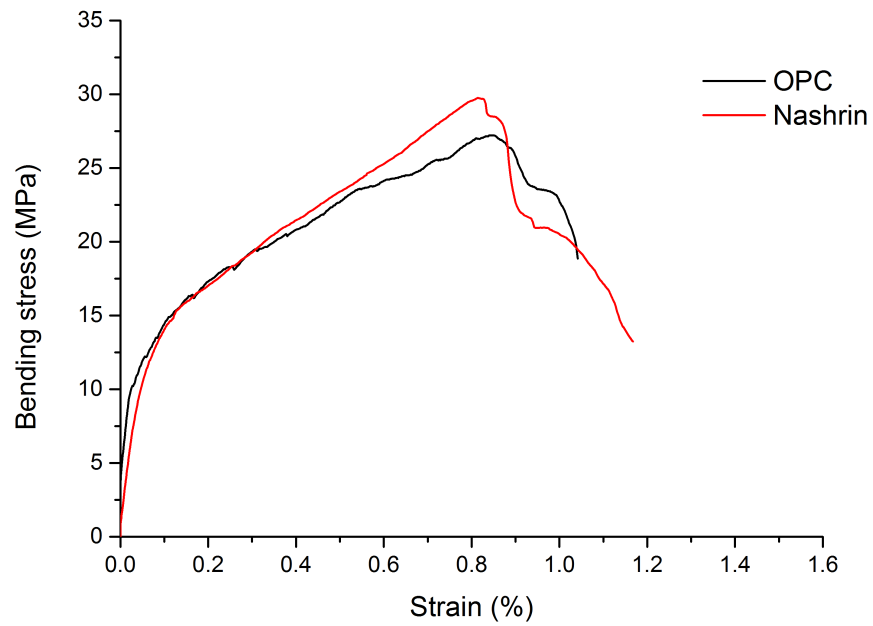


Figure 6.5.1 Stress-strain curves for unaged GRC composites, data from reference (Purnell and Beddows, 2005)

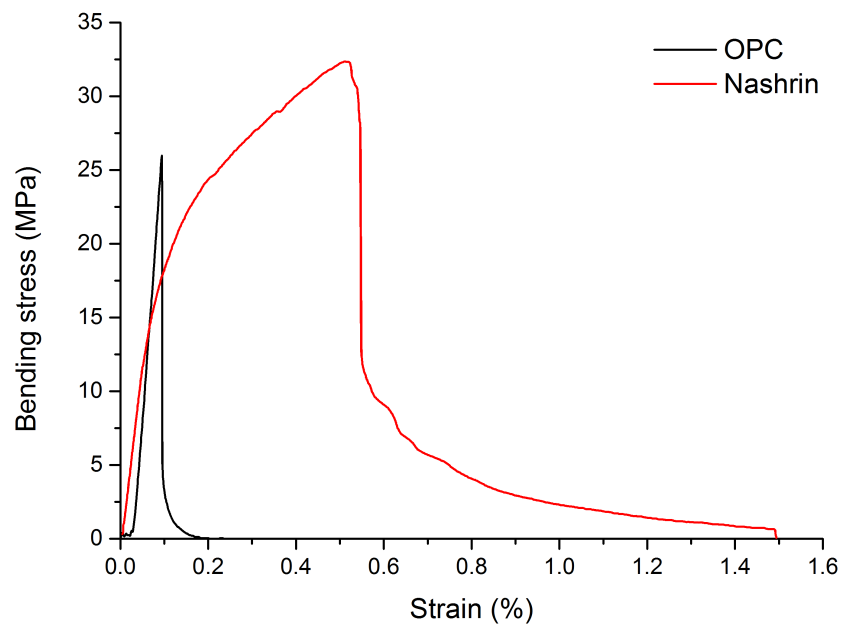


Figure 6.5.2 Stress-strain curves of GRC composites aged for 10 years

6.6 Summary of main findings

After ageing for 10 years at 25°C, significant difference has been observed between OPC/GRC and Nashrin/GRC in terms of microstructural evolution, failure mode and mechanical performances.

In the aged Nashrin/GRC composites, intermixture of C-S-H gel and ettringite are penetrating into the interfilamentary spaces but the overall spaces between glass fibres remain quite porous. It exhibit desirable composites mechanical properties after 10 years ageing; most of the toughness are still retained, making the material possess high proportion of ductility as well as composite strength. Microstructural study on a fractured surface further helps to explain its desirable mechanical performance. Most of the glass fibres are pulled out rather than fractured, spaces between fibres are quite vacant and interfacial zone between fibre and cement are significantly empty; all these beneficial microstructural features offer fibre the flexibility when forces are applied.

The aged OPC composites indicate considerably more brittle behaviour and both interfilamentary and interfacial zone showed severe densification with the ingress of intermixed CH and C-S-H at a fine scale. Severe fibre fracturing can be observed on the fractured surface, losing the bundled feature of glass fibres. However, there are insignificant changes in composite strength in with ageing in OPC/GRC.

Chapter 7- Results and discussion: Steel reinforced concrete

Hydration of CSA cement pastes at different ages (i.e. 7d, 28d, 90d and 1.5y) is studied in this chapter. In both 28d and 1.5y-aged steel reinforced CSA concrete, microstructural features at the interface are compared to the corresponding OPC concrete. Quantitative image analysis results at the interface are present in this chapter, by calculating different atomic ratios (Ca/Si, Al/Ca and S/Ca) as a function of distance away from steel.

7.1 DTA

7.1.1 CSA paste

DTA curves of hydrated CSA cement pastes with different curing regimes are presented in Fig. 7.1.1. In the sample cured for 7 days at 21°C, a prominent endotherm at 125°C is indicative of the generation of ettringite, although there may be interference from dehydration of CAH_{10} at similar temperatures (Scrivener and Campas, 2003; Berger *et al.*, 2011). Ettringite starts to form at the beginning of hydration (e.g. after 1 hour) until 2 days when gypsum is still available. Formation of CAH_{10} in hydrated CSA cement is rarely discussed in literature, probably from the hydration of Ye'elimite and belite in CSA cement. The subsequent broad endotherm at about 160°C has been assigned to the dehydration of stratlingite (C_2ASH_3) (Almusallam, 2001), produced from the reaction between remaining belite phases and aluminium hydroxide gels. The obvious step at 180-200°C is normally

associated with the presence of monosulfate. Monosulfate is produced from the hydration of calcium sulfoaluminate providing gypsum is consumed.

It is found out that with the progress of hydration for up to 90 days, endotherm within 125-180°C has become considerably broader and larger; there are no clear boundaries between those designated peaks for ettringite, CAH_{10} and stratlingite. The prominent peak is slightly shifting towards higher temperature, revealing a relative predominance of stratlingite over ettringite over curing for up to 90 days.

After curing for 1.5 years, significant changes have occurred regarding the hydration products in hydrated CSA cement. Small and broad peaks at ~120°C and 160°C still exist, correlating to the presence of ettringite, CAH_{10} and stratlingite respectively. But the most prominent peak is shifted to temperatures at ~200°C, which indicates the abundance of monosulfate in hydrated CSA paste, instead of ettringite, CAH_{10} and/or stratlingite for those early age samples. There is an additional small peak at ~300°C in the 1.5y-aged sample; this can be related to the formation of C_3AH_6 , which is supposed to derive from the conversion reaction of CAH_{10} with increasing curing periods (further discussed in section 7.2.1). Water loss of crystalline aluminium hydroxide is traceable in all the hydrated CSA cements with different curing ages, corresponding to a small blip at the steps between 280 and 300°C in DTA curves.

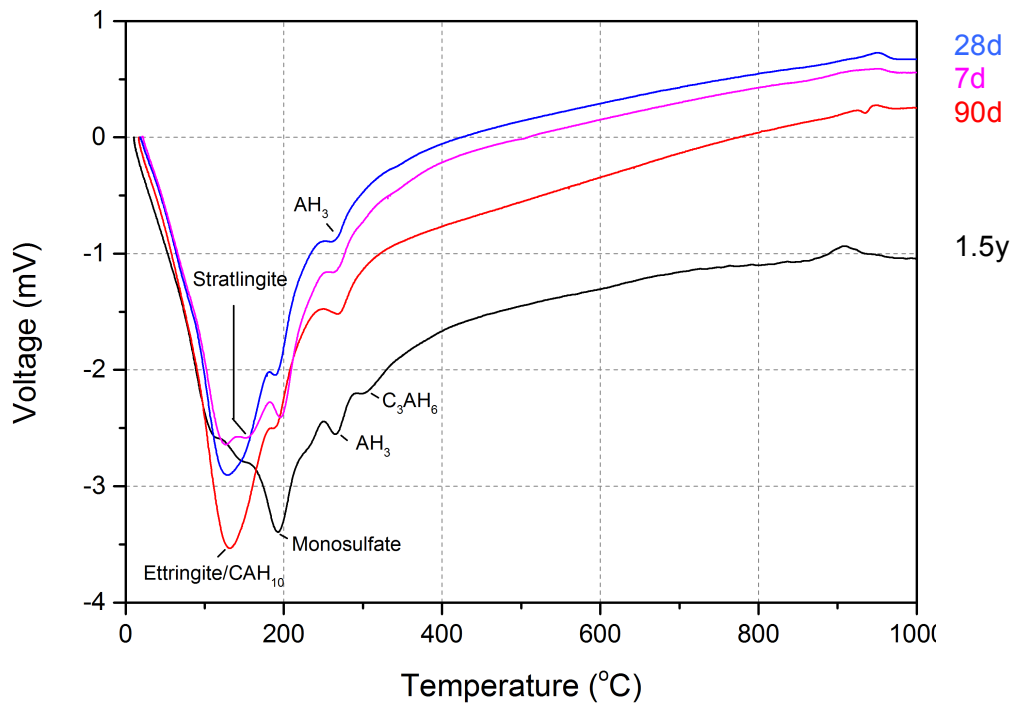


Figure 7.1.1 DTA results of CSA paste cured at 21°C for 7, 28, 90 days and 1.5 years

7.1.2 OPC paste

DTA curves of hydrated OPC paste cured at four different ages (i.e. 7 days, 28 days, 90 days and 1.5 years) are presented in Fig. 7.1.2. The curves within range of 100-130°C consist of three overlapping peaks, with a strong central endotherm at ~120°C. They can be corresponded to the evaporation of weakly bound pore water, dehydration of C-S-H gel and ettringite respectively, in the order of increasing dehydration temperatures. With curing age for up to 90 days, the strongest peak in the DTA curve becomes broader and larger, interfered by the increased formation of C-S-H gel. Subsequent considerably broad peak at ~170°C suggests the generation of AFm during hydration.

However in the 1.5 years-aged samples, these three broad endotherms at 100-170°C exhibit relatively comparable sizes, instead of a very strong central peak contained in samples at earlier ages. This indicates the decreased content of weakly bound pore water and massive formation of AFm phases in hydrated OPC pastes with the on-going curing.

The subsequent step at about 420°C is always associated with CH formation, which remains as one of the main hydration products in hydrated OPC pastes at all investigated ages. Relatively weak endotherm at 700°C in the DTA curves relates to the presence of calcite, which mainly results from the carbonation of CH.

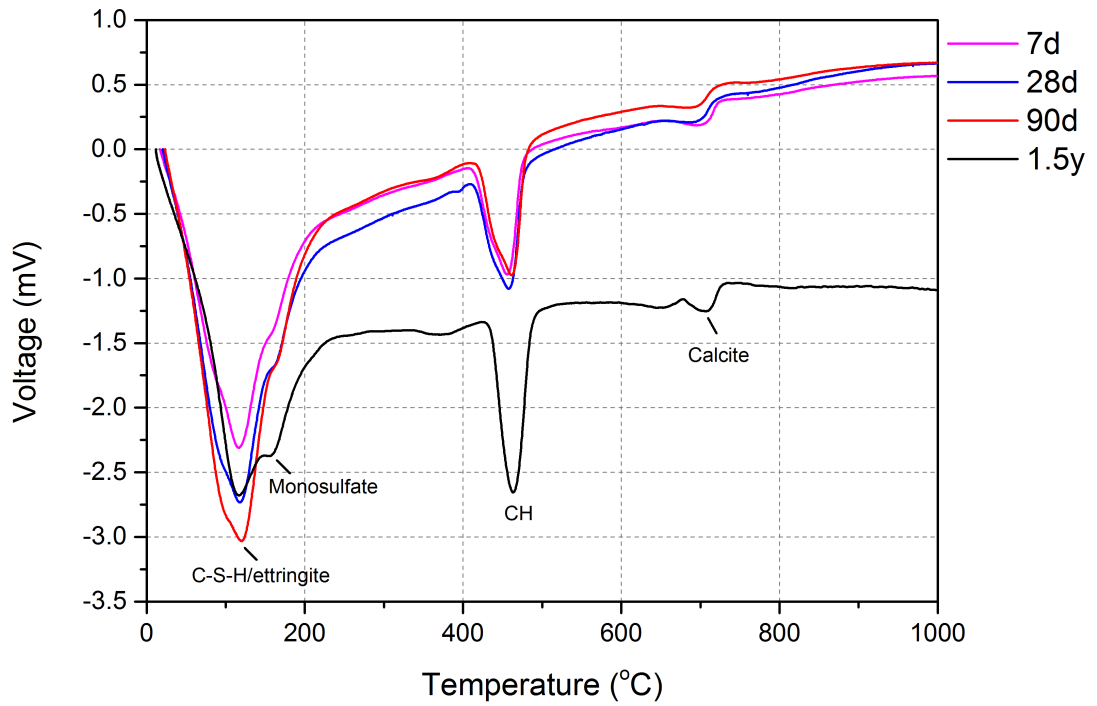


Figure 7.1.2 DTA results of OPC paste cured at 21°C for 7, 28, 90 days and 1.5 years

7.2 XRD

7.2.1 CSA paste

XRD pattern of the CSA cement powder (Fig. 7.2.1) shows that its major compounds are Ye'elite and belite, with very small amount of gypsum present.

XRD results of the hydrated CSA cement suggest a progressive depletion of Ye'elite with curing. Remnants of belite confirm that much more water is required to achieve a fully completed hydration of CSA cement compared to traditional Portland cement system, despite of a high w/c of 0.69 is used in this project. Significant remnants of belite demonstrate its comparatively slow hydration process. At all of the investigated ages, CH is always absent which agrees with the intrinsic hydration of CSA-based materials and the DTA data in section 7.1.1. Hydration products are initially ettringite and CAH_{10} , with increasing quantities of monosulfate and stratlingite at later ages. Increased formation of stratlingite is due to continuous consumption of belite and $Al(OH)_3$ gel. Ettringite is generated rapidly during the hydration of calcium sulfoaluminate and gypsum; after the depletion of gypsum, monosulfate starts to form. At later ages of 1.5 years, formation of C_3AH_6 is detected due to the conversion process of CAH_{10} (Eq. 7.1); stratlingite and monosulfate have become the main hydration products in aged hydrated CSA cement system.



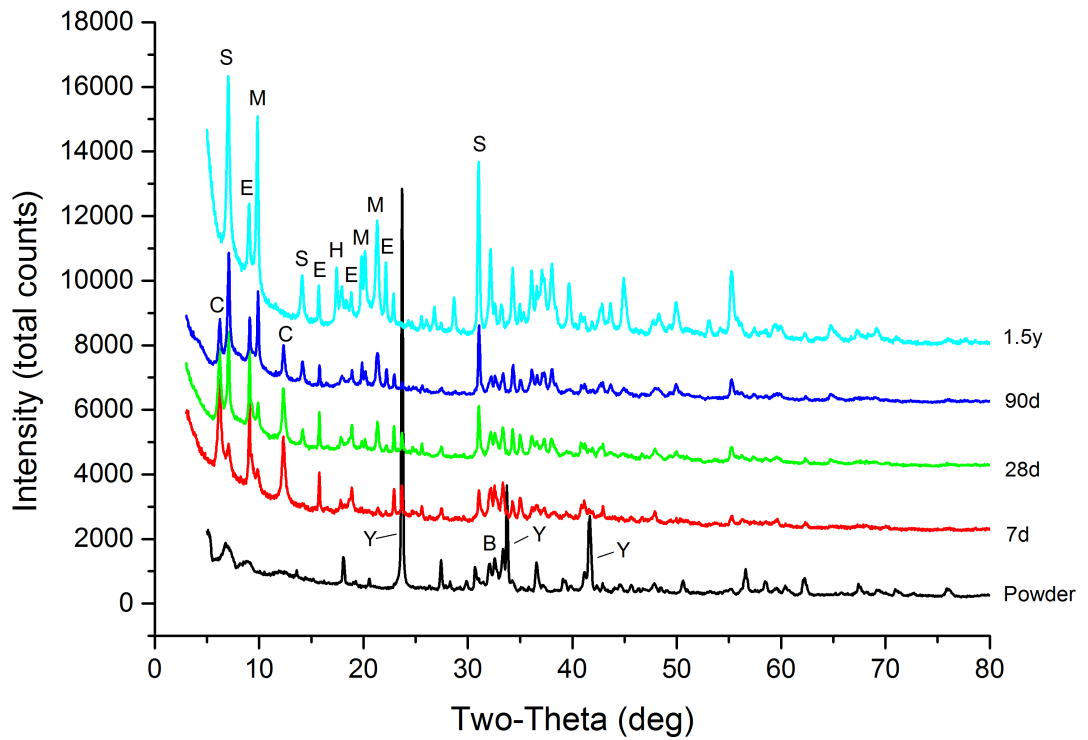


Figure 7.2.1 XRD analysis of CSA cements powder and hydrated CSA paste

(B: belite; C: CAH_{10} ; E: ettringite; H: C_3AH_6 ; M: monosulfate; S: stratlingite; Y: Ye'elimite)

7.2.2 OPC paste

Hydrated OPC paste with the same w/c as the CSA cement paste demonstrates large amounts of CH accumulation with increased curing time, which results from the hydration of C_3S at early age (Eq. 7.2) and C_2S at later age (Eq. 7.3). C_3A is quite reactive with water, producing ettringite as one of the hydration products that is also detected by XRD. Calcite is normally associated with the carbonation of CH, C-S-H gel and/or ettringite (Bertos *et al.*, 2004). Generation of ettringite in hydrated OPC paste at various ages in XRD is consistent with the above DTA curve in Fig. 7.1.2. Due to the amorphous nature of AFm phases, it is difficult to investigate by XRD but very small amount of AFm is still traceable in the XRD analysis.



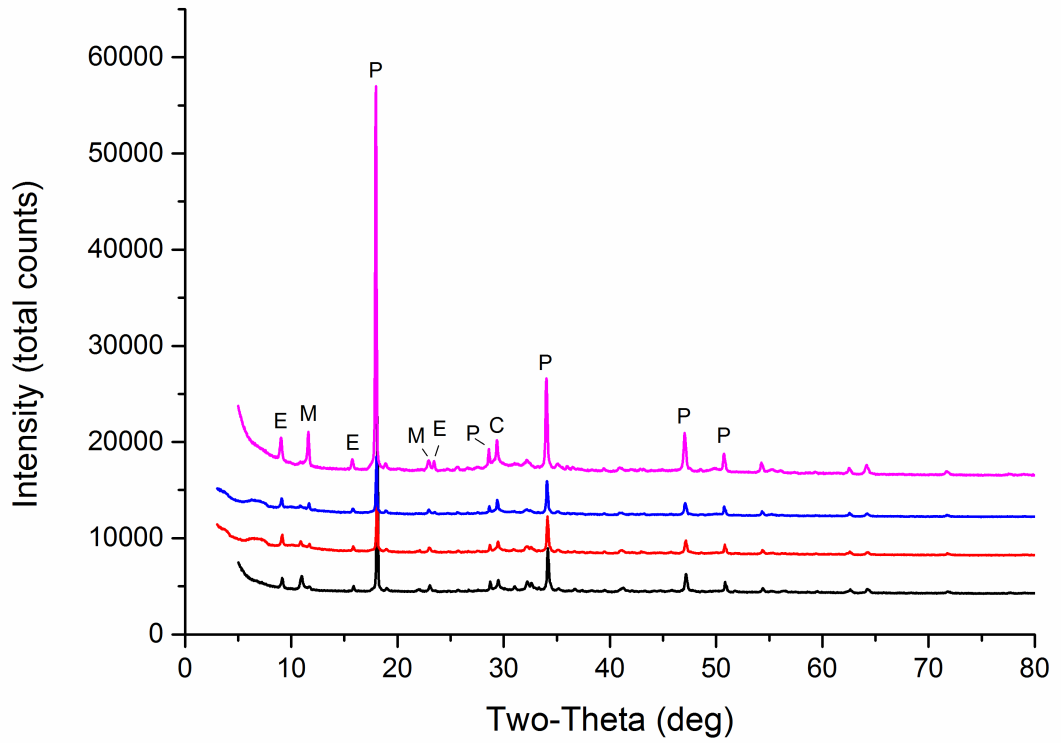


Figure 7.2.2 XRD analysis of hydrated OPC paste at w/c 0.69

(C: CaCO_3 ; E: ettringite; P: Ca(OH)_2 ; M: monosulfate;)

7.3 Microstructure in steel reinforced CSA concrete

7.3.1 Early-age microstructure

7.3.1.1 SEM

Ten BSE images and their corresponding elemental mappings were obtained in this research for qualitative analysis at the interface, which were randomly selected around the steel. One of the representative BSE image is present in Fig. 7.3.1.

Phases of interests such as unhydrated cement, C-S-H and pores can be differentiated according to grey scale in Fig. 7.3.1.a, which depends greatly on the electron density of materials. Steel bar displays as the lightest and are surrounded by a continuous rust layer with a thickness of about $22\mu\text{m}$. Within the concrete matrix, unhydrated cement clinker is easily identified due to its lightest grey scale, followed by C-S-H as light grey; AFt and AFm appear as dark grey. An enlarged BSE image in Fig. 7.3.1.b shows the existence of masses of prismatic-shaped ettringite crystals forming interlocking network with lengths of about $10\mu\text{m}$ in the matrix. It tends to locate in large voids.

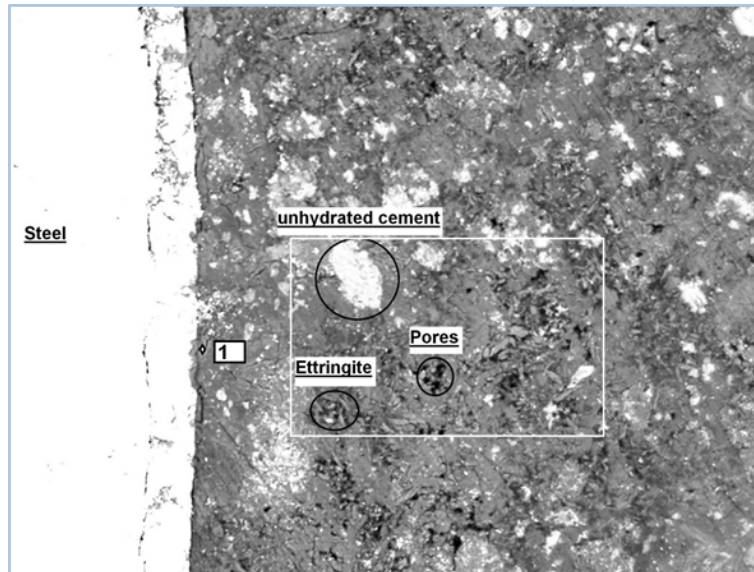
At the interfacial zone, cement has a very intimate contact with the reinforcement and less air voids are observed in the vicinity of the steel reinforcement than that in the bulk matrix. Current flow between the anode and cathode should be relatively restricted near the interfacial zone to some extent, reducing the possibility of electrochemical reaction.

Chapter 7- Results and discussion: Steel reinforced concrete

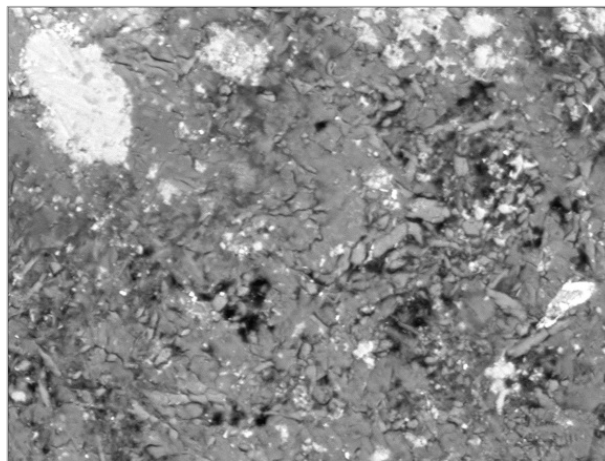
Based on the elemental mapping results (Fig. 7.3.1.d), there is clear chemical difference between the interface and bulk matrix, which confirms the bridge effect of reinforcement. In the mapping of Al, an aluminium-rich layer with various widths is precipitated at the interfacial zone. At the same time, a very thin layer of sulfate is accumulated along part of rebar, which may probably refer to AFt or AFm if associated with the Al and Ca mappings. Further EDX analysis for point 1 at the interface shows an extremely high Al/Ca ratio of 2.7, for which CaO and Al₂O₃ together occupy 90.6 wt.%. This indicates that an extremely high amount of aluminium is accumulated at the interface.

The current SEM results appear to confirm the 'wall effect' of the steel reinforcement, which separates the microstructure of interface from the bulk matrix. However no continuous crystal layer is observed along the interface in CSA concretes. This is morphologically similar to OPC concrete system, which has a non-contiguous CH precipitation layer at the interface according to literature (Head, 2001; Diamond and Huang, 2001; Scrivener, 2004).

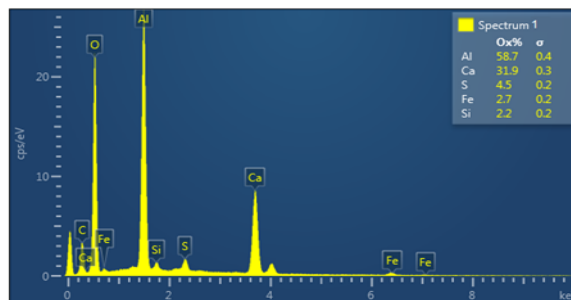
Chapter 7- Results and discussion: Steel reinforced concrete



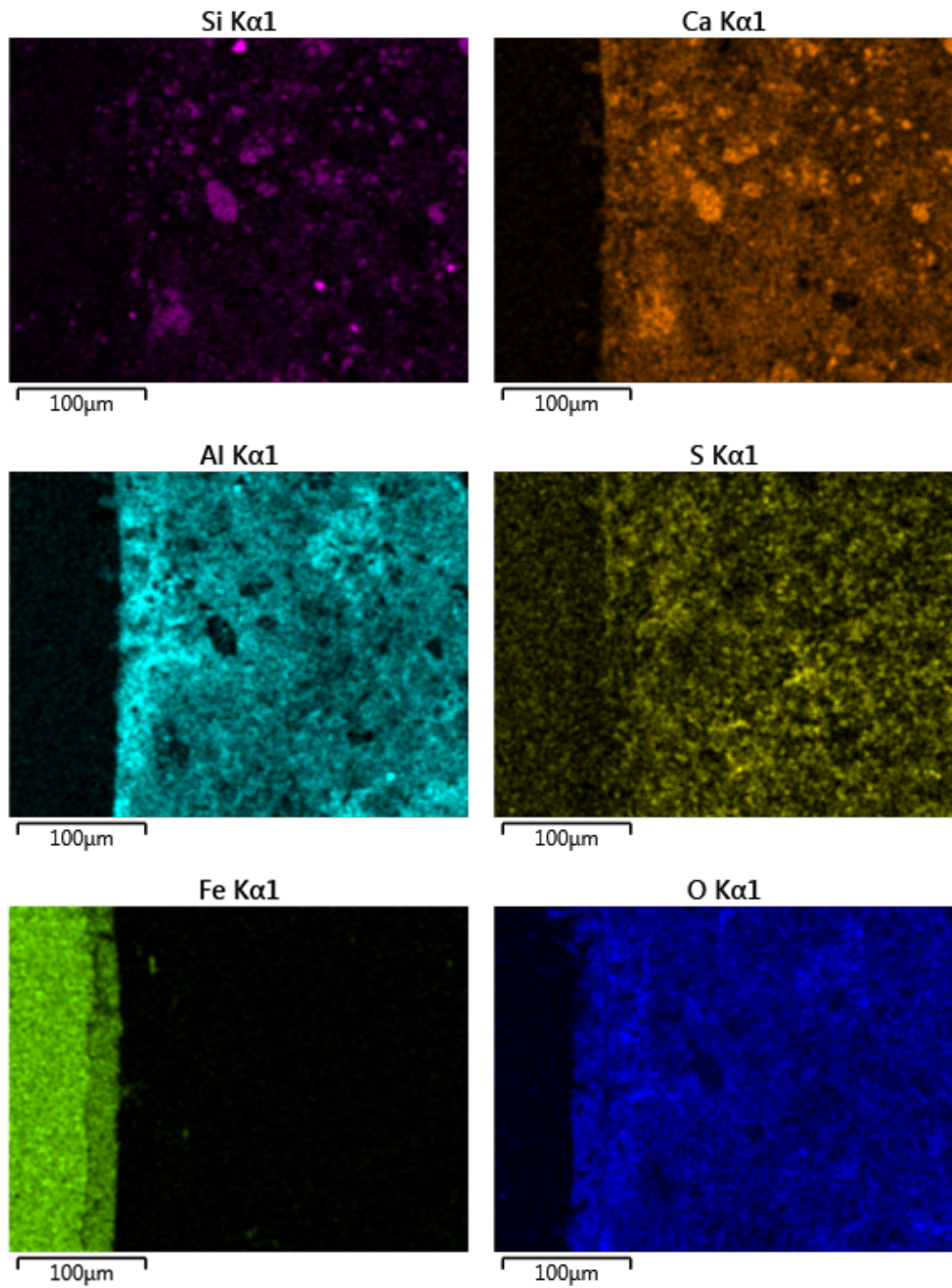
(a) BSE image of steel reinforced CSA concrete cured for 28 days, at a magnification of $\times 400$ (width of field $332\mu\text{m}$)



(b) Enlarged BSE image of a selected area in Fig.a (within square frames), at a magnification of $\times 1000$ (width of field $133\mu\text{m}$). Some needle-like ettringite crystals forming interlocking network can be observed within large air voids, which is the main hydration product of CSA cement



(c) Spot analysis on Point 1



(d) Element mapping of Si, Ca, Al, S, Fe and O in Fig a, at a magnification of $\times 400$.

Figure 7.3.1 Backscattered electron image of steel reinforced CSA concrete aged for 28 days

7.3.1.2 Microanalysis

Microanalysis within $5\ \mu\text{m}$ away from the steel surface on 28d-cured reinforced CSA concrete demonstrates widely scattered data (Fig. 7.3.2). In the Al/Ca vs. Si/Ca plot, Al/Ca from 0.75 to as high as 3.75 can be observed, indicating extremely high quantity of Al_2O_3 at the interface. The S/Ca against Al/Ca plot shows very scattered data; this can be attributed to the complex chemical nature of the phases near the reinforcement. Intermixtures of various hydration products are located in the vicinity of reinforcement, and it is difficult to be distinguished by SEM due to technical limitations. Therefore transmission electron microscope is necessary in future study in order to have a more profound investigation on the chemical of the hydration products near steel.

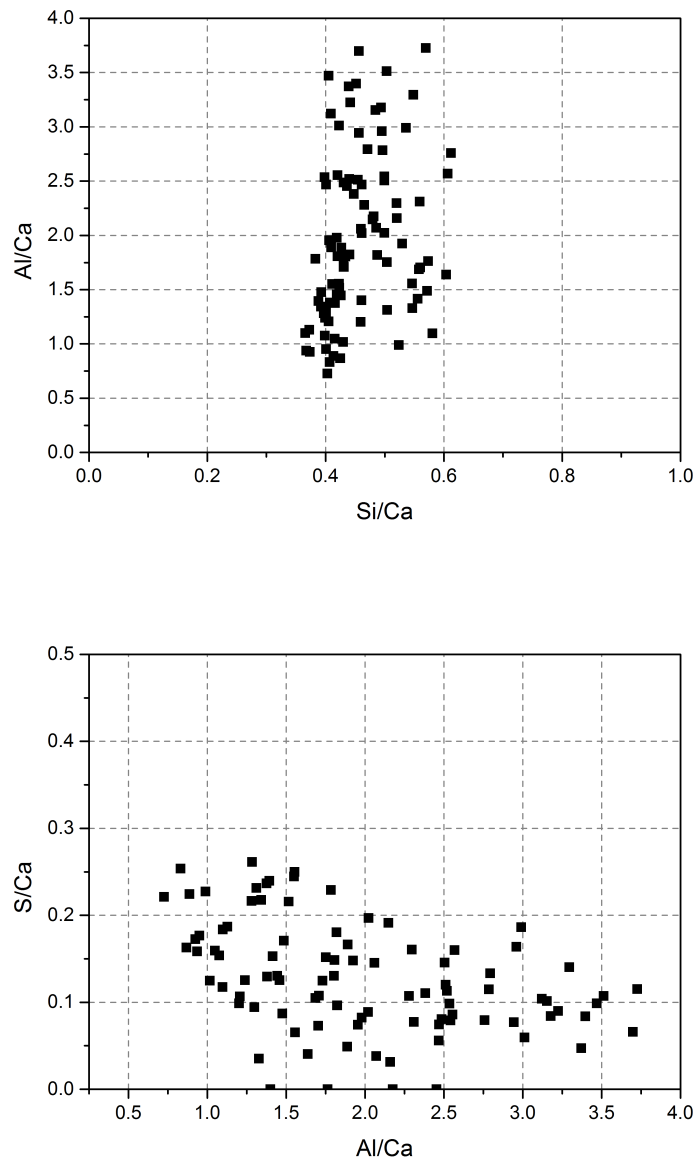


Figure 7.3.2 Microanalysis at the steel/concrete interface in CSA concrete aged for 28 days

7.3.2 Long-term microstructure

7.3.2.1 SEM

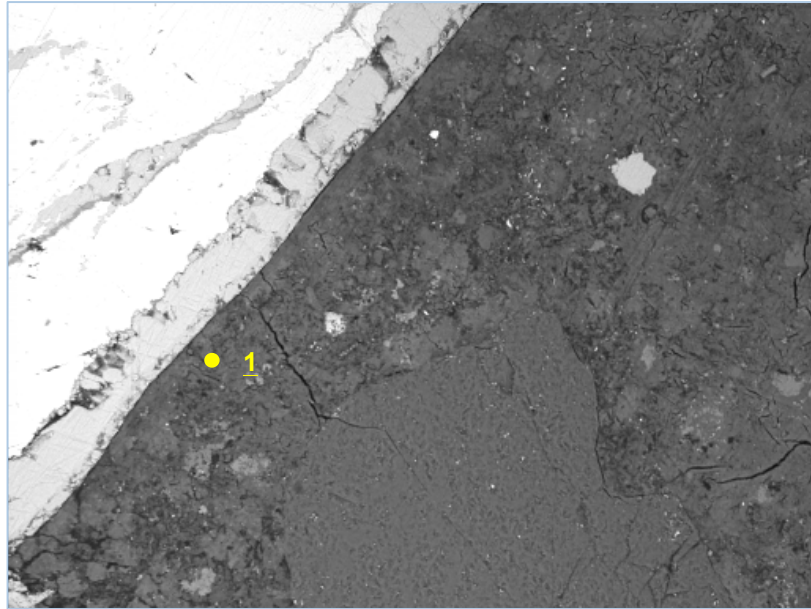
In order to give a general microstructural feature at the interface, ten sites were randomly chosen around the steel and sites with significant defects (e.g. large air voids) were avoided. One of the examples was present below.

Chapter 7- Results and discussion: Steel reinforced concrete

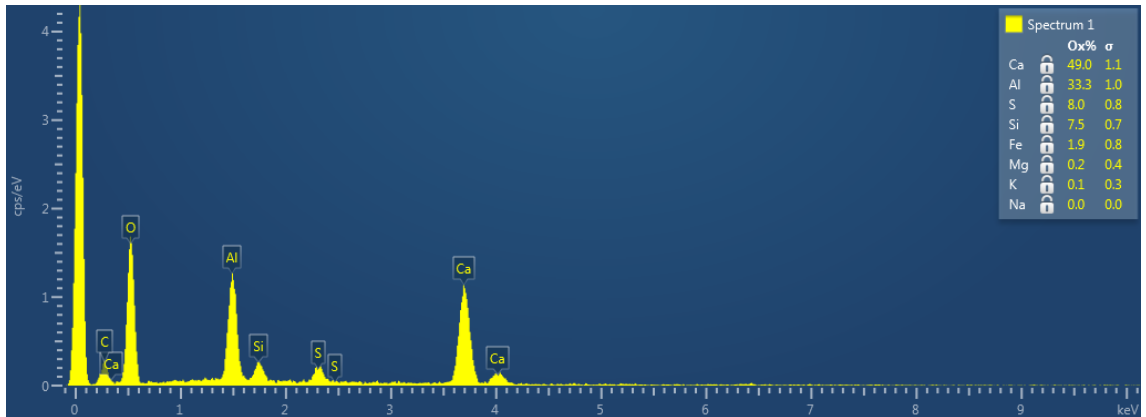
SEM image of the reinforced CSA concrete aged for 1.5 years (Fig. 7.3.3) indicates significantly dense microstructure both in the bulk matrix and at the steel/concrete interface. Hardly any unhydrated cement clinker can be found in the matrix, which suggests a nearly completed hydration. Spot analysis on Point 1 at the interface demonstrates that it contains 49.0 wt.% CaO and 33.3 wt.% Al₂O₃, with great quantities of CaO included.

In the mapping of aluminium, significant contrast can still be observed at the interfacial and in the bulk matrix; much more aluminium oxide is located at the interface than that in the matrix. However, compared to the 28 day-aged sample, reduced amount of aluminium precipitation at the interface is clear in the aged sample. This can be explained by continuous consumption of aluminium hydroxide and belite, forming stratlingite. According to the Ca and S mappings, increased quantities of calcium and sulfate are precipitated at the steel/concrete interface, compared to that in the 28 days aged sample (see Fig. 7.3.1.d). Transport properties of different ions in the vicinity of the steel regarding to early stage and long-term ageing are further discussed in section 7.5.2.

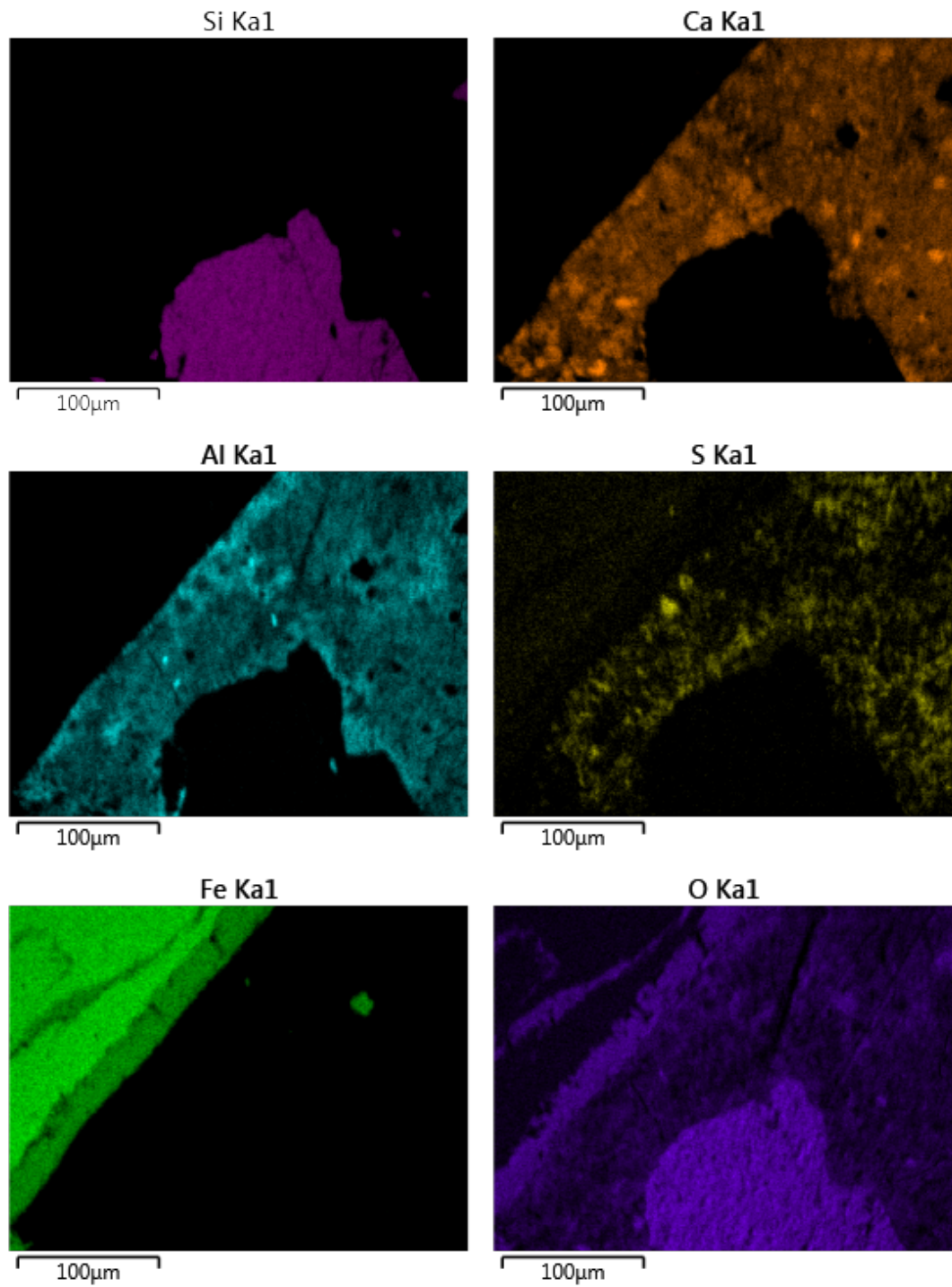
Chapter 7- Results and discussion: Steel reinforced concrete



(a) BSE image of steel reinforced OPC concrete cured for 1.5 years, at a magnification of $\times 400$ (width of field $332\mu\text{m}$)



(b) Spot analysis on Point 1 at the steel/concrete interface



(c) Elemental mappings of Si, Ca, Al, S, Fe, O

Figure 7.3.3 Microstructure study of steel reinforced CSA concrete aged for 1.5 years

7.3.2.2 Microanalysis

Microanalysis result for CSA concrete aged for 1.5 years in Fig. 7.3.4 shows significantly decreased Al/Ca atomic number ranging from 0.75 to up to 2.75, compared to that of 0.75-3.75 for the same material cured for 28 days (Fig. 7.3.2). This is consistent with the mapping results in the above section 7.3.2.1. Significant reduction of Al/Ca with the on-going curing can be related to the consumption of aluminium gel with belite, leaving the formation of stratlingite. In the microanalysis, data representative of stratlingite can be found, although interfered by lower Si/Ca and higher S/Ca ratio. Average Si/Ca atomic number in the 1.5y-aged sample is generally shifting towards higher value compared to that in the 28d-cured sample, suggesting the gradual inclusion of SiO_2 at the interface during hydration. In the S/Ca against Al/Ca plot, scattered data points suggest the complexity of the hydrated phases near steel, similarly to that in the 28d-aged sample (Fig. 7.3.2); therefore further investigation on the chemical composition of precipitated interfacial phases by transmission electron microscope is necessary.

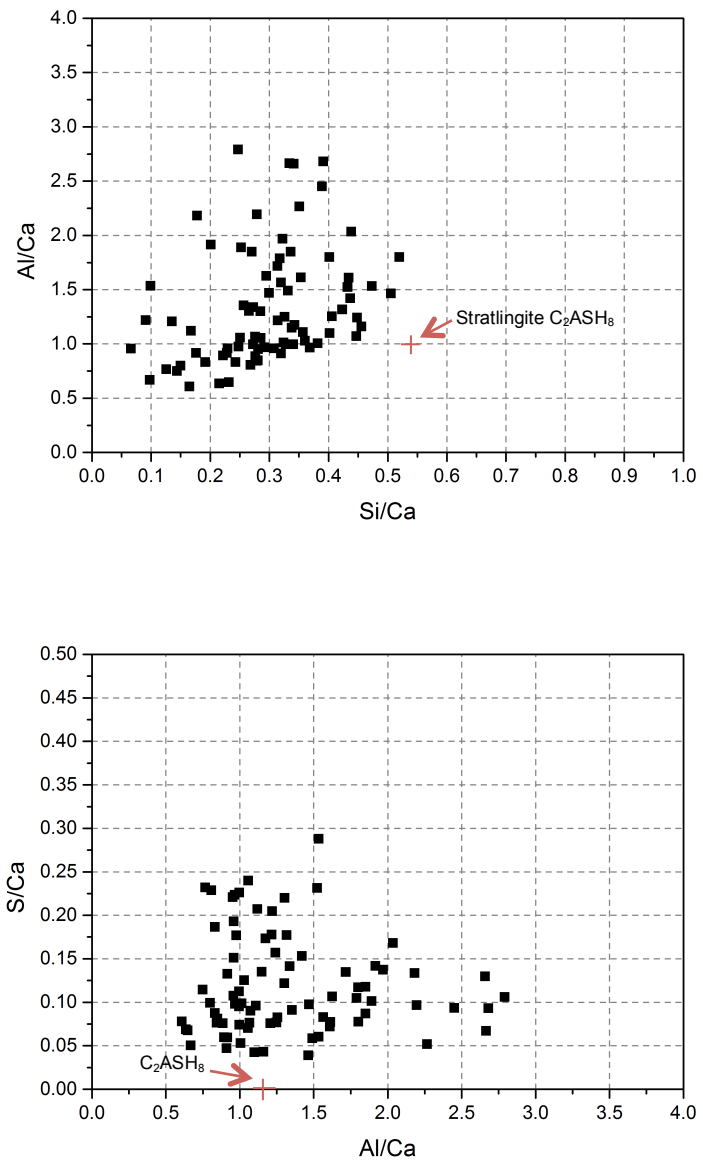


Figure 7.3.4 Scatter graphs of atomic ratios at the steel/concrete interface of reinforced CSA concrete, aged for 1.5 years

7.4 Microstructure in steel reinforced OPC concrete

7.4.1 Early-age microstructure

7.4.1.1 SEM

Ten sites were randomly chosen around the steel for microstructure studies at the interface in steel reinforced OPC concrete aged for 28 days and only one of the representative examples are illustrated in the thesis (Fig. 7.4.1).

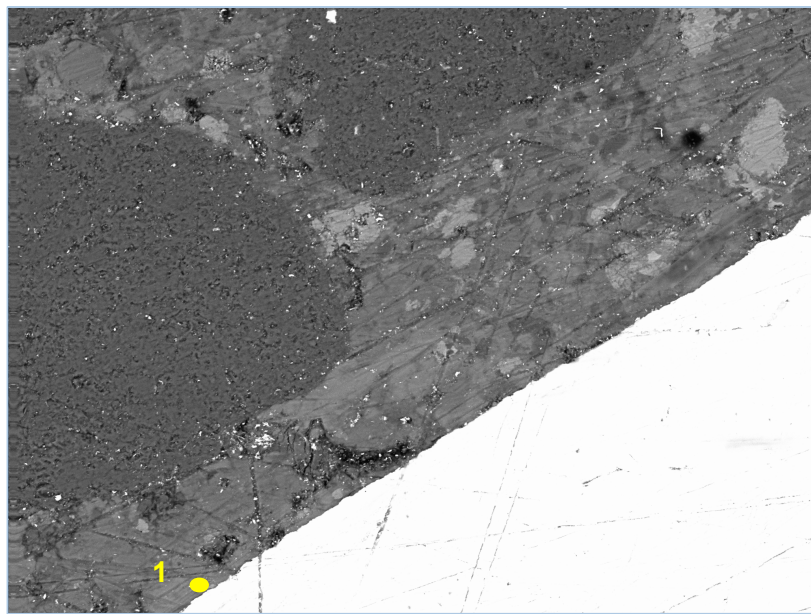
Even though it is aged for 28 days at 20°C, OPC concrete system with a relatively high w/c ratio of 0.69 has achieved most of its hydration degree; with almost none unhydrated cement clinker remaining in the bulk matrix (Fig. 7.4.1.a). Cement matrix has an overall intimate contact with the embedded steel reinforcement, despite some occasional interfacial defects such as air voids located in the vicinity of reinforcement. EDX spot analysis on Point 1 shows the extreme abundance of calcium near the reinforcement surface, accounting for as high as 93.2 wt.% (Fig. 7.4.1.b).

Elemental mapping of calcium (Fig. 7.4.1.c) indicates that there is a calcium-rich layer presented at the interfacial area with various lengths. Local inclusion of significant proportion of aluminium oxide can also be found partially near the steel surface, revealing the existence of AFt or AFm phases at the interface. There is not much silicon exists at this interfacial area according to the silicon mapping, revealing that C-S-H is at least not dominant at the interfacial zone at early curing stage.

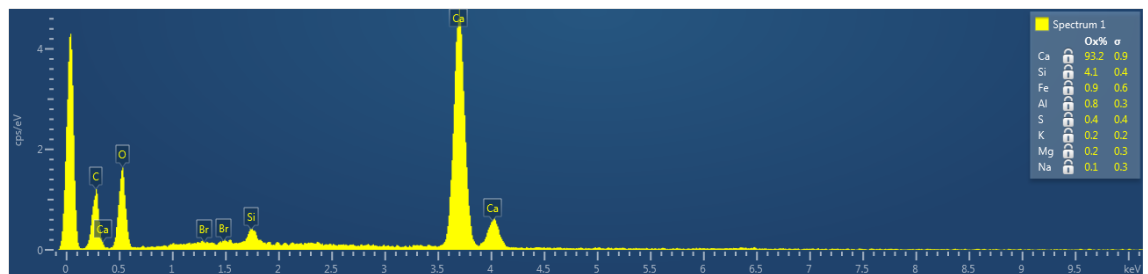
These results prove the inclusions of major CH and minor undesignated sulfoaluminate phase (e.g. AFt or AFm) are intermixed to some extent at the steel/concrete interface, rather than a continuous CH layer surrounded by

Chapter 7- Results and discussion: Steel reinforced concrete

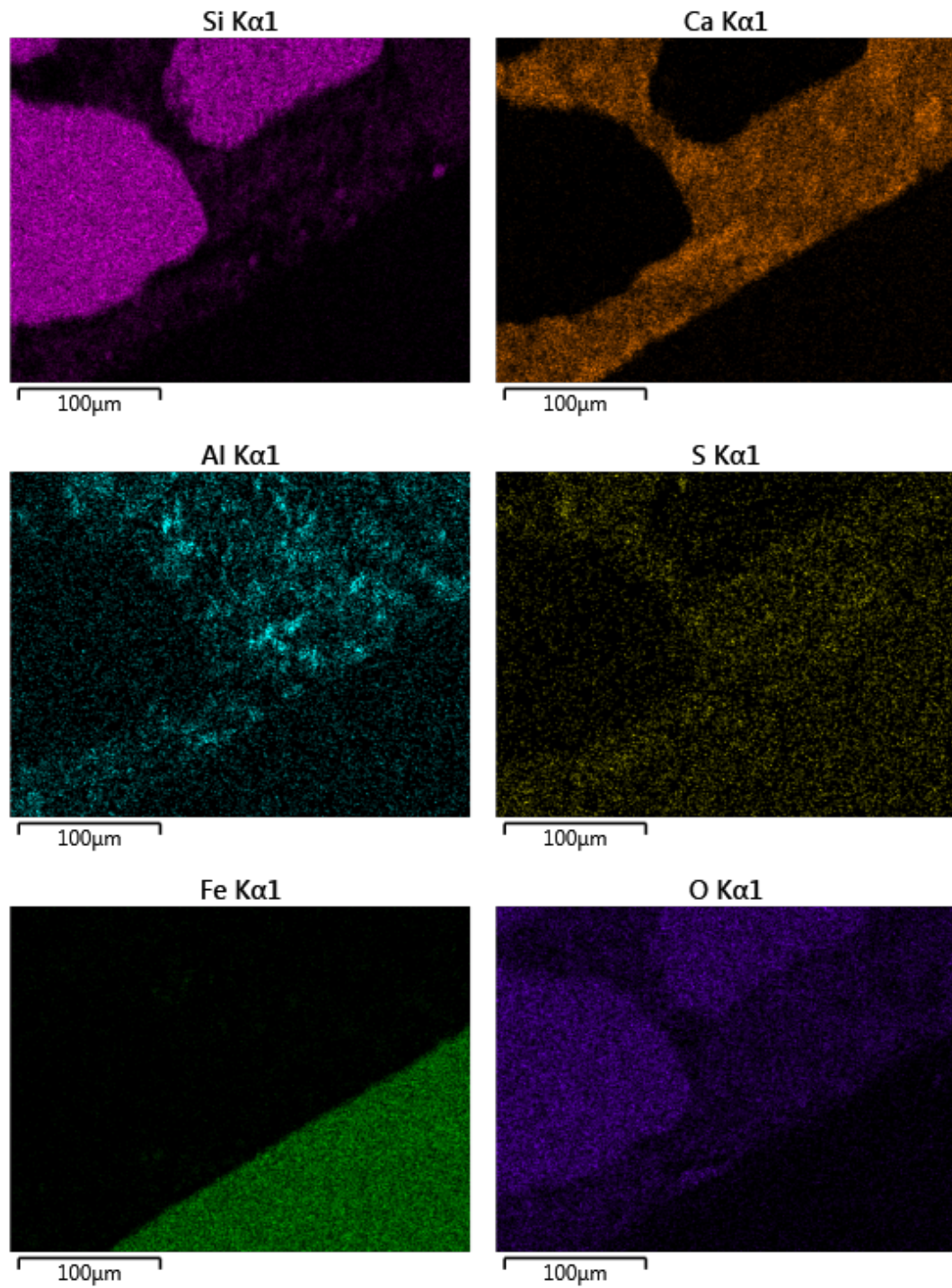
the reinforcement surface proposed in the earlier research (Page, 1975). Detailed chemical composition of the hydration products at interface is further discussed in next section 7.4.1.2.



(a) BSE image of steel reinforced OPC concrete cured for 28 days, at a magnification of x400 (width of field 332µm)



(b) Spot analysis on Point 1



(c) Elemental mappings of Si, Ca, Al, S, Fe and O

Figure 7.4.1 Microstructural study of steel reinforced OPC concrete cured for 28 days

7.4.1.2 Microanalysis

In the Al/Ca vs. Si/Ca plot (Fig. 7.4.2), cluster of data points are located near the origin, which represents the inclusion of crystalline CH precipitation at the steel/concrete interface. There are two obvious trend lines that data of C-S-H gel are growing towards, i.e. CH at the origin point and AFm (at Al/Ca=0.5, Si/Ca=0). The mean Ca/Si of the C-S-H gel is ~1.7. The main chemical compositions precipitated at the interfacial zone are mainly crystalline CH, intermixed with minor C-S-H gel and AFm. In the S/Ca towards Al/Ca plot, cluster of data can be found at the origin, which again proves the significant precipitation of CH at the interface. Growing trend line from C-S-H directing towards AFm (Al/Ca 0.5, S/Ca 0.25) is not clearly demonstrated in this plot owing to deficiency of sulfate.

Microanalysis at the steel/concrete interface of early-aged steel reinforced OPC concrete proves that CH is the major hydration product in this region, with slight inclusion of C-S-H and AFm as well.

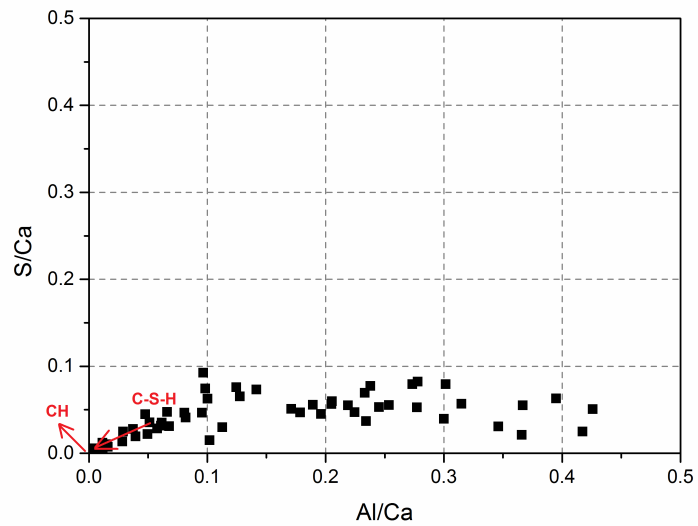
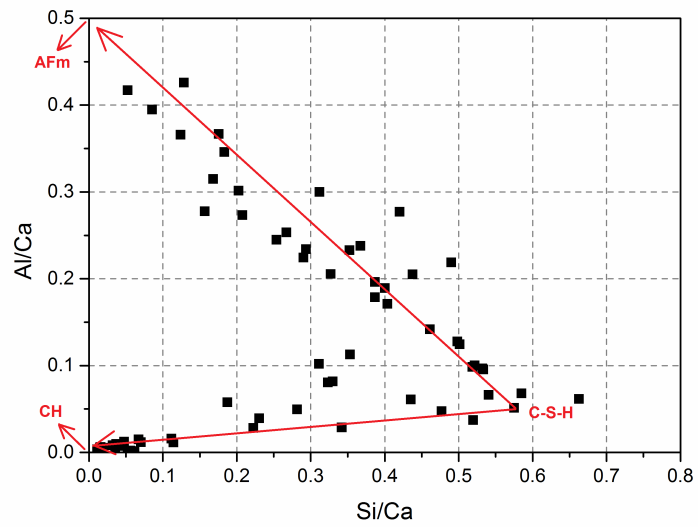


Figure 7.4.2 Scatter graphs of atomic ratios at the steel/concrete interface of reinforced OPC concrete, aged for 28 days

7.4.2 Long-term microstructure

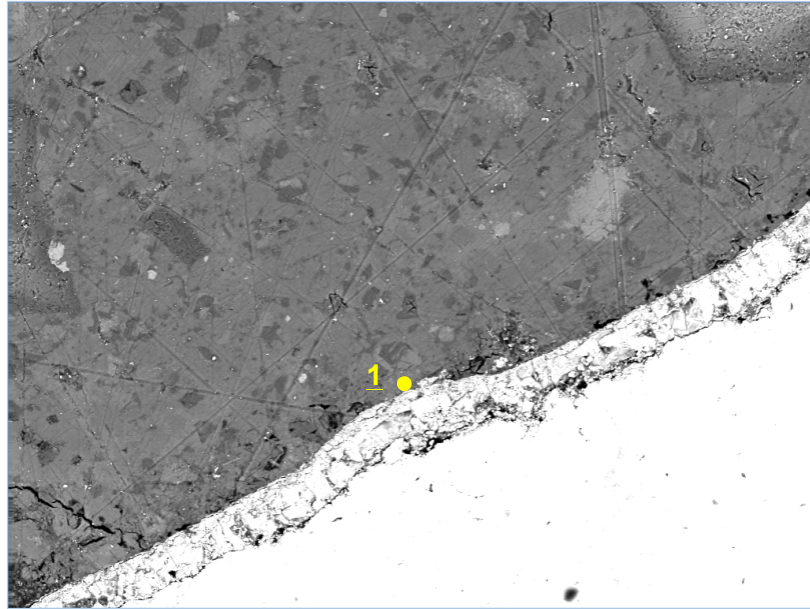
7.4.2.1 SEM

In order to have a general microstructure observation on the interface in 1.5y-aged steel reinforced OPC concrete, ten sites were randomly chosen around the steel. Within them, one representative example is present below.

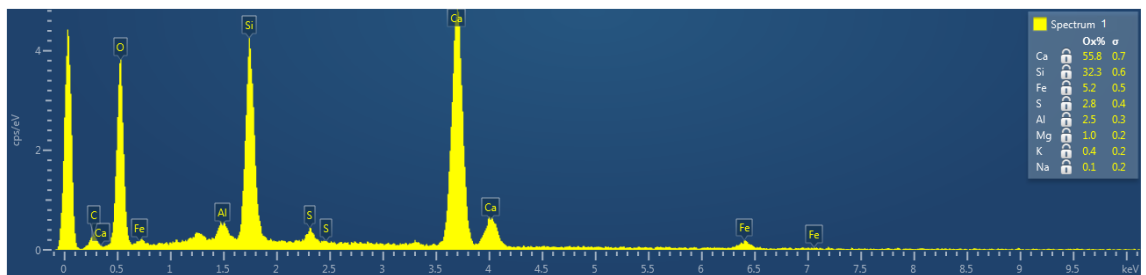
Chapter 7- Results and discussion: Steel reinforced concrete

Microstructure of 1.5 years-aged reinforced OPC concrete in Fig. 7.4.3.a shows that there is almost no unhydrated cement within the matrix, which suggests a completed hydration process. With the on-going hydration process, contact between cement and steel reinforcement becomes more intimate, only with a small amount of porosity displayed along the steel surface. Large amount of CaO and SiO₂ are accumulating at the interface according to elemental mappings (Fig. 7.4.3.c); moreover there is almost insignificant difference on the CaO content presence between interfacial zone and the bulk matrix. Limited amount of SO₃ and Al₂O₃ exist at the interfacial zone, suggesting the inclusion of calcium sulfoaluminate-based hydration products in this area. Further chemical study on the hydrated phases at interface is demonstrated in next section 7.4.2.2.

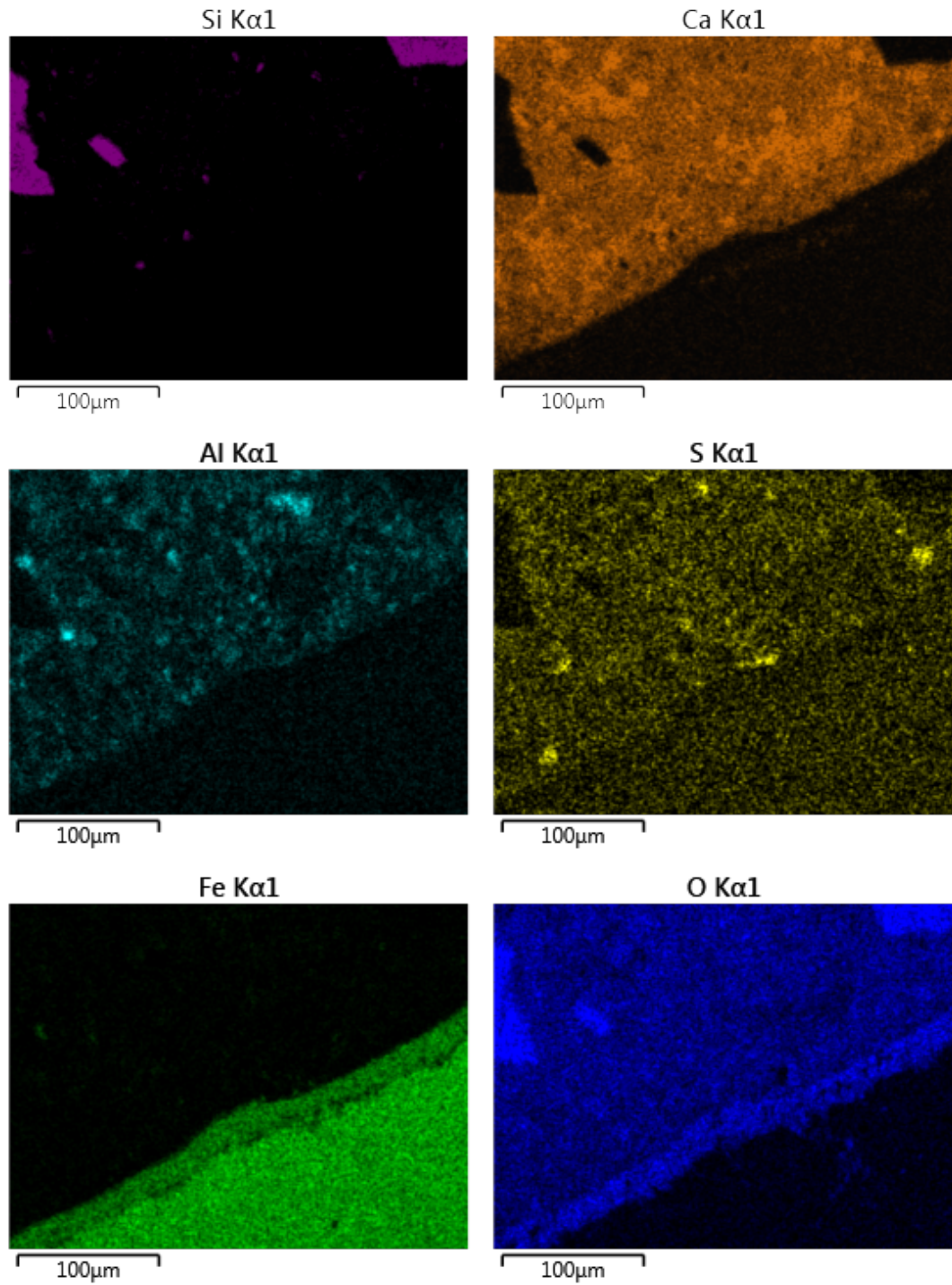
Chapter 7- Results and discussion: Steel reinforced concrete



(a) BSE image of steel reinforced OPC concrete cured for 1.5 year, at a magnification of x400 (width of field 332 μ m)



(b) Spot analysis on Point 1 at the steel/concrete interface



(c) Elemental mappings of Si, Ca, Al, S, Fe, O

Figure 7.4.3 Microstructure study of steel reinforced OPC concrete aged for 1.5 years

7.4.2.2 Microanalysis

In the Al/Ca towards Si/Ca plot, it suggests that main hydration product at the interface is C-S-H gel, as indicated by a series of clustered data near Si/Ca=0.55. Two growing trend lines from C-S-H gel in the direction towards both CH and AFm can be observed respectively, despite of some scattered data included. The mean Ca/Si ratio of the C-S-H gel is ~1.8. The S/Ca vs. Al/Ca plot further confirms the presence of C-S-H gel finely intermixed with CH at the interface between steel and concrete. However, pure crystalline CH phase is hardly detected at the origin after curing for 1.5 years, compared with the steel reinforced OPC concrete at early age, in which pronounced CH existence can be detected at the interface in microanalysis (Fig. 7.4.2). This denotes the gradual dissolution of CH over ageing at the steel/concrete interface, which consequently may increase the possibility of reinforcement corrosion due to the reduced buffering effect provided by CH layer at the interface to perform corrosion resistance of embedded reinforcement. Further information on the various ion movements at the interfacial zone is discussed in section 7.5.1.

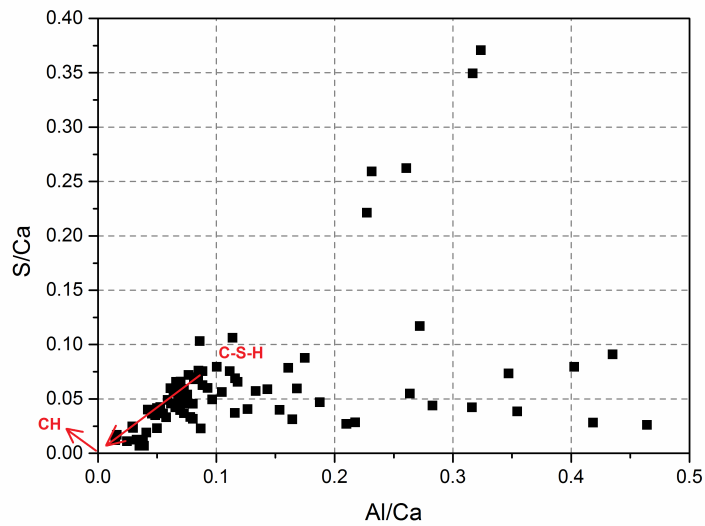
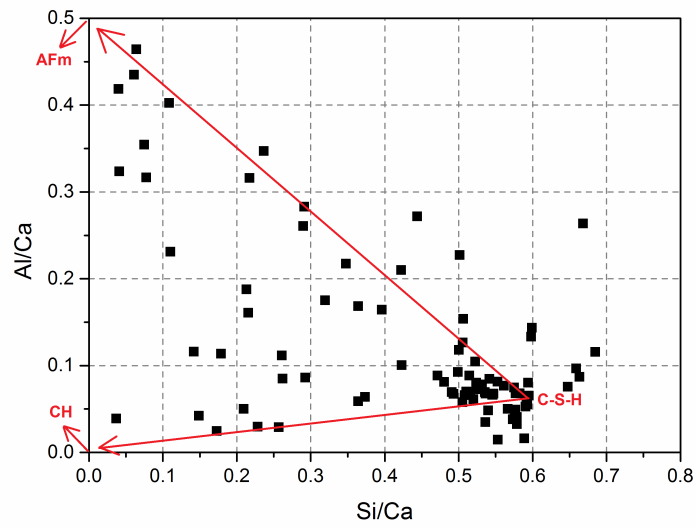


Figure 7.4.4 Scatter graph of atomic ratios at the steel/concrete interface of reinforced OPC concrete, aged for 1.5 years

7.5 Image analysis

7.5.1 Steel reinforced CSA concrete

Image analysis results of steel reinforced CSA concrete aged for both 28 days and 1.5 years are present in Fig. 7.5.1, focusing on the distribution of atomic ratios at the interfacial zone as a function of distance away from steel

surface. Steel/concrete interface with a width of $30\mu m$ is applied in this research, which was proved to be sufficient depth to monitor interfacial transition zone in previous research (Yang and Buenfeld, 2001; Scrivener *et al.*, 2004). Fifteen BSE images were randomly selected for each sample with a specific curing age, together with their corresponding elemental mappings. Elemental mappings were then read by Inca software pixel by pixel, finishing with a Microsoft Excel spread sheet containing the atomic information on each pixel; afterwards arithmetic calculations were necessary to achieve various atomic ratios, i.e. Ca/Si, Al/Ca and S/Ca (detailed information on the settings on acquiring quantified mappings are in section 5.8). At the end, average atomic ratios at the steel/concrete interface were calculated based on the fifteen sets of data. Error bars of standard deviations are added in each set of data to demonstrate statistical significance.

The results indicate that evolution of atomic ratio at the steel/concrete interface with increasing curing periods is less pronounced in the CSA sample compared to that in the traditional OPC concrete (in the following section 7.5.2). This may suggest less active and frequent transport and/or exchange of ions at the interfacial region. Ca to Si (Fig. 7.5.1.a) ratio stays at ~ 2.5 along interface in the 1.5 years-aged sample; it reduces slightly to ~ 2.25 in the 28 days-aged sample, despite of the initial increasing trend within the first $5\mu m$ away from steel surface. Error bars of standard deviations are added in Appendix A, which is less than 0.3.

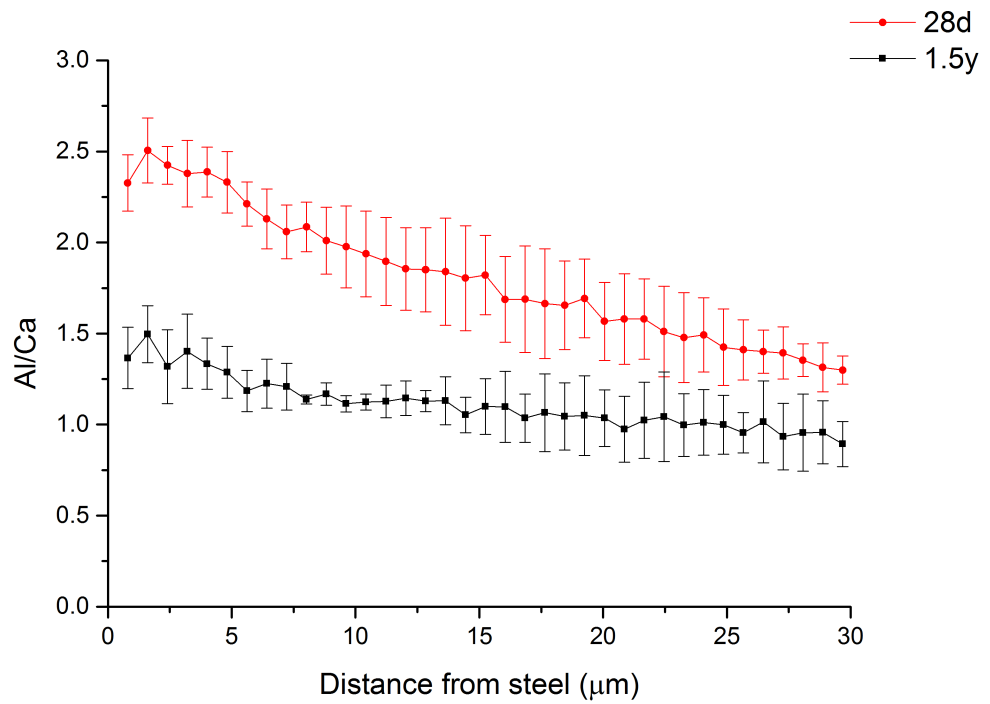
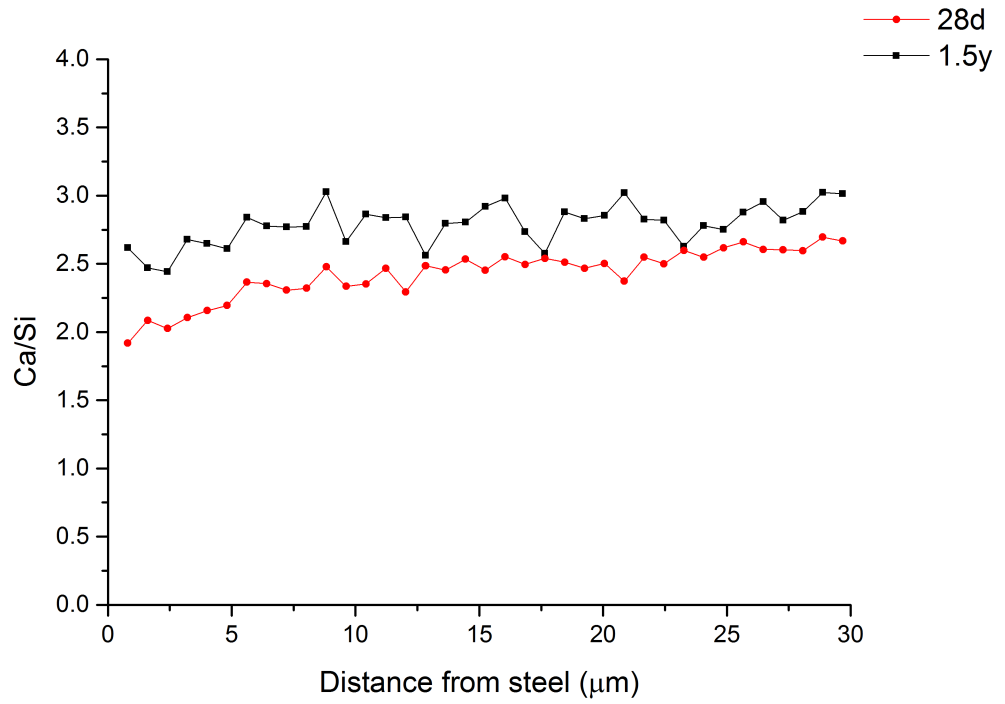
Extremely higher Al/Ca ratio of over 1.0 (in Fig. 7.5.1.b) can be observed generally at the interface in the CSA sample compared to that in the OPC sample (less than 0.3 in Fig. 7.5.2.b). This agrees with the high proportion of

Chapter 7- Results and discussion: Steel reinforced concrete

Al accumulation near the steel surface suggested by Al elemental mapping (see section 7.3.1.1 and 7.3.2.1). In the Al/Ca plot for steel reinforced CSA concretes, it shows decreasing Al to Ca ratio along the interfacial area with the progress of hydration at both curing ages. For example, the Al/Ca ratio reduces from 2.5 to 1.5 in the 28 days sample and a lower range from 1.5 to 1.0 is clear in the 1.5 years sample. The overall reduction in sample cured for 1.5 years can be explained by the continuous consumption of AH_3 with belite, leaving the generation of stratlingite as traced in the DTA curves (Fig. 7.1.1) and XRD results (Fig. 7.2.1) in hydrated CSA pastes. The corresponding error bars are within an acceptable range of 0.4.

Almost no obvious changes in S/Ca ratio with increasing curing age (in Fig. 7.5.1.c) can be observed. And the overall S to Ca ratio at the interface is slightly higher than that in the OPC concrete system (Fig. 7.5.2.c). Error bars of standard deviations are added separately in Appendix A, which is less than 0.05.

Chapter 7- Results and discussion: Steel reinforced concrete



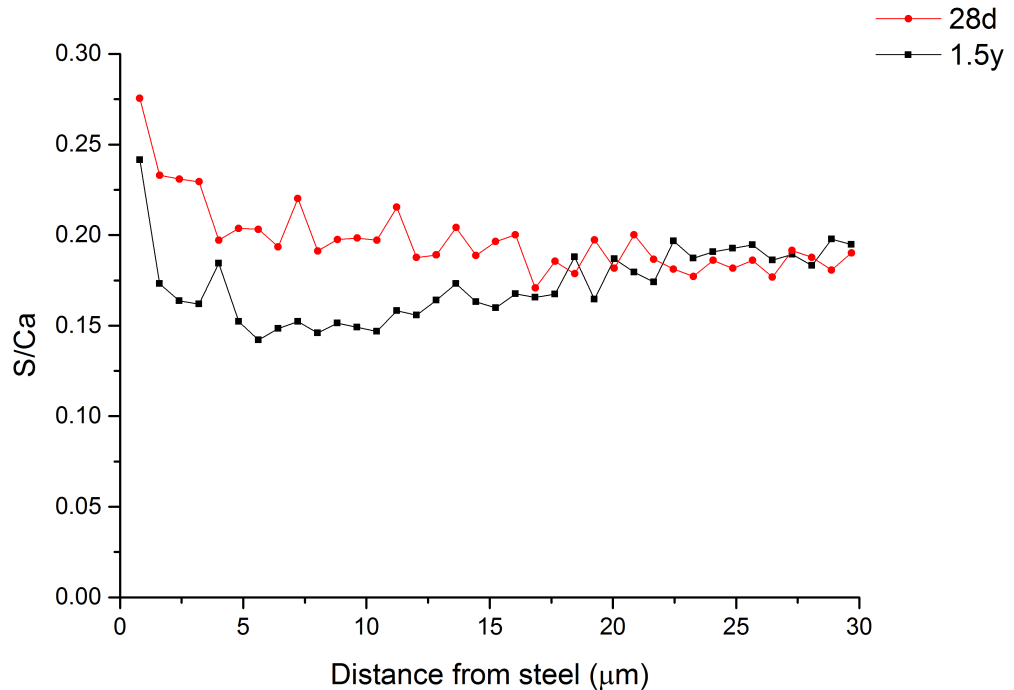


Figure 7.5.1 Image analysis on atomic ratios at the steel/concrete interface in reinforced CSA concrete

7.5.2 Steel reinforced OPC concrete

Image analysis results of steel reinforced OPC concretes aged for both 28 days and 1.5 years are presented in Fig. 7.5.2, illustrating the distribution of atomic ratios at the interfacial zone as a function of distance away from steel surface. Error bars of standard deviation are shown in the Ca/Si plot of 28 days-aged OPC sample (as in Fig. 7.5.2.a). The standard deviation at each data point is less than 0.4; this is within an acceptable range in consideration of the heterogeneous characteristics of cementitious materials.

In the Ca/Si plot, it shows significantly decreased Ca/Si value during curing for up to 1.5 years and there are insignificant changes on the Ca/Si ratio along the interfacial zone in both samples. For example in the 28 days-aged sample, Ca to Si ratio reaches as high as ~3.5 near the steel surface and

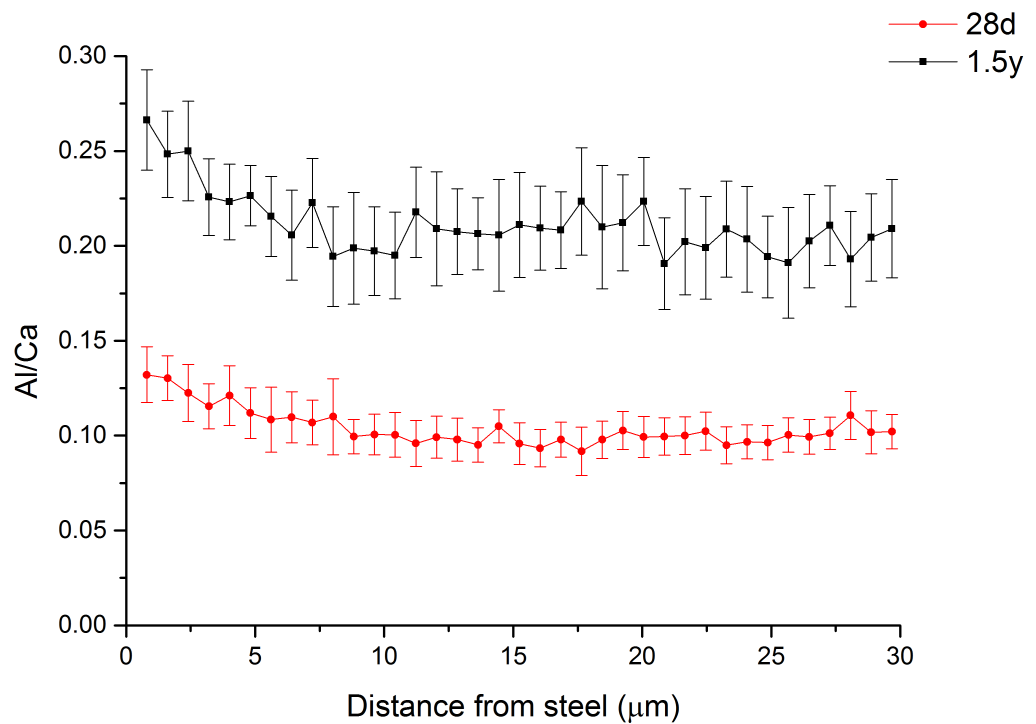
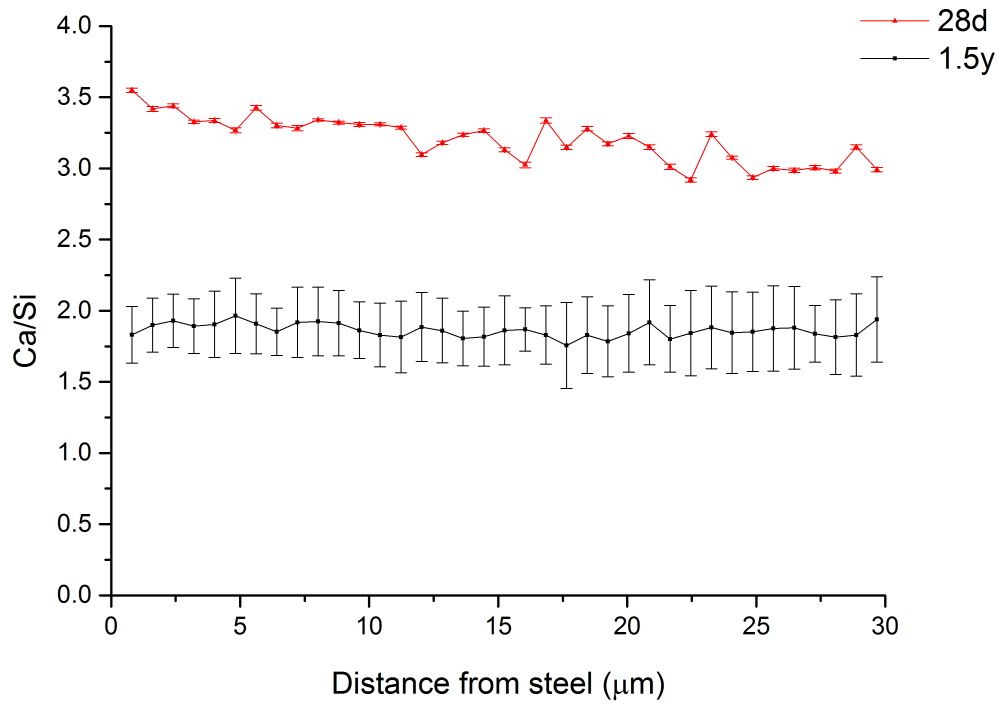
afterwards it stabilizes at ~ 3.25 along the interface, although with slight fluctuations at some data points. However, it is still far higher than the reported Ca to Si value of 1.2-2.3 in literature (Richardson, 1999; Richardson, 2008) for the outer C-S-H product in hardened cement paste. This is because chemical composition at the interface is mainly mixtures of crystalline CH and C-S-H gel, with a large proportion of CH precipitation included in this area (as indicated by the microanalysis in section 7.4.2.2), which results in a significantly higher Ca to Si ratio than normal C-S-H gel. After curing for 1.5 years in a foggy room, significant reduction of Ca to Si ratio to ~ 1.75 can be found along the interfacial zone. The decrease of Ca to Si ratio compared to that in the short-term cured sample can be interpreted by the gradual decrease of CH in the vicinity of steel, as stated in section 7.4.2.2.

In the Al/Ca plot, it is found that Al to Ca ratio increases to a great extent with the on-going curing. Al to Ca ratio is initially high near the steel surface, then falls gradually within the first $6\mu m$ at interface and maintains at a constant value afterwards. For example in the 28 days-aged sample, Al to Ca ratio starts from 0.125 near the steel surface and then keeps steadily at ~ 0.10 along the interface. In contrary, Al to Ca ratio in the 1.5 years-aged sample reaches as high as 0.275 on the steel surface and then reduces to ~ 0.2 afterwards. The higher Al/Ca ratio near steel surface is consistent with the decalcification of the matrix due to migration of CH. Error bars are within an acceptable range of 0.05.

Similar to the distribution of Al/Ca along the interface, overall S/Ca ratio increases considerably with progressive curing and there is initially higher S

Chapter 7- Results and discussion: Steel reinforced concrete

to Ca ratio within the first $6\mu\text{m}$ away from steel. The corresponding error bars stays in a reasonable range of 0.04.



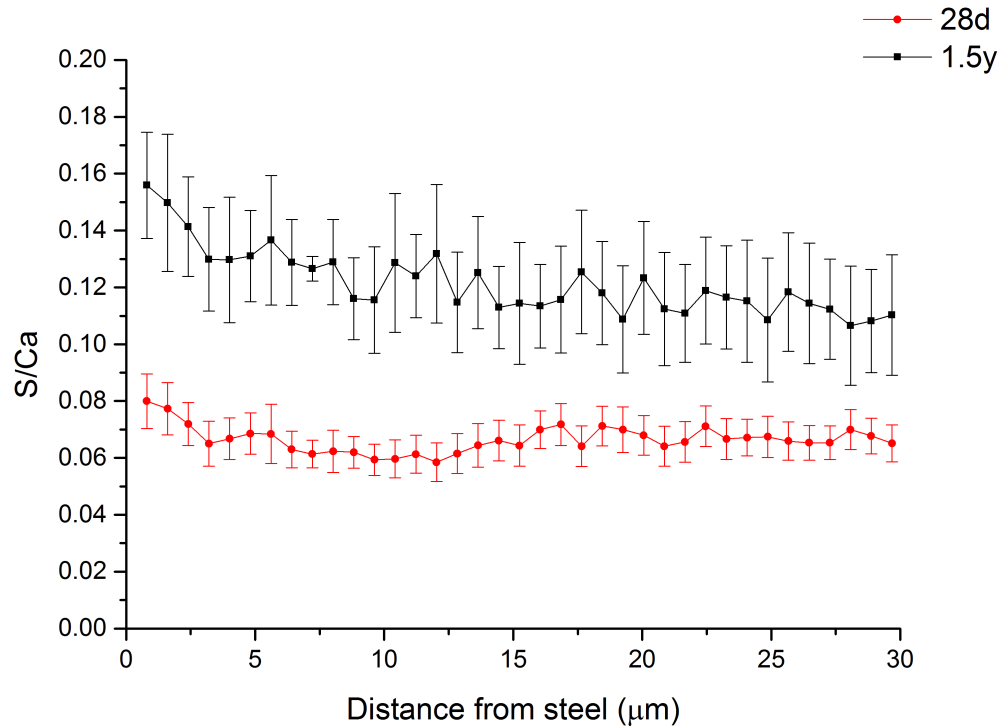


Figure 7.5.2 Image analysis on atomic ratios at the steel/concrete interface in reinforced OPC concrete

7.6 Summary of main findings

Complex hydration process occurs during the curing of CSA pastes. Hydration products are initially ettringite and CAH_{10} , with increasing generation of stratlingite and monosulfate afterwards. In the sample cured for 1.5 years, CAH_{10} is not traceable any more due to its conversion reaction to C_3AH_6 .

The microstructural studies of steel reinforced CSA concrete show the abundance of Al precipitation at steel/concrete interface, most of it being hydrated phases. With the on-going curing, this un-continuous Al layer is consumed to some extent due to the chemical reaction between AH_3 and belite, resulting in the formation of large amounts of stratlingite.

Chapter 7- Results and discussion: Steel reinforced concrete

Image analysis of steel reinforced CSA concrete indicates that there are insignificant changes on the Ca/Si and S/Ca along the interface in the 28 days and 1.5 years aged samples. Significant reduction of Al/Ca in the long-term aged sample is clear at the interfacial zone due to the chemical reaction between alumina gel and belite. However in the 1.5y-aged CSA sample, clear contrast still exists on the Al precipitation between the interface and bulk matrix, based on the Al elemental mapping.

In the reinforced OPC sample, the initial chemical layer rich in CH near the steel surface is suspected to be dissolved gradually to some extent with curing; and it is then mainly enriched with fine intermixtures of C-S-H gel and CH. This chemical change at the interface not only have vital importance on the pH value in this region but also destroys the CH layer which is supposed to act as buffering effect; both of which may lower the reinforcement corrosion resistant capacities in steel reinforced concrete systems.

Chapter 8- General discussion

General discussion on the nature of interface is present in this chapter; different microstructure features at interface can be observed in different types of reinforcements.

8.1 Chemical composition at the interface

8.1.1 Glass fibre/cement interface

Thin section images of unaged OPC/GRC demonstrated that spaces between fibres remained almost empty at early ages, and were then gradually filled with the penetrated hydrated phases with ageing (see Fig. 6.4.1 and Fig. 6.4.2). Microanalysis at the interfilamentary spaces in aged OPC/GRC suggested the presence of finely intermixed CH and C-S-H gel (Fig. 6.4.4). This is different to the previously reported studies on OPC/GRC (Devekey and Majumdar, 1970; Katz and Bentur, 1996; Butler *et al.*, 2009b); most of which stated that the ingressed hydration phase was predominantly crystalline CH. Inclusion of the amorphous C-S-H gel at the interfilamentary spaces may act as adhesive binder to help bond with the large CH crystals firmly, forming a rather rigid bonding composite structure as is shown on fractured surfaces (Fig. 6.4.5). The likely influence of the penetrated C-S-H/CH intermixtures on the composites' mechanical performances is further discussed in section 8.3.

Evolution of both the interfilamentary and interfacial microstructure in aged Nashrin/GRC is almost insignificant and the interfilamentary spaces have

been filled with ingressed hydration phases at the early age (Fig. 6.3.1-6.3.3). It was found that the penetrated interfilamentary products are mainly C-A-S-H gel intermixed with ettringite according to the microanalysis (Fig. 6.3.6); this is in agreement with the corresponding XRD results, which indicated that the main crystalline hydration product was ettringite in the Nashrin-based matrix.

8.1.2 Steel/concrete interface

Microanalysis on reinforced OPC concrete indicated that chemical phases located at the interface were mainly mixtures of CH and C-S-H gel at both investigated ages (28 days and 1.5 years), with minor calcium sulfoaluminate phases (such as AFm) included as well. This agrees with the previous work (Horne *et al.*, 2007; Li and Hu, 2001), in which it was stated that calcium sulfoaluminate hydrate phases might also be present at the steel/concrete interfacial area, finely intermixed with C-S-H gel on a scale too fine to be resolved in BSE images.

There was a lack of chemical investigation at the steel/concrete interface in reinforced CSA concrete in literature. In the present work, it was found out that chemical compounds located at the steel/CSA cement interface were mainly hydrated alumina gel at early ages (Fig. 7.3.1.d). With the progress of curing, decreased amount of alumina gel was observed near steel due to its chemical reaction with the remaining belite phases (Fig. 7.3.3.c), causing the formation of stratlingite (as is indicated by microanalysis in Fig. 7.3.4). This is confirmed by the substantially decreased Al/Ca ratio along the interfacial region with prolonged curing periods from image analysis (Fig. 7.5.2).

8.2 Ion transport at steel/concrete interface

Microanalysis at the interface between steel bar and OPC concrete suggested slight reduction of CH at ages of 1.5 years compared to that at 28 days (Fig. 7.4.2 and Fig. 7.4.4); this was also confirmed by the quantitative image analysis, in which a general reduction of ~16% in Ca/Si ratio can be observed over the interface at 1.5 years relative to that at 28 days (see Fig. 7.5.1).

Similar quantitative image analysis by Horne (Horne *et al.*, 2007) revealed substantially preferential CH precipitation near the steel bar (as presented below in Fig. 8.2.1), occupying ~16-20 wt.% of the total interfacial compounds compared to a CH concentration of 10-12 wt.% at rest of the interface and the bulk cement. In his work, it also suggested slightly increased CH near the steel surface with increasing curing ages; for example, the highest CH concentration reaches ~16 wt.% at ~5 μ m away from steel surface at 3 days, then increases to ~18 wt.% at 28 days and approximately 20 wt.% CH can be observed near steel at 365 days.

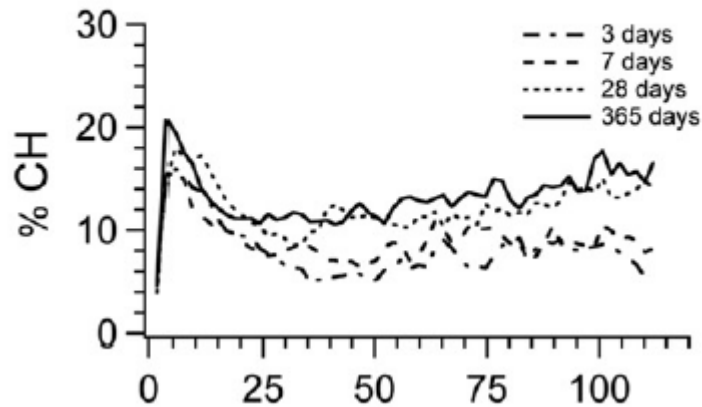


Figure 8.2.1 Calcium hydroxide phase gradient in the interfacial region between cement paste and vertically cast steel at four ages in a concrete with a w/c ratio of 0.70, from reference (Horne *et al.*, 2007)

Combined the image analysis results in the present study with the work done by Horne (Horne, 2004; Horne *et al.*, 2007), it can therefore be postulated that there might be a saturation period of curing, during which progressive CH formation happens at the steel/concrete interface. This is due to the bleeding occurred near steel surface, resulting in a layer of water film around the steel surface, which facilitates the Ca^{2+} ions to transport from the bulk matrix to the spaces near steel; and Ca^{2+} will crystalize to form CH crystals once its concentration has reached the oversaturation state. The duration of the saturation period could be potentially controlled by varying factors e.g. environmental exposure condition, changes of alkalinity in the pore solution (i.e. owing to carbonation) and density of the hydration phases; all of them can significantly affect the ion permeability rate towards interfacial zone. At longer curing ages after the potential saturation period, CH concentrated near the steel surface begins to decrease gradually, presumably due to pH drop in the bulk matrix (e.g. owing to carbonation). The decreased quantity

of CH at interfacial region is undesirable for the corrosion resistance behaviour as the CH around steel is initially expected to act as a buffering effect to protect steel from corrosion, or at least at longer ages.

In steel reinforced CSA concrete system, accumulation of alumina gel can be observed near steel surface from elemental mappings at both ages of 28 days and 1.5 years (Fig. 7.3.1 and Fig. 7.3.3). Quantitative image analysis in Fig. 7.5.2 suggests that ion transportation at interfacial region in CSA concrete is less active than that in the OPC concrete, only with limited proportion of alumina gel consumed by reactions with belite; changes of Ca/Si and S/Ca ratios along the whole interfacial zone is insignificant at ages for up to 1.5 years. This relatively stable chemical environment within the interface is favourably beneficial for maintaining alkalinity around the steel to some extent, at least for longer periods during ageing. Therefore corrosion resistance of the steel reinforcement can be enhanced, as there is less change of pH near the embedded steel surface relative to that in steel reinforced OPC concrete.

8.3 Accuracy of hot water accelerated ageing tests

In the unaged samples investigated in a previous project (Purnell and Beddows, 2005), OPC and Nashrin composites exhibit comparable bending performances (see Fig. 6.5.1); both of them are favourably ductile with a similar ultimate strain of ~0.8%. After ageing for 10 years at 25 °C, remarkable changes have occurred regarding to their bending performances.

Chapter 8- General discussion

Bending performance of the aged OPC/GRC indicates extreme brittleness, with a low ultimate strain value of 0.09% (Fig. 6.5.2). Nevertheless, composite strength reduction was not found. This is inconsistent with the previous hot water accelerated ageing results (Purnell and Beddows, 2005; Butler *et al.*, 2010; Butler *et al.*, 2009b; Orłowsky and Raupach, 2008); most of the results demonstrated substantially decreased bending strength besides extreme brittleness. For example, previous research by Purnell (Purnell and Beddows, 2005) stated that OPC/GRC composites were badly degraded with regard to strength after hot water accelerated ageing for 140 days at 50°C (as shown in Fig. 8.3.1), which is equivalent to about 8 years ageing at 25°C (Purnell and Beddows, 2005); and the bending strength were significantly reduced from 27MPa at 0 day to ~11MPa after 140 days. Mechanical performance of GRC composites made by Portland cement was also investigated by Butler (Butler *et al.*, 2010) using hot water accelerated tests, as presented in Fig. 8.3.2. The results showed that bending resistance decreased dramatically after 360 days at an elevated temperature of 40°C, compared with reference samples cured at 20°C at the age of 28 days. The bending strength reduced approximately 50% after accelerated ageing for 360 days at 40°C, i.e. from 10MPa at 20°C for 28 days to ~5MPa after 360 days at 40°C.

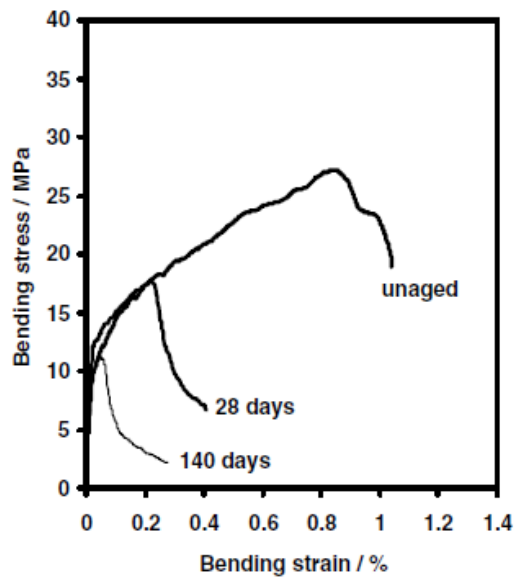


Figure 8.3.1 Evolution of bending performance of OPC/GRC by hot water accelerated ageing at 50°C; from reference (Purnell and Beddows, 2005)

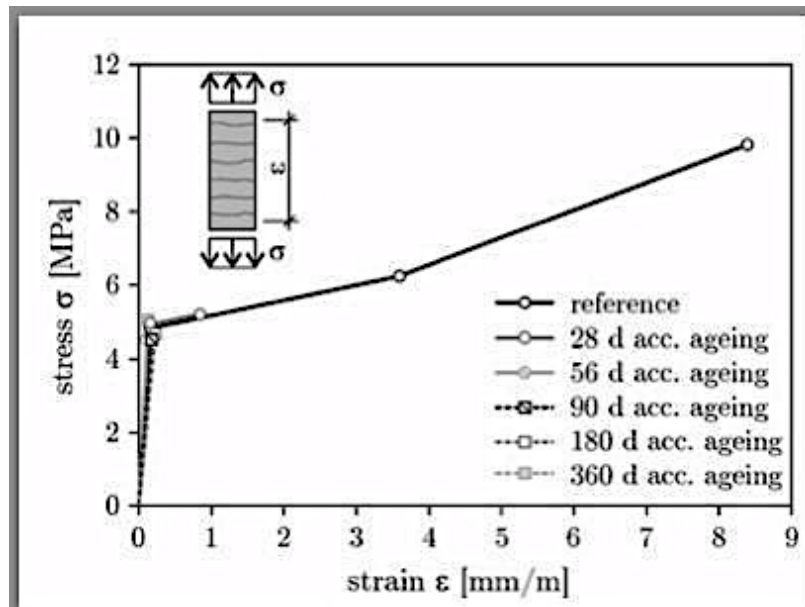


Figure 8.3.2 Stress-strain curves for the GRC specimens made of CEMI 32.5R, accelerated at 40°C/99% RH with reference sample cured at 20°C/66% RH for 28 days, from reference (Butler *et al.*, 2010)

Chapter 8- General discussion

Based on the durability results obtained from hot water accelerated ageing in literature and 'real ageing' tests in this study, consensus can be reached on the severe loss of brittleness in aged GRC composites (due to extreme matrix densification). Nevertheless different opinions exist on their bending strengths after ageing; as discussed above, hot water accelerated aged samples from literature showed severe reduction in composites strength but OPC samples cured at 10 years under normal temperature in this study suggest almost no strength loss during ageing. This would suggest that densification mechanisms are more important than fibre weakening mechanism with regard to long-term performance of GRC composites.

Microstructural reasons for the retained composites strength under normal temperature in the long term can be explained as follows. During ageing over 10 years at 25°C, bonding between glass fibres are gradually enhanced by the infilling of finely intermixed CH and C-S-H gel adhering on fibre surface. The ingressed C-S-H gel helps to produce firmer connection between the relatively large CH crystals, leading to enhanced bond and anchorage to the cement matrix eventually. As a consequence, it turns the GRC composites into rather rigid integrities as a whole; fibres and cement matrix are carrying the load together to give very high composite strength, but the embedded glass fibres under this circumstance have lost most of their flexibilities to add post-peak ductility to the composites. On the other hand, changes at the interface between glass fibre and cement are also highly related to the brittle mechanical performances of aged OPC/GRC composites. Lack of flexibility at this region is the main reason to the extreme composite brittleness due to severe filling of hydration products at

Chapter 8- General discussion

the interfacial zone. As a consequence, during cracking process it fails to absorb the cracking energy through flexible movement and thus loses the ability to suppress the propagation of cracks.

It can be concluded that under normal curing temperatures, even though severe brittleness occurs, glass fibres are still able to add strength to the composites, maintaining the bending strength of aged composites similar, or at least not markedly reduced, to the newly produced un-degraded GRC composites. This may raise concerns on previously established fibre weakening mechanism in GRC composites, which is already widely used in the durability studies on GRC composites; fibre densification mechanism. Like other durability models, hot water accelerated ageing technique might not be perfectly accurate in predicting the real degradation process of GRC composites as a intrinsically different hydration and/or degradation process may be developed at higher curing temperatures. As a consequence it is thus unable to provide exactly the true information on real ageing performances of normal aged GRC composites. However, it might still be very useful in developing new types of GRC materials, by comparing composites made with different matrix formulations and/or varying glass fibre types in a reasonable timescale, prior to a further thorough investigation of the newly modified composites with potentially enhanced performances.

The concept of the accuracy of hot water accelerated ageing also applies to the Nashrin/GRC. In the present study, GRC composites modified by Nashrin retain most of its toughness after 10 years ageing at 25°C (Fig. 6.5.2). The material exhibits great ductility with ultimate strain of 0.55%, compared to the original 0.8% strain for the unaged sample (Fig. 6.5.1).

Chapter 8- General discussion

More importantly, reduction of bending strength was not found in the present study (from 30MPa for the unaged sample to ~32MPa after 10 years). This is slightly different from the previous studies obtained from hot water accelerated ageing tests (Purnell and Beddows, 2005); it revealed that after curing at 50°C for 316 days (this is equivalent to about 6 years ageing at 25°C) (Purnell and Beddows, 2005), GRC modified by Nashrin still exhibited greater toughness compared to the corresponding OPC composites, but tensile strength reduction from ~30MPa in the unaged sample to ~20MPa after 316 days at 50°C was also observed compared to the unaged samples (Fig. 8.3.3).

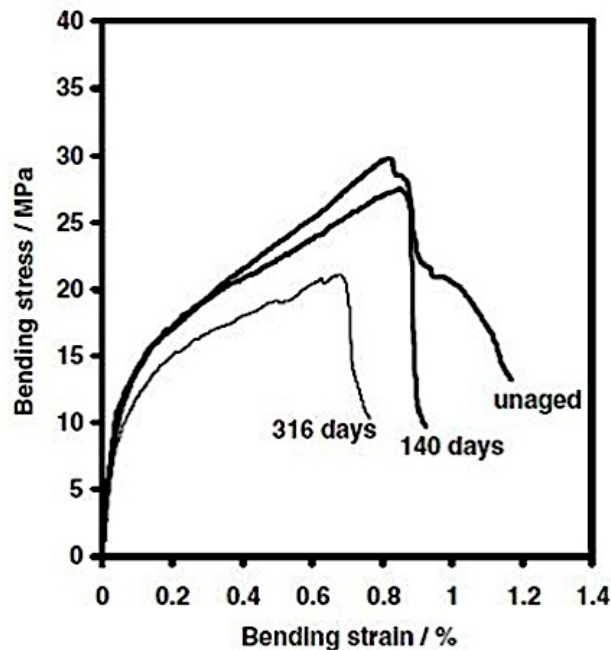


Figure 8.3.3 Evolution of bending performance of Nashrin/GRC by hot water accelerated ageing at 50°C; from reference (Purnell and Beddows, 2005)

According to the mechanical performance of Nashrin/GRC cured at 25°C for 10 years (Fig. 6.5.2), it can be better concluded that addition of calcium sulfoaluminate cement-based materials in GRC composites can provide

beneficial advantages over traditional GRC composites, both in terms of microstructure development and mechanical performances in the long term.

By comparing accelerated ageing and normal ageing for both GRC materials, it can be summarised that accelerated ageing testing cannot completely fulfil its potential to provide true information on the degradation process of GRC composites. Severe composite strength reduction has not been found in both Nashrin/GRC and OPC/GRC under normal ageing; this is different to most of the previous research, which proposed that degradation of GRC composites is a combination of significant reductions in both strength and ductility as time develops (whereas only brittleness is confirmed in the present study). It would appear that at ageing temperatures closer to those encountered in-service, mechanisms that lead to enhanced fibre-matrix bond (densification, precipitation of both CH and C-S-H at the interface and between the fibres, etc.) might have a greater role to play in degradation than mechanisms associated with fibre weakening.

8.4 General discussion on the importance of interface

Durability of reinforced cement composites is highly dependent on the corrosion resistance of embedded reinforcement, which is significantly dependent on the nature of the interface. Interface with low porosity can act as an isolation zone physically between embedded reinforcement and surrounding cementitious materials, by preventing the deleterious ions transporting towards the reinforcement. Regarding to the aspects affecting the interface quality, factors such as matrix formulations, reinforcement types, curing conditions and the ambient environment are all considered.

Chapter 8- General discussion

Glass fibres used in this study are bundled features so not all of the fibres are in direct contact with the bulk cement matrix. Hydrated phases have the preference to ingress into the limited interfilamentary spaces as well as the interface between fibre and cement; but this extent of ingress is highly dependent on types of cement matrix. For example in the traditional OPC matrix, ingress of generated CH/C-S-H mixture (into spaces between glass fibres and the interface) is not prominent at the early age, but the penetration continues to occur with curing, causing severe bundle filling at longer age. In the Nashrin matrix, hydration products of ettringite and C-A-S-H gel are occupying the interfilamentary and interfacial zone at the early age and there are insignificant microstructure changes at the interface as curing develops. This is due to the extremely rapid hydration of calcium sulfoaluminate phase contained in the Nashrin materials, generating ettringite within the first 1-2 days.

Steel bar/concrete interface presents totally different topographic and chemical features in comparison to that in the GRC composites. Preferential ion accumulation can be observed around the steel bar during curing owing to the bleeding on steel bar surface. For example in the OPC concrete system, permeation rate of Ca^{2+} are pronounced near steel surface, generating a non-continuous CH layer in the vicinity of steel bar. Dominant Al^{3+} tends to transport near the steel surface during curing in the reinforced CSA concrete. This hydrated alumina gel layer around steel surface can reduce the contact area of embedded steel reinforcement and cement matrix physically; on the other hand, this layer contains mixtures of hydrated alumina phases (e.g. stratlingite and/or highly alkaline AH_3). Thus it can

maintain a medium pH value near steel (the minimum reported pore solution pH value is 8.5 (Glass *et al.*, 2000)), which is of significant importance to sustain the passive state of reinforcement for longer periods. Even after curing for 1.5 years, thick layer of hydrated alumina gel with varying thickness can be found near the rebar surface in CSA concrete.

Therefore it can be concluded that microstructure evolution at the interface is intrinsically related to the durability properties of the reinforced composites in the long term. Degradation of reinforced composites is mainly due to the chemical changes at the interfacial area, causing reinforcement corrosion (e.g. for steel reinforced concrete) and/or lack of reinforcement flexibility (e.g. for GRC composite) to some extent by the hydrated phases at the interface.

8.5 Application of CSA cement

Based on this study, confidence on the application of CSA cement in GRC and steel reinforced concrete systems are reinforced to greater extent. Addition of CSA cement in GRC composites demonstrates favourable mechanical properties in the long term compared to the OPC formulation; no strength reduction is observed after aged for 10 years and the material retains most of its ductility at the same time. This can be attributed to the hydration nature of CSA cement, which produces no CH and a beneficial pore solution with low alkalinity.

Application of CSA cement in steel bar reinforced concrete is also proved to be acceptable. After curing for 1.5 years in a standard fog room, the steel/concrete interface are still in good quality with a thick layer of hydrated

Chapter 8- General discussion

alumina gel surrounding the rebar, protecting the embedded reinforcement from corrosion by maintaining a relatively high pH near steel.

Chapter 9- Conclusions and future work

9.1 General conclusions

- CSA cement is beneficial to produce GRC composites with improved durability, attributed to the relatively porous interfacial and interfilamentary space in the long term compared to aged OPC/GRC.
- Application of CSA cement in steel reinforced concrete system is proved to be practical, at least during standard curing in foggy room for up to 1.5 years; steel/concrete interface is still in good quality. Large amount of hydrated alumina gel is precipitating at the steel/concrete interface at both shorter and longer ages, and less active ion transport can be observed near steel surface.
- Chemical and microstructural evolution at the interface is highly related to the corrosion resistance of embedded reinforcements.
In aged steel reinforced OPC concrete, decreased amount of CH at the interface may cause pH drop around steel, which consequently accelerates the reinforcement corrosion process.
In aged GRC composites, lack of flexibility at the interface results from the severe filling of CH/C-S-H intermixture at this region, which consequently lead to extreme brittleness of the composites.
- In the degradation mechanisms of GRC composites, it is suggested in this research that densification mechanisms are more important than fibre weakening mechanism with regard to long-term performance of GRC composites.

Chapter 9- Conclusions and future work

- Updated imaging analysis technique can be successfully obtained by applying quantified elemental mappings, with a wider range of applications compared to the traditional imaging analysis technique.

9.2 Future work

- Future work is to investigate the electrochemical behaviour of steel embedded in CSA concrete. It can provide indirect information on the corrosion process of reinforcement, which may further assess the application of CSA cement in reinforced structures. Associated with the microstructural and chemical changes at the interface during ageing, it is expected that the influence of interface quality on the corrosion process can be further established.
- Continue to compare the phase changes and ion transportation at the interfacial zone in steel reinforced OPC and CSA concretes in longer periods, by quantitative image analysis of the atomic ratios and microanalysis near the steel surfaces.
- Study the calorimetry of hydrated CSA cement during the first 28 days to have a more comprehensive understanding of the hydration process, particularly within the first 24h.
- TEM investigation on the interfacial phases at steel/CSA concrete interface is necessary in order to have a better understanding on the chemicals at interface.

References

- ADOLFSSON, D., N. MENAD, E. VIGGH and B. BJÖRKMAN. 2007. Hydraulic properties of sulphoaluminate belite cement based on steelmaking slags. *Advances in cement research*, 19(3), pp.133-138.
- ALBINO, V., R. CIOFFI, M. MARROCCOLI and L. SANTORO. 1996. Potential application of ettringite generating systems for hazardous waste stabilization. *Journal of Hazardous Materials*, 51(1-3), pp.241-252.
- ALKHALAF, M. N. and C. L. PAGE. 1979. STEEL-MORTAR INTERFACES - MICROSTRUCTURAL FEATURES AND MODE OF FAILURE. *Cement and Concrete Research*, 9(2), pp.197-207.
- ALMUSALLAM, A. A. 2001. Effect of degree of corrosion on the properties of reinforcing steel bars. *Construction and Building Materials*, 15(8), pp.361-368.
- ALONSO, C., C. ANDRADE, M. CASTELLOTE and P. CASTRO. 2000. Chloride threshold values to depassivate reinforcing bars embedded in a standardized OPC mortar. *Cement and Concrete Research*, 30(7), pp.1047-1055.
- ALONSO, C., C. ANDRADE, M. CASTELLOTE and P. CASTRO. 2001. Chloride threshold values to depassivate reinforcing bars embedded in a standardized OPC mortar - Reply to discussion. *Cement and Concrete Research*, 31(5), pp.839-840.
- ALONSO, M. and M. SANCHEZ. 2009. Analysis of the variability of chloride threshold values in the literature. *Materials and corrosion*, 60(8), pp.631-637.
- AMLEH, L. and A. GHOSH. 2006. Modeling the effect of corrosion on bond strength at the steel-concrete interface with finite-element analysis. *Canadian Journal of Civil Engineering*, 33(6), pp.673-682.
- ANGST, U., B. ELSENER, C. K. LARSEN and O. VENNESLAND. 2009. Critical chloride content in reinforced concrete - A review. *Cement and Concrete Research*, 39(12), pp.1122-1138.
- ANN, K. Y. and H.-W. SONG. 2007. Chloride threshold level for corrosion of steel in concrete. *Corrosion Science*, 49(11), pp.4113-4133.
- ANSTICE, D. J., C. L. PAGE and M. M. PAGE. 2005. The pore solution phase of carbonated cement pastes. *Cement and Concrete Research*, 35(2), pp.377-383.

References

- ARJUNAN, P., M. R. SILSBEE and D. M. ROY. 1999. Sulfoaluminate-belite cement from low-calcium fly ash and sulfur-rich and other industrial by-products. *Cement and Concrete Research*, 29(8), pp.1305-1311.
- BARHUM, R. and V. MECHTCHERINE. 2013. Influence of short dispersed and short integral glass fibres on the mechanical behaviour of textile-reinforced concrete. *Materials and structures*, 46(4), pp.557-572.
- BARTOS, P. J. M. and W. Z. ZHU. 1996. Effect of microsilica and acrylic: Polymer treatment on the ageing of GRC. *Cement & Concrete Composites*, 18(1), pp.31-39.
- BENTUR, A. 1985. Mechanisms of potential embrittlement and strength loss of glass fiber reinforced cement *In: Proceedings of durability of glass fibre reinforced concrete symposium*, pp.109-123.
- BENTUR, A. 2000. Role of interfaces in controlling durability of fiber-reinforced cements. *Journal of Materials in Civil Engineering*, 12(1), pp.2-7.
- BENTUR, A., M. BENBASSAT and D. SCHNEIDER. 1985. DURABILITY OF GLASS-FIBER-REINFORCED CEMENTS WITH DIFFERENT ALKALI-RESISTANT GLASS-FIBERS. *Journal of the American Ceramic Society*, 68(4), pp.203-208.
- BENTUR, A. and S. MINDESS. 1990. *Fibre reinforced cementitious composites*. London: London : Elsevier Applied Science.
- BERETKA, J., N. SHERMAN, M. MARROCCOLI, A. POMPO and G. VALENTI. 1997. Effect of composition on the hydration properties of rapid-hardening sulfoaluminate cements. *In: Proceedings of the 10th International Congress on the Chemistry of Cement: SINTEF Civil & Environmental Engineering, Cement & Concrete: Norway*, p.2ii029.
- BERGER, S., G. AOUAD, C. CAU DIT COUMES, P. LE BESCOP and D. DAMIDOT. 2013. Leaching of calcium sulfoaluminate cement pastes by water at regulated pH and temperature: Experimental investigation and modeling. *Cement and Concrete Research*, 53, pp.211-220.
- BERGER, S., C. C. D. COUMES, P. LE BESCOP and D. DAMIDOT. 2011. Influence of a thermal cycle at early age on the hydration of calcium sulphoaluminate cements with variable gypsum contents. *Cement and Concrete Research*, 41(2), pp.149-160.
- BERTOS, M. F., S. SIMONS, C. HILLS and P. CAREY. 2004. A review of accelerated carbonation technology in the treatment of cement-based materials and sequestration of CO₂. *Journal of Hazardous Materials*, 112(3), pp.193-205.

References

- BIRYUKOVICH, K. and D. YU. 1964. *Glass fibre reinforced cement*. Civil Engineering Research Association.
- BRANDT, A. M. 2008. Fibre reinforced cement-based (FRC) composites after over 40 years of development in building and civil engineering. *Composite Structures*, 86(1-3), pp.3-9.
- BUTLER, M., V. MECHTCHERINE and S. HEMPEL. 2009a. Effect of Matrix Composition on the Durability of Concretes Reinforced with Glass Fibre Fabric. *Beton- Und Stahlbetonbau*, 104(8), pp.485-495.
- BUTLER, M., V. MECHTCHERINE and S. HEMPEL. 2009b. Experimental investigations on the durability of fibre-matrix interfaces in textile-reinforced concrete. *Cement & Concrete Composites*, 31(4), pp.221-231.
- BUTLER, M., V. MECHTCHERINE and S. HEMPEL. 2010. Durability of textile reinforced concrete made with AR glass fibre: effect of the matrix composition. *Materials and Structures*, 43(10), pp.1351-1368.
- CABRERA, J. G. 1996. Deterioration of concrete due to reinforcement steel corrosion. *Cement & Concrete Composites*, 18(1), pp.47-59.
- CARMEN MARTIN-SEDENO, M., A. J. M. CUBEROS, A. G. DE LA TORRE, G. ALVAREZ-PINAZO, L. M. ORDONEZ, M. GATESHKI and M. A. G. ARANDA. 2010. Aluminum-rich belite sulfoaluminate cements: Clinkering and early age hydration. *Cement and Concrete Research*, 40(3), pp.359-369.
- CASTEL, A., T. VIDAL, R. FRANCOIS and G. ARLIGUIE. 2003. Influence of steel-concrete interface quality on reinforcement corrosion induced by chlorides. *Magazine of Concrete Research*, 55(2), pp.151-159.
- CHEN, I. A., C. W. HARGIS and M. C. G. JUENGER. 2012. Understanding expansion in calcium sulfoaluminate-belite cements. *Cement and Concrete Research*, 42(1), pp.51-60.
- CHEN, I. A. and M. C. G. JUENGER. 2011. Synthesis and hydration of calcium sulfoaluminate-belite cements with varied phase compositions. *Journal of Materials Science*, 46(8), pp.2568-2577.
- COHEN, Z. and A. PELED. 2010. Controlled telescopic reinforcement system of fabric-cement composites - Durability concerns. *Cement and Concrete Research*, 40(10), pp.1495-1506.
- COHEN, Z. and A. PELED. 2012. Effect of nanofillers and production methods to control the interfacial characteristics of glass bundles in textile fabric cement-based composites. *Composites Part a-Applied Science and Manufacturing*, 43(6), pp.962-972.

References

- COLLIER, N., J. SHARP, N. MILESTONE, J. HILL and I. GODFREY. 2008. The influence of water removal techniques on the composition and microstructure of hardened cement pastes. *Cement and Concrete Research*, 38(6), pp.737-744.
- COUTTS, R. S. P. 2005. A review of Australian research into natural fibre cement composites. *Cement & Concrete Composites*, 27(5), pp.518-526.
- CSIZMADIA, J., G. BALÁZS and F. D. TAMÁS. 2001. Chloride ion binding capacity of aluminoferrites. *Cement and Concrete Research*, 31(4), pp.577-588.
- CUYPERS, H., J. WASTIELS, P. VAN ITTERBEECK, E. DE BOLSTER, J. ORLOWSKY and M. RAUPACH. 2006. Durability of glass fibre reinforced composites experimental methods and results. *Composites Part a-Applied Science and Manufacturing*, 37(2), pp.207-215.
- DAMTOFT, J. S., J. LUKASIK, D. HERFORT, D. SORRENTINO and E. M. GARTNER. 2008. Sustainable development and climate change initiatives. *Cement and Concrete Research*, 38(2), pp.115-127.
- DARWIN, D. and M. N. ABOUZEID. 1995. Application of automated image analysis to the study of cement paste microstructure. *In: S. DIAMOND, S. MINDESS, F. P. GLASSER, L. W. ROBERTS, J. P. SKALNY and L. D. WAKELEY, eds. Microstructure of Cement-Based Systems/Bonding and Interfaces in Cementitious Materials.* pp.3-12.
- DAY, R. 1981. Reactions between methanol and Portland cement paste. *Cement and Concrete Research*, 11(3), pp.341-349.
- DESCHNER, F., B. MUENCH, F. WINNEFELD and B. LOTHENBACH. 2013. Quantification of fly ash in hydrated, blended Portland cement pastes by backscattered electron imaging. *Journal of Microscopy*, 251(2), pp.188-204.
- DEVEKEY, R. C. and A. J. MAJUMDAR. 1970. INTERFACIAL BOND STRENGTH OF GLASS FIBRE REINFORCED CEMENT COMPOSITES. *Journal of Materials Science*, 5(2), pp.183-&.
- DIAMOND, S. 2001. Considerations in image analysis as applied to investigations of the ITZ in concrete. *Cement & Concrete Composites*, 23(2-3), pp.171-178.
- DIAMOND, S. and D. BONEN. 1995. A re-evaluation of hardened cement paste microstructure based on backscatter SEM investigations. *In: S. DIAMOND, S. MINDESS, F. P. GLASSER, L. W. ROBERTS, J. P. SKALNY and L. D. WAKELEY, eds. Microstructure of Cement-Based Systems/Bonding and Interfaces in Cementitious Materials.* pp.13-22.

References

- DIAMOND, S. and J. D. HUANG. 2001. The ITZ in concrete - a different view based on image analysis and SEM observations. *Cement & Concrete Composites*, 23(2-3), pp.179-188.
- ENFEDAQUE, A., D. CENDON, F. GALVEZ and V. SANCHEZ-GALVEZ. 2010. Analysis of glass fiber reinforced cement (GRC) fracture surfaces. *Construction and Building Materials*, 24(7), pp.1302-1308.
- ENFEDAQUE, A., D. CENDON, F. GALVEZ and V. SANCHEZ-GALVEZ. 2011. Failure and impact behavior of facade panels made of glass fiber reinforced cement(GRC). *Engineering Failure Analysis*, 18(7), pp.1652-1663.
- ENFEDAQUE, A., L. SANCHEZ PARADELA and V. SANCHEZ-GALVEZ. 2012. An alternative methodology to predict aging effects on the mechanical properties of glass fiber reinforced cements (GRC). *Construction and Building Materials*, 27(1), pp.425-431.
- ENFEDAQUE DIAZ, A., L. SANCHEZ PARADELA and V. SANCHEZ-GALVEZ. 2010. The effect of silica fume and metakaolin on glass-fibre reinforced concrete (GRC) ageing time. *Materiales De Construccion*, 60(300), pp.67-82.
- FAMY, C., K. L. SCRIVENER and A. K. CRUMBIE. 2002. What causes differences of C-S-H gel grey levels in backscattered electron images? *Cement and Concrete Research*, 32(9), pp.1465-1471.
- FANG, C. Q., K. LUNDGREN, L. G. CHEN and C. Y. ZHU. 2004. Corrosion influence on bond in reinforced concrete. *Cement and Concrete Research*, 34(11), pp.2159-2167.
- GALLÉ, C. 2001. Effect of drying on cement-based materials pore structure as identified by mercury intrusion porosimetry: a comparative study between oven-, vacuum-, and freeze-drying. *Cement and Concrete Research*, 31(10), pp.1467-1477.
- GAO, S. L., E. MADER and R. PLONKA. 2004. Coatings for glass fibers in a cementitious matrix. *Acta Materialia*, 52(16), pp.4745-4755.
- GAO, S. L., E. MAEDER and R. PLONKA. 2007. Nanostructured-coatings of glass fibers: Improvement of alkali resistance and mechanical properties. *Acta Materialia*, 55(3), pp.1043-1052.
- GARCÍA-MATÉ, M., A. G. DE LA TORRE, L. LEÓN-REINA, E. R. LOSILLA, M. A. ARANDA and I. SANTACRUZ. 2014. Effect of calcium sulfate source on the hydration of calcium sulfoaluminate eco-cement. *Cement and Concrete Composites*.

References

- GARCÍA-MATÉ, M., I. SANTACRUZ, Á. G. DE LA TORRE, L. LEÓN-REINA and M. A. ARANDA. 2012. Rheological and hydration characterization of calcium sulfoaluminate cement pastes. *Cement and Concrete Composites*, 34(5), pp.684-691.
- GARTNER, E. 2004. Industrially interesting approaches to "low-CO₂" cements. *Cement and Concrete Research*, 34(9), pp.1489-1498.
- GEORGIN, J. F., J. AMBROISE, J. PERA and J. M. REYNOUARD. 2008. Development of self-leveling screed based on calcium sulfoaluminate cement: Modelling of curling due to drying. *Cement & Concrete Composites*, 30(9), pp.769-778.
- GLASS, G. K., B. REDDY and N. R. BUENFELD. 2000. The participation of bound chloride in passive film breakdown on steel in concrete. *Corrosion Science*, 42(11), pp.2013-2021.
- GLASS, G. K., R. YANG, T. DICKHAUS and N. R. BUENFELD. 2001. Backscattered electron imaging of the steel-concrete interface. *Corrosion Science*, 43(4), pp.605-610.
- GLASSER, F. P., J. MARCHAND and E. SAMSON. 2008. Durability of concrete - Degradation phenomena involving detrimental chemical reactions. *Cement and Concrete Research*, 38(2), pp.226-246.
- GLASSER, F. P. and L. ZHANG. 2001. High-performance cement matrices based on calcium sulfoaluminate-belite compositions. *Cement and Concrete Research*, 31(12), pp.1881-1886.
- GLINICKI, M. and A. BRANDT. 2007. Quantification of glass fibre–cement interfacial properties by SEM-based push-out test. In: *Proc 5th int RILEM workshop high performance fiber reinforced cement composites, Proc*, pp.343-355.
- HARGIS, C. W., A. P. KIRCHHEIM, P. J. MONTEIRO and E. M. GARTNER. 2013. Early age hydration of calcium sulfoaluminate (synthetic ye'elimate,) in the presence of gypsum and varying amounts of calcium hydroxide. *Cement and Concrete Research*, 48, pp.105-115.
- HAYASHI, M., S. STATO, AND H. FUJII. 1985. Some ways to improve durability of GFRC. In: *Durability of Glass Fibre Reinforced Concrete Symposium*, Chicago. Prestressed Concrete Institute.
- HEAD, M. 2001. *Influence on the interfacial transition zone (ITZ) on the properties of concrete*. PhD thesis thesis, University of Leeds.
- HEMPEL, R., M. BUTLER, S. HEMPEL and H. SCHORN. 2007. Durability of textile reinforced concrete. *ACI Special Publication*, 244.

References

- HEMPEL, S. and M. BUTLER. 2007. Microscopic investigations on durability of textile-reinforced concrete. *Proceedings of the 11th euroseminar on microscopy applied to building materials. Porto (CD-ROM)*.
- HORNE, A. T. 2004. *Microstructure of interfaces in steel reinforced concrete*. Ph.D thesis, University of Leeds.
- HORNE, A. T., I. G. RICHARDSON and R. M. D. BRYDSON. 2007. Quantitative analysis of the microstructure of interfaces in steel reinforced concrete. *Cement and Concrete Research*, 37(12), pp.1613-1623.
- HUGHES, J. M. and H. WEILL. 1991. ASBESTOSIS AS A PRECURSOR OF ASBESTOS RELATED LUNG-CANCER - RESULTS OF A PROSPECTIVE MORTALITY STUDY. *British Journal of Industrial Medicine*, 48(4), pp.229-233.
- JANOTKA, I. and L. KRAJCI. 1999. An experimental study on the upgrade of sulfoaluminate-belite cement systems by blending with Portland cement. *Advances in Cement Research*, 11(1), pp.35-41.
- JANOTKA, I., L. KRAJCI and S. C. MOJUMDAR. 2002. Influence of Portland cement addition to sulphoaluminate-belite cement on hydration and mechanical properties of hardened mortars. *Ceramics-Silikaty*, 46(3), pp.110-116.
- JANOTKA, I., L. KRAJCI, A. RAY and S. C. MOJUMDAR. 2003. The hydration phase and pore structure formation in the blends of sulfoaluminate-belite cement with Portland cement. *Cement and Concrete Research*, 33(4), pp.489-497.
- JOHN, D. A., A. B. POOLE and I. SIMS. 1998. *Concrete Petrography*. London: Arnold Publishers.
- JUENGER, M. C. G., F. WINNEFELD, J. L. PROVIS and J. H. IDEKER. 2011. Advances in alternative cementitious binders. *Cement and Concrete Research*, 41(12), pp.1232-1243.
- KALOGRIDIS, D., G. C. KOSTOGLLOUDIS, C. FTIKOS and C. MALAMI. 2000. A quantitative study of the influence of non-expansive sulfoaluminate cement on the corrosion of steel reinforcement. *Cement and Concrete Research*, 30(11), pp.1731-1740.
- KASSELOURI, V., P. TSAKIRIDIS, C. MALAMI, B. GEORGALI and C. ALEXANDRIDOU. 1995. A STUDY ON THE HYDRATION PRODUCTS OF A NON-EXPANSIVE SULFOALUMINATE CEMENT. *Cement and Concrete Research*, 25(8), pp.1726-1736.

References

- KATZ, A. and A. BENTUR. 1996. Mechanisms and processes leading to changes in time in the properties of CFRC. *Advanced Cement Based Materials*, 3(1), pp.1-13.
- KJELLEN, K., A. MONSØY, K. ISACHSEN and R. DETWILER. 2003. Preparation of flat-polished specimens for SEM-backscattered electron imaging and X-ray microanalysis—importance of epoxy impregnation. *Cement and Concrete Research*, 33(4), pp.611-616.
- KOLEVA, D. A., J. HU, A. L. A. FRAAIJ, P. STROEVEN, N. BOSHKOV and J. H. W. DE WIT. 2006. Quantitative characterisation of steel/cement paste interface microstructure and corrosion phenomena in mortars suffering from chloride attack. *Corrosion Science*, 48(12), pp.4001-4019.
- L.ZHANG, M. Z. S., Y.M. WANG. 1999. Development of the use of sulfo- and ferro-aluminate cements in China. *Advances in Cement Research*, 11, pp.15-21.
- LECOMTE, I., C. HENRIST, M. LIEGEOIS, F. MASERI, A. RULMONT and R. CLOOTS. 2006. (Micro)-structural comparison between geopolymers, alkali-activated slag cement and Portland cement. *Journal of the European Ceramic Society*, 26(16), pp.3789-3797.
- LEONARD, S. and A. BENTUR. 1984. IMPROVEMENT OF THE DURABILITY OF GLASS-FIBER REINFORCED CEMENT USING BLENDED CEMENT MATRIX. *Cement and Concrete Research*, 14(5), pp.717-728.
- LI, X., Y. ZHANG, X. SHEN, Q. WANG and Z. PAN. 2014. Kinetics of calcium sulfoaluminate formation from tricalcium aluminate, calcium sulfate and calcium oxide. *Cement and Concrete Research*, 55, pp.79-87.
- LI, Y. and S. G. HU. 2001. The microstructure of-the interfacial transition zone between steel and cement paste. *Cement and Concrete Research*, 31(3), pp.385-388.
- LIAO, Y. S., X. S. WEI and G. W. LI. 2011. Early hydration of calcium sulfoaluminate cement through electrical resistivity measurement and microstructure investigations. *Construction and Building Materials*, 25(4), pp.1572-1579.
- LITHERLAND, K. L., OAKLEY DR, PROCTOR BA. 1981. The use of accelerated ageing procedures to predict the long-term strength of grc composites. *Cem Concr Res*, 11, pp.455-466.

References

- LIU, M.-Y., H.-G. ZHU, N. A. SIDDIQUI, C. K. Y. LEUNG and J.-K. KIM. 2011. Glass fibers with clay nanocomposite coating: Improved barrier resistance in alkaline environment. *Composites Part a-Applied Science and Manufacturing*, 42(12), pp.2051-2059.
- LUZ, C. A., J. C. ROCHA, M. CHERIAF and J. PERA. 2006. Use of sulfoaluminate cement and bottom ash in the solidification/stabilization of galvanic sludge. *Journal of Hazardous Materials*, 136(3), pp.837-845.
- MAJUMDAR, A. and V. LAWS. 1991. *Glass fibre reinforced cement*. Oxford: BSP Professional Books.
- MARIKUNTE, S., C. ALDEA and S. P. SHAH. 1997. Durability of glass fiber reinforced cement composites: Effect of silica fume and metakaolin. *Advanced Cement Based Materials*, 5(3-4), pp.100-108.
- MECHLING, J.-M., A. LECOMTE, A. ROUX and B. LE ROLLAND. 2013. Sulfoaluminate cement behaviours in carbon dioxide, warm and moist environments. *Advances in Cement Research*, 26(1), pp.52-61.
- MEDEIROS, M. H. and P. HELENE. 2009. Surface treatment of reinforced concrete in marine environment: Influence on chloride diffusion coefficient and capillary water absorption. *Construction and building materials*, 23(3), pp.1476-1484.
- MICHALSKE, T. A. and S. W. FREIMAN. 1983. A MOLECULAR MECHANISM FOR STRESS-CORROSION IN VITREOUS SILICA. *Journal of the American Ceramic Society*, 66(4), pp.284-288.
- MIN, D. and T. MINGSHU. 1994. FORMATION AND EXPANSION OF ETTRINGITE CRYSTALS. *Cement and Concrete Research*, 24(1), pp.119-126.
- MOHAMMED, T. U. and H. HAMADA. 2001. A discussion of the paper "Chloride threshold values to depassivate reinforcing bars embedded in a standardized OPC mortar" by C. Alonso, C. Andrade, M. Castellote, and P. Castro. *Cement and Concrete Research*, 31(5), pp.835-838.
- MUTHUPRIYA, P. 2013. AN EXPERIMENTAL INVESTIGATION ON EFFECT OF GGBS AND GLASS FIBRE IN HIGH PERFORMANCE CONCRETE. *International Journal of Civil Engineering*.
- NASSER, A., A. CLEMENT, S. LAURENS and A. CASTEL. 2010. Influence of steel-concrete interface condition on galvanic corrosion currents in carbonated concrete. *Corrosion Science*, 52(9), pp.2878-2890.
- NEFF, D., J. HARNISCH, M. BECK, V. L'HOSTIS, J. GOEBBELS and D. MEINEL. 2011. Morphology of corrosion products of steel in concrete under

References

macro-cell and self-corrosion conditions. *Materials and Corrosion-Werkstoffe Und Korrosion*, 62(9), pp.861-871.

NOURREDINE, A. 2011. Influence of curing conditions on durability of alkali-resistant glass fibres in cement matrix. *Bulletin of Materials Science*, 34(4), pp.775-783.

ORLOWSKY, J. and M. RAUPACH. 2006. Modelling the loss in strength of AR-glass fibres in textile-reinforced concrete. *Materials and Structures*, 39(6), pp.635-643.

ORLOWSKY, J. and M. RAUPACH. 2008. Durability model for AR-glass fibres in textile reinforced concrete. *Materials and Structures*, 41(7), pp.1225-1233.

ORLOWSKY, J., M. RAUPACH, H. CUYPERS and J. WASTIEIS. 2005. Durability modelling of glass fibre reinforcement in cementitious environment. *Materials and Structures*, 38(276), pp.155-162.

PACHECO-TORGAL, F. and S. JALALI. 2011. Cementitious building materials reinforced with vegetable fibres: A review. *Construction and Building Materials*, 25(2), pp.575-581.

PAGE, C. L. 1975. Mechanism of corrosion protection in reinforced concrete marine structures. *Nature* 258, pp.514-515.

PAGE, C. L. 2009. Initiation of chloride-induced corrosion of steel in concrete: role of the interfacial zone. *Materials and Corrosion-Werkstoffe Und Korrosion*, 60(8), pp.586-592.

PAGE, C. L. P. A. M. M. 2007. *Durability of concrete and cement composites*. Cambridge: Cambridge : Woodhead Publishing ; Boca Raton, Fla. : CRC Press, c2007.

PAUL, A. 1977. Chemical durability of glasses; a thermodynamic approach. *Journal of materials science*, 12(11), pp.2246-2268.

PELED, A., J. JONES and S. SHAH. 2005. Effect of matrix modification on durability of glass fiber reinforced cement composites. *Materials and structures*, 38(2), pp.163-171.

PERA, J. and J. AMBROISE. 2004. New applications of calcium sulfoaluminate cement. *Cement and Concrete Research*, 34(4), pp.671-676.

PEYSSON, S., J. PERA and M. CHABANNET. 2005. Immobilization of heavy metals by calcium sulfoaluminate cement. *Cement and Concrete Research*, 35(12), pp.2261-2270.

References

- PINCHIN, D. J. and D. TABOR. 1978. INTERFACIAL PHENOMENA IN STEEL FIBER REINFORCED CEMENT .1. STRUCTURE AND STRENGTH OF INTERFACIAL REGION. *Cement and Concrete Research*, 8(1), pp.15-24.
- POPESCU, C. D., M. MUNTEAN and J. H. SHARP. 2003. Industrial trial production of low energy belite cement. *Cement & Concrete Composites*, 25(7), pp.689-693.
- POURBAIX, M. 1974. APPLICATIONS OF ELECTROCHEMISTRY IN CORROSION SCIENCE AND IN PRACTICE. *Corrosion Science*, 14(1), pp.25-82.
- PROCTOR, B. A., D. R. OAKLEY and K. L. LITHERLAND. 1982. DEVELOPMENTS IN THE ASSESSMENT AND PERFORMANCE OF GRC OVER 10 YEARS. *Composites*, 13(2), pp.173-179.
- PURNELL, P. 2007. *Degradation of fibre-reinforced cement composites*. Durability of Concrete and Cement Composites.
- PURNELL, P. and J. BEDDOWS. 2005. Durability and simulated ageing of new matrix glass fibre reinforced concrete. *Cement & Concrete Composites*, 27(9-10), pp.875-884.
- PURNELL, P., J. CAIN, P. VAN ITTERBEECK and J. LESKO. 2008. Service life modelling of fibre composites: A unified approach. *Composites Science and Technology*, 68(15-16), pp.3330-3336.
- PURNELL, P., N. R. SHORT and C. L. PAGE. 2001. A static fatigue model for the durability of glass fibre reinforced cement. *Journal of Materials Science*, 36(22), pp.5385-5390.
- PURNELL, P., N. R. SHORT, C. L. PAGE and A. J. MAJUMDAR. 2000. Microstructural observations in new matrix glass fibre reinforced cement. *Cement and Concrete Research*, 30(11), pp.1747-1753.
- PURNELL, P., N. R. SHORT, C. L. PAGE, A. J. MAJUMDAR and P. L. WALTON. 1999. Accelerated ageing characteristics of glass-fibre reinforced cement made with new cementitious matrices. *Composites Part a-Applied Science and Manufacturing*, 30(9), pp.1073-1080.
- QUILLIN, K. 2001. Performance of belite-sulfoaluminate cements. *Cement and Concrete Research*, 31(9), pp.1341-1349.
- RICHARDSON, I. G. 1999. The nature of C-S-H in hardened cements. *Cement and Concrete Research*, 29(8), pp.1131-1147.
- RICHARDSON, I. G. 2008. The calcium silicate hydrates. *Cement and Concrete Research*, 38(2), pp.137-158.

References

- SABIR, B. B., S. WILD and J. BAI. 2001. Metakaolin and calcined clays as pozzolans for concrete: a review. *Cement & Concrete Composites*, 23(6), pp.441-454.
- SAILLIO, M., V. BAROGHEL-BOUNY and F. BARBERON. 2014. Chloride binding in sound and carbonated cementitious materials with various types of binder. *Construction and Building Materials*, 68, pp.82-91.
- SCRIVENER, K. and A. CAMPAS. 2003. Calcium aluminate cements. *Advanced concrete technology: Constituent materials*, 2, pp.1-2.
- SCRIVENER, K. L. 2004. Backscattered electron imaging of cementitious microstructures: understanding and quantification. *Cement & Concrete Composites*, 26(8), pp.935-945.
- SCRIVENER, K. L., A. FULLMANN, E. GALLUCCI, G. WALENTA and E. BERMEJO. 2004. Quantitative study of Portland cement hydration by X-ray diffraction/Rietveld analysis and independent methods. *Cement and Concrete Research*, 34(9), pp.1541-1547.
- SHI, C., A. F. JIMÉNEZ and A. PALOMO. 2011. New cements for the 21st century: the pursuit of an alternative to Portland cement. *Cement and Concrete Research*, 41(7), pp.750-763.
- SHI, X., N. XIE, K. FORTUNE and J. GONG. 2012. Durability of steel reinforced concrete in chloride environments: An overview. *Construction and Building Materials*, 30, pp.125-138.
- SNOECK, D., L. VELASCO, A. MIGNON, S. VAN VLIERBERGHE, P. DUBRUEL, P. LODEWYCKX and N. DE BELIE. 2014. The influence of different drying techniques on the water sorption properties of cement-based materials. *Cement and Concrete Research*, 64, pp.54-62.
- SOYLEV, T. A. and R. FRANCOIS. 2003. Quality of steel-concrete interface and corrosion of reinforcing steel. *Cement and Concrete Research*, 33(9), pp.1407-1415.
- STUTZMAN, P. 2004. Scanning electron microscopy imaging of hydraulic cement microstructure. *Cement & Concrete Composites*, 26(8), pp.957-966.
- SURYAVANSHI, A. and R. NARAYAN SWAMY. 1996. Stability of Friedel's salt in carbonated concrete structural elements. *Cement and Concrete Research*, 26(5), pp.729-741.
- TELESCA, A., M. MARROCCOLI, M. PACE, M. TOMASULO, G. VALENTI and P. MONTEIRO. 2014. A hydration study of various calcium sulfoaluminate cements. *Cement and Concrete Composites*, 53, pp.224-232.

References

- VALENTI, G. L., M. MARROCCOLI, M. L. PACE and A. TELESCA. 2012. Discussion of the paper "Understanding expansion in calcium sulfoaluminate-belite cements" by I.A. Chen et al., *Cem. Concr. Res.* 42 (2012) 51-60. *Cement and Concrete Research*, 42(11), pp.1555-1559.
- VAN ITTERBEECK, P., P. PURNELL, H. CUYPERS, T. TYSMANS, J. ORLOWSKY and J. WASTIELS. 2012. Durability models for GRC: uncertainties on strength predictions. *Plastics Rubber and Composites*, 41(2), pp.77-87.
- VAN ITTERBEECK, P., P. PURNELL, H. CUYPERS and J. WASTIELS. 2009. Study of strength durability models for GRC: Theoretical overview. *Composites Part a-Applied Science and Manufacturing*, 40(12), pp.2020-2030.
- VIDAL, T., A. CASTEL and R. FRANCOIS. 2007. Corrosion process and structural performance of a 17 year old reinforced concrete beam stored in chloride environment. *Cement and Concrete Research*, 37(11), pp.1551-1561.
- WANG, Y. T. and S. DIAMOND. 1995. An approach to quantitative image analysis for cement pastes. *In: S. DIAMOND, S. MINDESS, F. P. GLASSER, L. W. ROBERTS, J. P. SKALNY and L. D. WAKELEY, eds. Microstructure of Cement-Based Systems/Bonding and Interfaces in Cementitious Materials.* pp.23-32.
- WERNER, A. M. and D. A. LANGE. 1999. Quantitative image analysis of masonry mortar microstructure. *Journal of Computing in Civil Engineering*, 13(2), pp.110-115.
- WINNEFELD, F. and S. BARLAG. 2009. Influence of calcium sulfate and calcium hydroxide on the hydration of calcium sulfoaluminate clinker. *Zkg International*, 62(12), pp.42-53.
- WINNEFELD, F. and B. LOTHENBACH. 2010. Hydration of calcium sulfoaluminate cements - Experimental findings and thermodynamic modelling. *Cement and Concrete Research*, 40(8), pp.1239-1247.
- WONG, H. S., M. K. HEAD and N. R. BUENFELD. 2006. Pore segmentation of cement-based materials from backscattered electron images. *Cement and Concrete Research*, 36(6), pp.1083-1090.
- YANG, R. and N. R. BUENFELD. 2001. Binary segmentation of aggregate in SEM image analysis of concrete. *Cement and Concrete Research*, 31(3), pp.437-441.
- YILMAZ, V. T. and F. P. GLASSER. 1991. REACTION OF ALKALI-RESISTANT GLASS-FIBERS WITH CEMENT .2. DURABILITY IN CEMENT

References

MATRICES CONDITIONED WITH SILICA FUME. *Glass Technology*, 32(4), pp.138-147.

YONEZAWA, T., V. ASHWORTH and R. P. M. PROCTER. 1988. PORE SOLUTION COMPOSITION AND CHLORIDE EFFECTS ON THE CORROSION OF STEEL IN CONCRETE. *Corrosion*, 44(7), pp.489-499.

ZHANG, J. and G. W. SCHERER. 2011. Comparison of methods for arresting hydration of cement. *Cement and Concrete Research*, 41(10), pp.1024-1036.

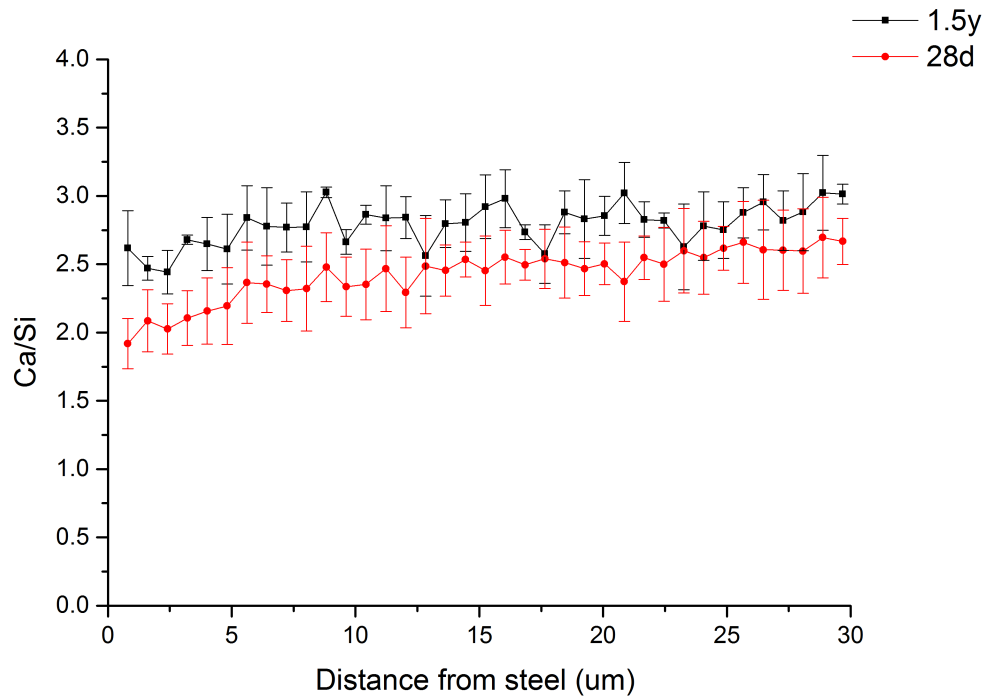
ZHANG, L. and F. P. GLASSER. 2005. Investigation of the microstructure and carbonation of CSA-based concretes removed from service. *Cement and Concrete Research*, 35(12), pp.2252-2260.

ZHANG, R., A. CASTEL and R. FRANCOIS. 2011. Influence of steel-concrete interface defects owing to the top-bar effect on the chloride-induced corrosion of reinforcement. *Magazine of Concrete Research*, 63(10), pp.773-781.

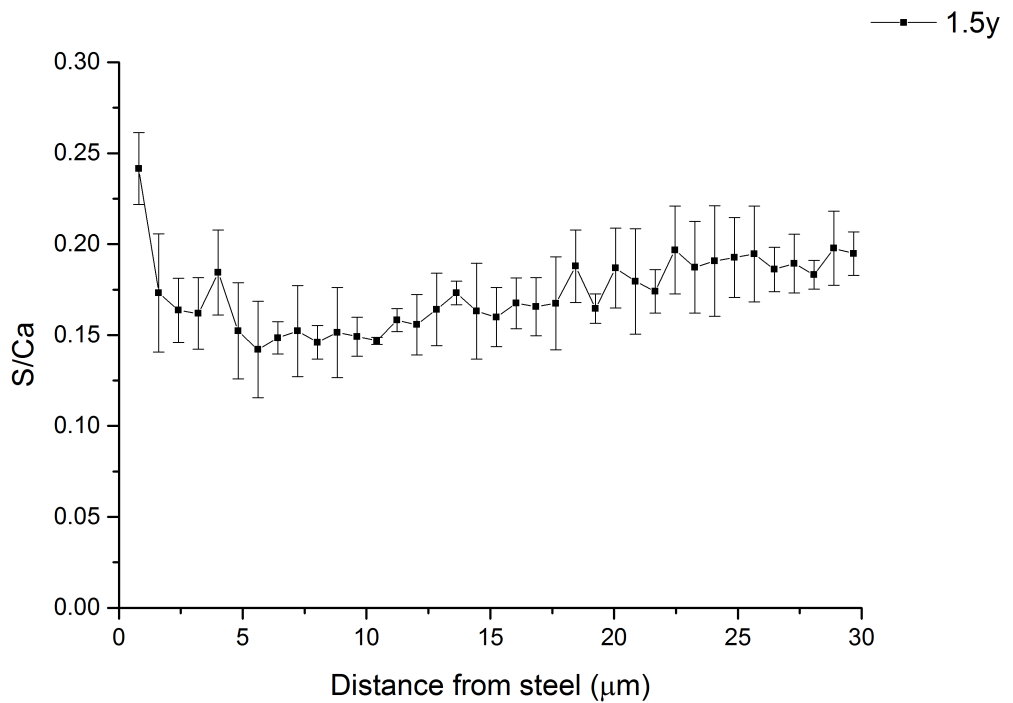
ZHOU, Q., N. B. MILESTONE and M. HAYES. 2006. An alternative to Portland Cement for waste encapsulation - The calcium sulfoaluminate cement system. *Journal of Hazardous Materials*, 136(1), pp.120-129.

ZHU, W. and P. J. M. BARTOS. 1997. Assessment of interfacial microstructure and bond properties in aged GRC using a novel microindentation method. *Cement and Concrete Research*, 27(11), pp.1701-1711.

Appendix A



Ca/Si ratio for CSA concretes



References

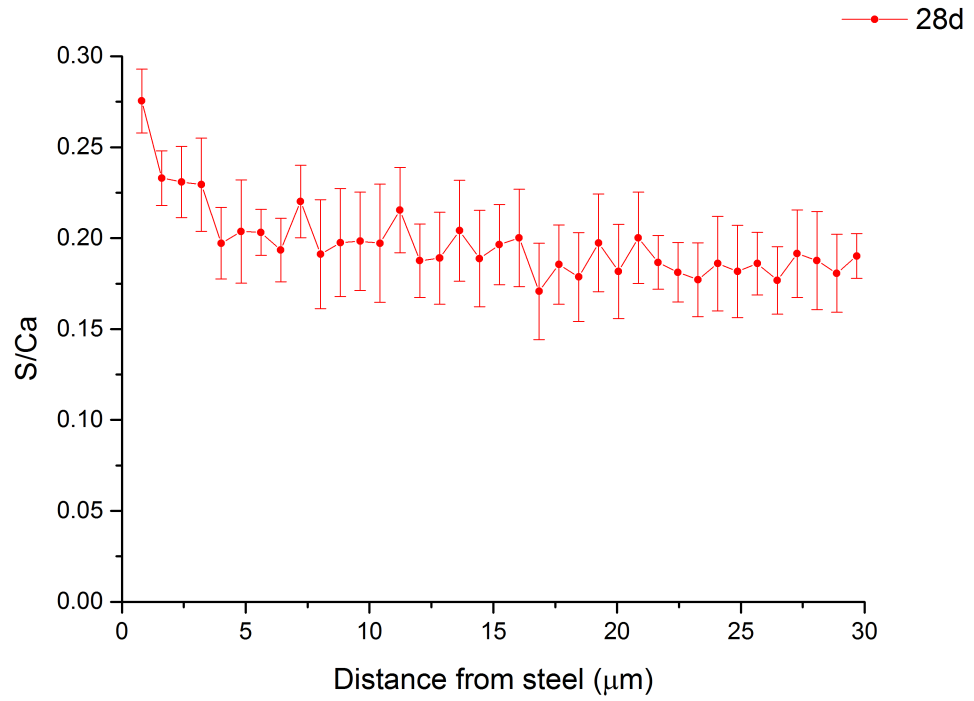


Figure 10.1 Image analysis on S/Ca at the interface between CSA cement and steel

Appendix B

List of publications

M. Song, et al., Microstructure of interface between fibre and matrix in 10-year aged GRC modified by calcium sulfoaluminate cement, *Cem. Concr. Res.*, 2015;

M. Song, et al., Microstructure of steel/concrete interface in low-carbon concrete, conference paper at 32nd *Cement and Concrete Science*.